ABSTRACT

DESIGN OF THREE-DIMENSIONAL
AXON STRETCH GROWTH DEVICE

by
Fayekah Assanah

Spinal Cord Injury (SCI) causes destruction and degeneration of axons in the white matter of the spinal cord, resulting in functional loss and paralysis. A successful treatment of SCI requires axons to regenerate across damaged regions. Current studies focus on identifying mechanisms to promote axon regeneration in lesions and have yet to be successful in preventing nerve degeneration due to scar tissue formation. Establishing axonal bridges over long distances of SCI lesions remains a challenge, resulting in poor functional recovery. Instead of relying on promoting axon regeneration into lesions, Pfister et al. has developed a transplantable nervous tissue construct spanned by stretch grown axon tracts. These tracts of living axons are intended to act as a bridge to facilitate axon outgrowth from the nerve construct to the host nerves over long SCI lesions. While axon stretch growth is fast and efficient, the current approach uses a two-dimensional (2D) culture system, posing a challenge for uniform distribution of DRG explants throughout the culture. This yields in a less than optimal number of axon tracts being stretched.

The research objective of this thesis is to increase the number/density of axons that are stretched grown by using three-dimensional (3D) cultures. This thesis work involves modification of the existing 2D axon stretch growth device to achieve axon growth in 3D cultures. The design includes separating two 3D hydrogel cell cultures using a porous nylon mesh to constrain each half of the culture. Optimal mechanical

properties of the collagen hydrogel and nylon mesh pore sizes are tested for mechanical support, best axon outgrowth, and the number of axons available for stretch growth. Phase contrast and fluorescent microscopy are used to determine axon outgrowth in the hydrogel and through the nylon mesh. Live staining with fluorescent intracellular dyes and confocal microscopy are used to quantify the cross sectional areas of axon bundles stretched using the 2D device. This provides insight into developing a quantification method for axons grown in the 3D setup to determine the efficiency and the growth mechanism of axons in 3D cultures.

DESIGN OF THREE-DIMENSIONAL
AXON STRETCH GROWTH DEVICE

by
Fayekah Assanah

A Dissertation
Submitted to the Faculty of
New Jersey Institute of Technology
in Partial Fulfillment of the Requirements for the Degree of
Master of Science in Biomedical Engineering

Department of Biomedical Engineering
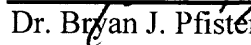
January 2008

Blank Page

APPROVAL PAGE

DESIGN OF THREE-DIMENSIONAL
AXON STRETCH GROWTH DEVICE
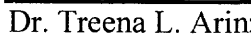
Fayekah Assanah

Dr. Bryan J. Pfister, Dissertation Advisor   Date
Assistant Professor of Biomedical Engineering, NJIT

Dr. Michael Jaffe, Committee Member   Date
Research Professor of Biomedical Engineering, NJIT

Dr. Treena L. Arinzeh, Committee Member   Date
Assistant Professor of Biomedical Engineering, NJIT

BIOGRAPHICAL SKETCH

Author: Fayekah Assanah

Degree: Master of Science

Date: January 2008

Undergraduate and Graduate Education:

- Master of Science in Biomedical Engineering,
  New Jersey Institute of Technology, Newark, NJ, 2008

- Bachelor of Science in Electrical Engineering,
  University of Virginia, Charlottesville, Virginia, 2005

Major: Biomedical Engineering

To my mother, my friend, my strength and my guardian angel who taught me to believe in myself and keep my head high through the rough times of life. She is my blessings from Allah; she is the person dearest to my soul.

ACKNOWLEDGMENT

TABLE OF CONTENTS

LIST OF TABLES

LIST OF FIGURES

Figure   **Page**

Figure   **Page**

Figure   **Page**

CHAPTER 1
INTRODUCTION

1.1 Introduction

An estimated 450,000 people live in the United States with Spinal Cord Injury (SCI) and approximately 11,000 new cases of SCI result each year [1]. About 10,000 are permanently paralyzed, and many die as a result of their injuries [2]. The annual cost of medical care for treating SCI has been estimated at about $11 billion [3, 4]. Although some SCI injuries allow for recovery to a certain degree, others result in complete paralysis of the body from below the site of injury [4]. Injuries to the spinal cord are classified as functionally incomplete or complete [5]. In incomplete injury, sensation to certain body parts still survive, as compared to complete injury, where, signals coming from the brain to the body parts are completely obstructed by nerve damage [5, 6]. Thus, it is very difficult to repair the functional loss in a complete spinal cord injury.

Research has focused on many techniques to repair and treat SCI. To fully understand the methods and approaches, it is important to understand the functional elements of the spinal cord and how injury to the spine can result in paralysis. The following section in this chapter briefly describes the essential components of the spinal cord, how spinal cord injury may lead to functional loss and explains the factors that hinder axon outgrowth after chronic SCI. This chapter also discusses the different techniques used to repair SCI and the advantages and disadvantages of such approaches.

In the later sections of this chapter, the axon stretch growth device designed by Pfister et al is described and how this technique presents a unique insight into repairing SCI. This is followed by the discussion of the goal of this thesis work.

1.2 Spinal Cord Injury

The nervous system consists of two main divisions: the central nervous system (CNS), which includes the brain and the spinal cord, and the peripheral nervous system (PNS), which is composed of the cranial, spinal, and autonomic nerves that exit the spinal cord and connects to the limbs and organs of the body. The spinal cord is about 18 inches long and extends from the base of the brain, down the middle of the back, to about the waist (Figure 1.1). The upper motor neurons (UMNs) lie within the spinal cord and their function is to carry messages back and forth from the brain to the spinal nerves along the spinal tract. The spinal nerves that branch out from the spinal cord to the other parts of the body are the lower motor neurons (LMNs). Nerve fibers enter and exit the cord through the spinal roots: (1) the ventral root sends signals to the periphery, (2) the dorsal roots brings information from the periphery through the Dorsal Root Ganglia (DRG) into the spinal cord up to the brain [7, 8]. The DRG is a group of sensory nerve cell bodies that pass sensory information to neurons in the spinal cord so it can be analyzed by the brain. The spinal nerves, mentioned above, communicate with specific areas of the body: carrying sensory messages from the brain to the other body parts and organs (also called effector organs) and from the rest of the body back to the brain.

Figure 1.2 shows the cross-sectional area of the spinal cord [8], the pathway of signals inbetween the effector muscle and the spinal cord, the Dorsal Root Ganglion (DRG), the interneuron and the synaptic connections.
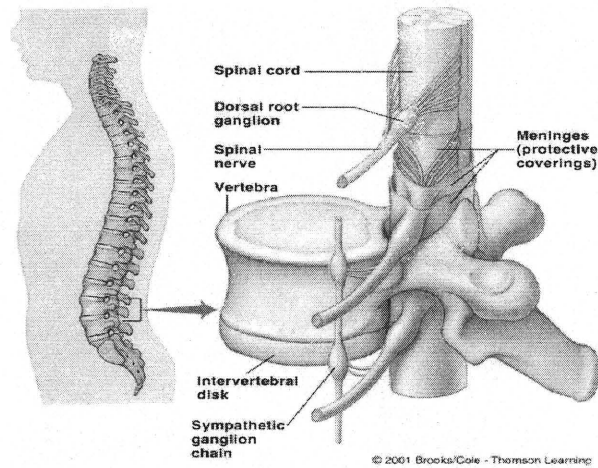
Figure 1.1 The spinal column showing the Dorsal Root Ganglion, Spinal Nerve and the Spinal cord [8].
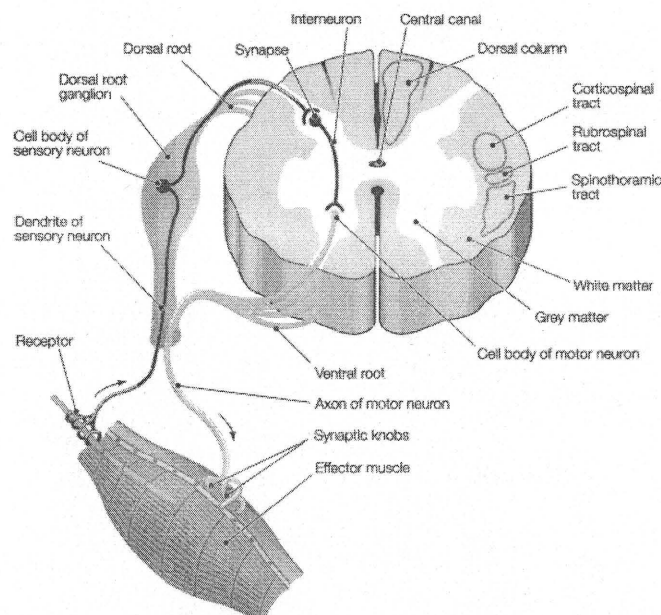
Figure 1.2 Cross section of the spinal cord showing the Dorsal Root Ganglion, the synaptic connection, the interneuron, and the pathway of signals to and from the effector muscle [9].

The functional unit of the nervous system is the neuron. The neuron consists of a cell body, dendrites and an axon. The dendrites serve as antennas to receive signals from other neurons. The axon on the other hand, is longer than the dendrites and transmits nervous signals, over long distances, away from the cell body of the neuron to the synapse of the post synaptic neuron in the effector organs. In other words, axons carry signals up and down the spinal cord between the brain and the rest of the body [8]. The signals that are carried by the axons over such long distances, through the spinal cord are called axon potentials. The synapse is the junction between neurons where transmission of signals occurs. In a synapse, signals are transmitted from the axon terminal of the pre-synaptic neuron to the receiving end of the post synaptic neuron of the effector organ. At the post synaptic neuron, the signals are transmitted through chemicals called neurotransmitters.

The Figure 1.3 is an illustration of the structure of a neuron and its axons and dendrites. It also shows the synapse and the transmission of signals from the cell body of the neuron to the post synaptic neuron at the synaptic cleft. Thus, the spinal cord acts as a passageway for all the nervous/axon tracts carrying signals to and from the brain to the rest of the body. The spinal cord, in turn, is supported and protected by the spinal column.

Damage to the spinal cord can impair various nervous system functions such as memory, cognition, language, and voluntary movement [4]. Spinal Cord Injury occurs as a result of a traumatic blow to the spine that fractures or dislocates the spinal discs and the vertebrae, displaces bone fragments and tears ligaments or spinal cord tissues. As a result, nerve tracts and axons in the white matter tracts of the spinal cord are crushed [5, 11].
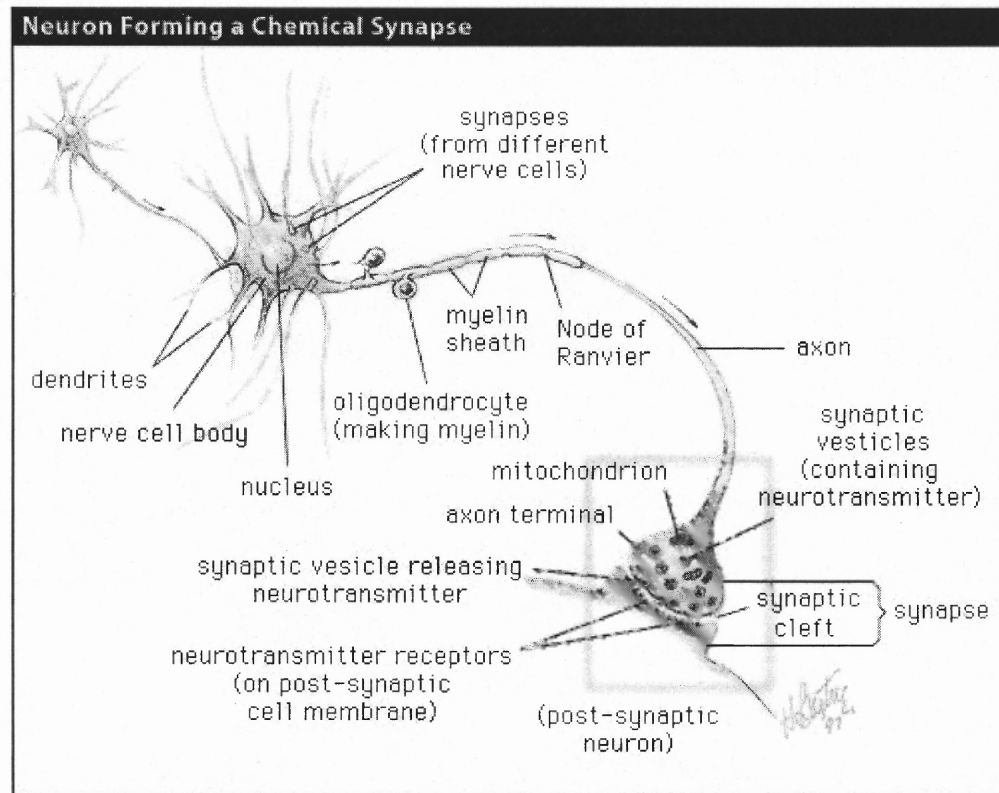
Figure 1.3 Illustration of a neuron, axons and dendrites and formation of a synapse [10].

The injury causes compression of the spinal cord that can lead to the degeneration of nerve fibers distal to the lesion and the eventual death of disconnected neurons. This loss of axonal connections results in the interruption of communication between nerve cell bodies and their targets causing permanent motor and/or sensory functional loss below the site of injury [5, 11, 12, 13].

After Spinal Cord Injury, a series of events take place as a natural response of the body to heal the injury and also re-establish the functional connection of signals through the spinal cord. In order to understand the effects of Spinal Cord Injury, it is important to understand this cascade of events. The following sections describe the sequences

involved in axon regeneration and the factors that hinder axon outgrowth, in further details.

1.2.1 Inhibitory Factors that Hinder Axon Regeneration after Spinal Cord Injury

When axon tracts are damaged in SCI, regeneration of such axons is difficult because damaged tissue releases biological factors that inhibit axon growth. Major sources of inhibitory factors are: (1) CNS myelin made by oligodendrocytes (neuroglia that forms the myelin sheaths enveloping the axons [8]) and (2) Glial scar formed at the injury site [14, 15]. The non-permissive property of the white matter in the spinal cord is associated with the breakdown products of myelin (protein components of the CNS myelin) which account for most of the CNS axon regeneration failure [15, 16]. On the other hand, the glial cells (supporting cells of the central nervous system) create a glial 'scar', creating a barrier against axon growth. Scar tissues, in turn, prevent axons from regenerating into the lesions. Ischemia, on the other hand, deprives the tissue of oxygen, glucose and other nourishment. Excess leakage of plasma from the damaged blood vessels causes the spinal cord to swell, killing many interneurons and glial cells. The dead cells aggravate the injury, causing many undamaged interneurons in neighboring uninjured regions to undergo apoptosis and/ or demyelination. Furthermore, large cavities in the cord tissue results as inflammatory response bring neutrophils and macrophages into the lesion to ingest bacteria and cellular debris [4, 5, 15].

1.2.2 Axon Regeneration after Spinal Cord Injury

After Spinal Cord Injury, axon regeneration in the CNS involves a cascade of complex sequences [17]. Once axons are transected, new axons have to sprout and grow into and through the lesion at the site of injury to reestablish functional connections with the disconnected targets [4]. After chronic injury, as a result of the body's natural defense, the lesion site is greatly occupied by dense scar tissues filled with fibroblasts, astrocytes, meningeal cells, and a variety of inhibitory molecules derived from the CNS myelin. These cells and the factors that greatly hinder axon regeneration are discussed in the next section. Axons are free to sprout around the scar region but these axons fail to elongate and retrace their original pathway to reach their intended targets, thus, permanently losing functional connections [4, 15]. In Figure 1.4 the axons and glial/macrophages are shown to degenerate beyond the injury or lesion site because of the damage to the functional connection. New axons sprout at the injury site but fail to regenerate and grow towards their previous targets.

As a result of the axon disconnections, signals coming from the brain no longer reach their destinations to the effector organs. Alternately, signals from the rest of the body fail to travel back to the brain. This causes paralysis of body parts and motor and sensory functional loss.

Functional recovery becomes feasible only if regeneration of injured spinal axon tracts can reconnect with their original targets. The factors discussed above hinder axon regeneration over long distances. The following section of this chapter discusses the various methods and techniques involved in repairing spinal cord injury.
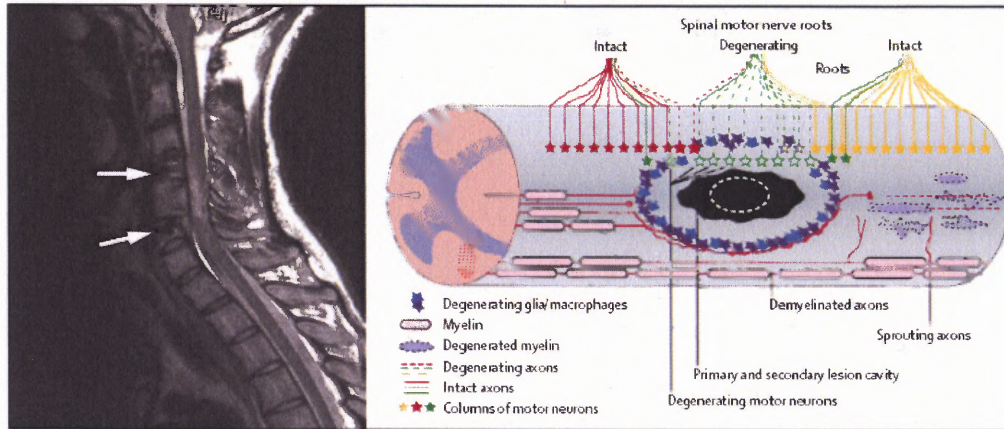
Figure 1.4 Axons, glial cells are shown to degenerate beyond the injury or lesion site [4].

1.3 Research in Spinal Cord Injury

The success of any regeneration therapy depends on restoring functional connections by improving axon tract regeneration in the spinal cord [4, 18]. A lot of research has focused on repairing SCI through several techniques. The most common approaches to repair nerve fiber injuries in the spinal cord are: (1) Cellular replacement, (2) Transplantation of biomaterials. The following sections discuss these two approaches and how researchers have applied these techniques to repair Spinal Cord Injury.

1.3.1 Cellular Replacement

Cellular replacement is an approach where severed nerve fibers are encouraged to grow by providing stimulatory substances and/or removing inhibitory molecules from the environment which make scarred tissue non-permissive for regeneration. It also includes preventing scar formation by inhibition of collagen biosynthesis [5].

Cellular replacement has been applied to repair SCI to (1) fill the cavity created at the injury site, (2) provide permissive environment to improve axon outgrowth and (3)

replace dead cells (neurons or myelinating cells e.g. oligodendrocytes) [5]. Different cell types such as Schwann cells, olfactory en-sheathing glial cells, neural stem cells, embryonic and adult stem cells have been used for this purpose.

Schwann cells are a cell type located in the PNS, rather than in the CNS [4]. The role of Schwann cells largely involves myelination and ensheathing of peripheral nerve fibers. The potential of Schwann cell to facilitate the neuronal repair has been widely noted [5, 19, 20, 21]. Researchers have replaced injured cells of SCI by Schwann cells. It has been observed that Schwann cells are seen to promote CNS nerve tract repair because of their production of neuronal trophic factors, such as nerve growth factor (NGF), brain-derived neurotrophic factor (BDNF), and ciliary neurotrophic factor (CNTF) that all help promote axon regeneration by inhibiting the effects of CNS myelination [20, 21, 22].

Olfactory ensheathing glial cells (OEGs) are a specialized type of CNS glial cells that support and guide the growth of newly formed axons from the olfactory mucosa of the nasal passages to the olfactory bulbs [4, 23]. OEG migration is not obstructed by the CNS glial scars and they are able to enter both gray and white matter, potentially attracting regenerating axons. In the last few years, the efficacy of OEGs in promoting axonal regeneration in the injured adult mammalian CNS has been extensively examined [24, 25, 26, 27, 28, 29, 30].

McDonald et al., Ogawa Y et al., T. Veizovic et al. and other groups [25, 31, 32, 33] have shown the remarkable potential of transplanted neural stem cells (NSCs) to promote functional recovery. Neural stem cells are defined as multi-potential and self-renewing cells that are able to generate all the major cell types in the adult CNS. Multi-potential means that a single neural stem cell may give rise to various neuronal or glial

cell types depending upon the specific environmental cues [4]. Researchers have seen that NSCs assist in the formation of functional synapses as well as help in remodeling the injured tissue and increase the tissue plasticity when transplanted into the adult CNS.

McDonald et al., Keirstead HS et al., and Zeng X et al. [34, 35, 36] have transplanted embryonic stem cells (ESCs) (rodent and human) into injured spinal cord. ESCs have a remarkable ability to self renew and they can also be genetically manipulated in vitro [4, 5]. The implanted cells tend to survive, integrate and differentiate into glial and neuronal phenotypes at the injury site and eventually induce some level of locomotor recovery. However, ESCs replacement present many ethical issues unlike in the case of adult stem cells (ASCs) which are also becoming increasing popular for CNS repair [5, 37]. For instance, a number of studies have evaluated the potential of bone marrow stroma cells (BMSCs) from adults for the treatment of SCI. These cells are attractive for autologous transplantation because they can be easily isolated and expanded in culture and delivered to the injury site [5].

Although cell transplantation/replacement has been successful in axon regeneration, this method and its strategies have turned out to be more complex than initially anticipated [5]. This is partly due to the underestimated influence of factors such as lineage restriction and the variable immune response to the engrafted population [4, 38]. SCI injuries tend to span several centimeters in length and cell replacement techniques can only enhance axon regeneration over a much smaller distance. Therefore, fully recovering the axonal tract and encouraging axons to grow towards their lost targets to completely bridge the lesion in a short time still remains a challenge.

1.3.2 Transplantation of Biomaterials

Transplantation refers to the method of reconstruction of the glial pathway by biomaterial scaffolds and nerve constructs [5, 18]. A scaffold is defined as a temporary framework or substrate to support cells. Prior to the emergence of tissue engineering and cellular replacement for repairing SCI, strategies to bridge or replace the lesions relied upon the utilization of biomaterials to form scaffolds and artificial transplants [39]. Figure 1.5 illustrates the general concept behind bridging the lesion site with a substrate made of different biomaterials and size comparable to the native tissue. Current research involve the use of polymeric materials, both non-degradable (e.g polyvinyl chloride [9, 40], polyethylene [41, 45]), and degradable (e.g. polyglycolic acid [42], collagen [43]) to build the bridges. The bridges or the constructs are usually tubular in structure in order to match the geometrical structure of the spinal cord. These brides also act as a guidance channel for the regenerating axons [44, 45]. It directs cell behaviors such as migration, proliferation, differentiation and apoptosis which encourage a favorable environment for cell-cell and cell-matrix communication [4, 18]. Some scaffold materials have been incorporated with neutrophic factors such as NGF and BDNF to encourage axon outgrowth [46, 47]. The applications of biodegradable materials for constructing guidance channels may offer an advantage compared over the nondegradable construct, as they timely degrade from the implantation site and do not require an additional surgical intervention for removal from the body [4, 48, 49, 50].
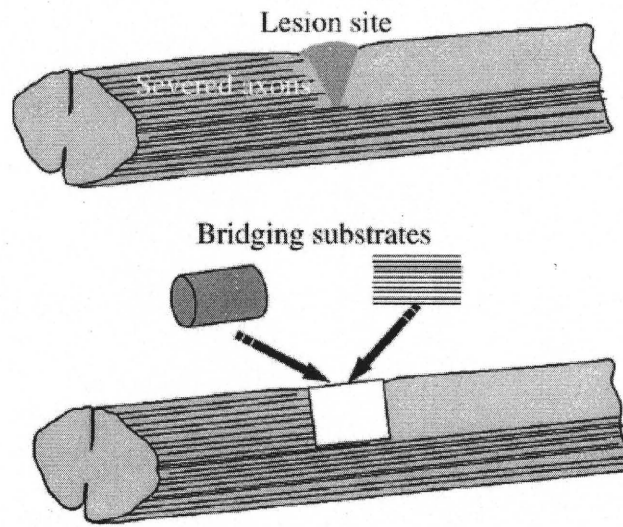
Figure 1.5 Illustration of the concept of bridging the lesion in CNS injury by a substrate made of various biomaterials [4].

Various techniques have focused on using different polymeric hydrogels for supporting axon regeneration. W. Plant et al. have used poly 2-hydroxyethyl methacrylate (HEMA) collagen sponges to provide a highly porous, mechanically stable 3D network structure able to house a population of glial cells to assist in axon outgrowth. However, results show that the number of regrowing axons is limited and the sponge of HEMA give little protection to peripheral glial cells when implanted inside the host cell [51].

A. Jain et al. have studied axonal growth in 3D scaffold of agarose, optimized with embedded drug delivery system: BDNF. The results demonstrate that the agarose gel conforms to the shape of the spinal cord cavity. BDNF reduces the reactivity of the astrocytes and the production of chondroitin sulfate proteoglycans (CSPGs) and enhances the ability of regenerating nerve fibers to enter the hydrogel scaffold [12].

Other investigators have proposed scaffolds to guide regenerating fibers by providing an oriented surface on which to grow [15, 20, 21, 22]. For example, P. Prang et

al. have assessed the capacity of anisotropic capillary hydrogels (ACH) channels to promote directed axonal regrowth in the injured mammalian CNS. Results show that the ACH is able to promote highly oriented axon regeneration in vitro and in vivo in the injured mammalian CNS leading to appropriate target re-enervation in vitro [45]. Although guidance channels have shown promise in directed regeneration of axons in the spinal cord, issues regarding biocompatibility and biodegradability are yet to be resolved.

A few techniques have seen the possibility of transplanting grafting tissues such as peripheral nerves [5], genetically modified fibroblasts [12, 52, 53], and intact fetal spinal cords [54] into the spinal cord to promote axon bridges across spinal cord lesions. Although these techniques have shown success, the use of artificial nerve grafts, constructs and scaffolds made of certain biomaterials arise a major concern regarding biocompatibility and biodegradability in the host cell that can induce unwanted chemical cues to the other cells of the body.

The methods described above prove to be worthwhile and effective in promoting axon growth. However, as mentioned earlier, SCI lesions can span upto several centimeters in length and it is seen that axons cannot regenerate over long distances on their own because of the factors discussed above. Additionally, for long distances, the transected axon segment at the injury site degenerates even before axons can reach their original targets. Therefore, it is a challenge to regenerate the axons uni-directionally towards its original targets, over long distances.

Instead of relying on the promotion of axon regeneration into lesions by the methods discussed above, Pfister et al. has developed a transplantable nervous tissue construct spanned by stretch grown axon tracts. The hypothesis is that living axon tracts

act as a bridge to facilitate axon outgrowth from the nerve construct to the host nerves [13]. Unlike the techniques mentioned above, this approach allows repairing lesions that span several centimeters in length because, here, axons are rapidly elongated at an escalated rate to stretch grow upto several centimeters under the application of mechanical forces. In addition, axon tracts in this construct are not myelinated making them non-immunogenic when transplanted. The axon tracts are supported by natural hydrogel such as collagen to form the construct. Hence, the properties of the construct can be matched to that of the spinal cord. The following section explains the concept behind applying mechanical forces to stretch axons and the method of axon stretch growth using the custom designed axon stretch growth device by Pfister et al.

1.4 Axon Stretch Growth in Spinal Cord Injury

The axon stretch growth method by Pfister et al., involves an *in vitro* tissue engineering method to rapidly elongate numerous axon bundles under the application of mechanical forces. The forces from stretching induce the longitudinal growth of axons at rates up to 1cm/day in comparison to the natural growth rate of axons by a growth cone which is approximately 1mm/day [13]. Before discussing the design and the method of axon stretch growth it is important to understand the concept behind the growth of axons under the application of external mechanical forces. The following section discusses the hypotheses behind axon stretch growth.

1.4.1 Concept behind Axon Stretch Growth

The concept behind the method of axon stretch growth is regulated by mechanical tension [55, 56, 57]. Growth cone mediated growth is not the only way axons grow [55]. Growth cones pull on the axon to activate unknown stretch-sensitive mechanisms that, in turn, stimulate axon growth. It is believed that in growth-cone mediated axonal elongation, microtubules are added at the distal end of the growth cone as the axon cylinder grows in length [55].

After synaptic connections are established at the axon terminals, the axons grow by co-ordinating with the surrounding tissue [55]. As the body of an organism grows, it exerts tension on its axons, and stimulates axonal growth. Tensional forces in the axons are the mechanisms that regulate chemical reactions of microtubules assembly and disassembly, which in turn, drives axonal elongation and retraction, respectively. As explained by Bray et al., nerve cells respond to the axial tension applied to them by increasing the length and number of microtubules and neurofilaments by assembling membrane components. The tension causes the axons to activate unknown stretch sensitive mechanism that in turn stimulates axonal outgrowth [58]. As the axons elongate, the tension is dissipated and the axons add mass to accommodate the increased length. Hence, axons do not stretch elastically but behave more viscoelastic, as the axons slowly adapt to the tension [55]. This growth by the application of external mechanical forces is called towing. It is hypothesized that in the towing mode, the mass addition of axons is interstitial around the entire length of the axons [59, 60].

1.4.2 Axon Stretch Growth Device

The axon stretch growth device designed by Pfister et al. applies the concept of towing, discussed above, to rapidly elongate axons grown inbetween two cell cultures. The axon stretch growth device or the bioreactor is a custom designed axon expansion chamber consisting of a linear motion table, stepper motor and a controller as shown in Figure 1.6. The chamber houses an axon stretching frame that is enclosed with a CO_2 exchange port. The axon stretching frame is connected by means of metal rods to a linear motion table which is in turn connected to the stepper motor that drives the linear displacements.
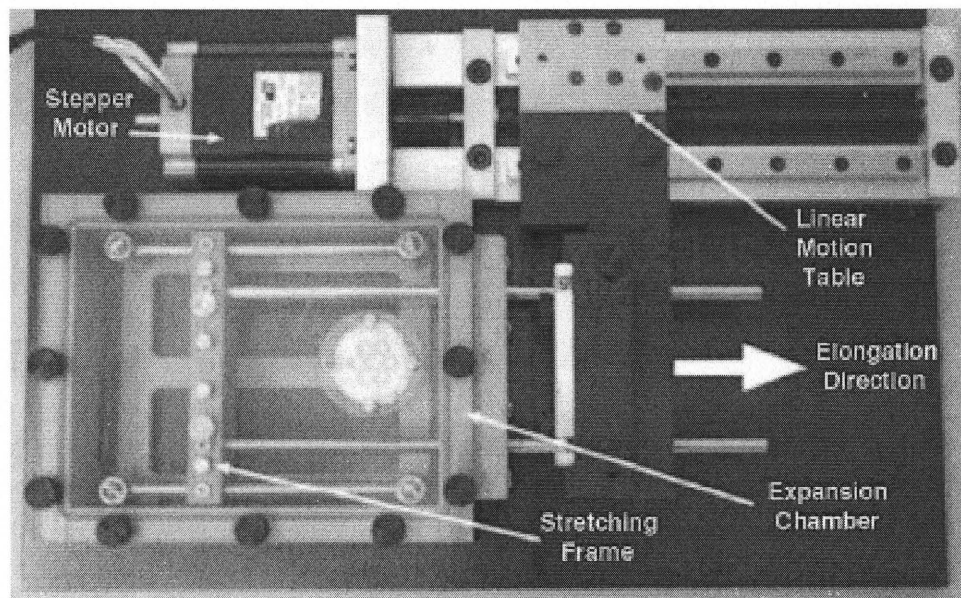
Figure 1.6 Axon Stretch Growth System. The system contains an expansion chamber with carbon dioxide exchange port, a linear motion table and a stepper motor [13].
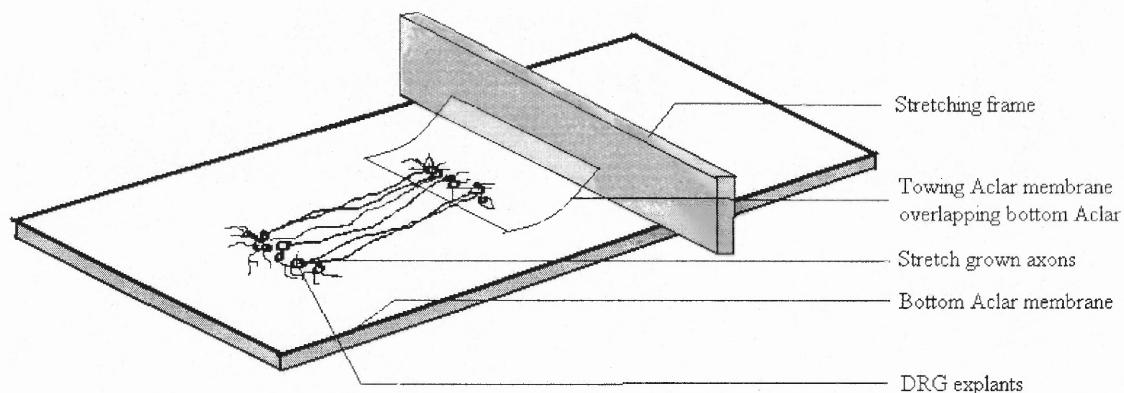
Figure 1.7 Set-up of two-dimensional axon stretch growth mechanism.

Inside the chamber, the stretching frame separates two adjoining Aclar membranes (Figure 1.7). The bottom membrane covers the entire bottom surface of the stretching frame and serves as the stationary substrate where a population of neurons, embryonic Dorsal Root Ganglion (DRG) explants, is cultured. The bottom membrane is overlapped with a towing Aclar membrane (connected to the stretching frame) that supports another population of neurons. Axons are allowed to grow across the interface of the two substrates into the population of neurons on either side.

As the stretching frame moves uni-directionally, the overlapping Aclar membrane is displaced across the bottom Aclar membrane stretching the axons inbetween the two cell cultures. The microstepper motor and controller is run by SiProgrammer software (Servo Systems, Montville, NJ). The software enables the controller and the microstepper motor to apply stepwise escalated stretch to the stretching frame. In other words, the rate of stretching is increased in a variable stepwise fashion. The linear motion table (shown in Figure 1.6) converts the stepwise rotation of the stepper motor into stepwise linear displacements that allows the stretching frame to displace through discrete linear

distances. Figure 1.8 and Figure 1.9 shows the linear motion of the stretching frame. In Figure 1.8 (a), the two neural cultures are together allowing for axon growth from one culture to the other. In Figure 1.8 (b), as the stretching frame is displaced uni-directionally, the two cultures separate and the interconnecting axons are stretched.

Figure 1.9 is the schematic of axon stretch growth showing the overlapping Aclar membranes. As the towing Aclar membrane is uni-directionally displaced the interconnecting axons are stretched.
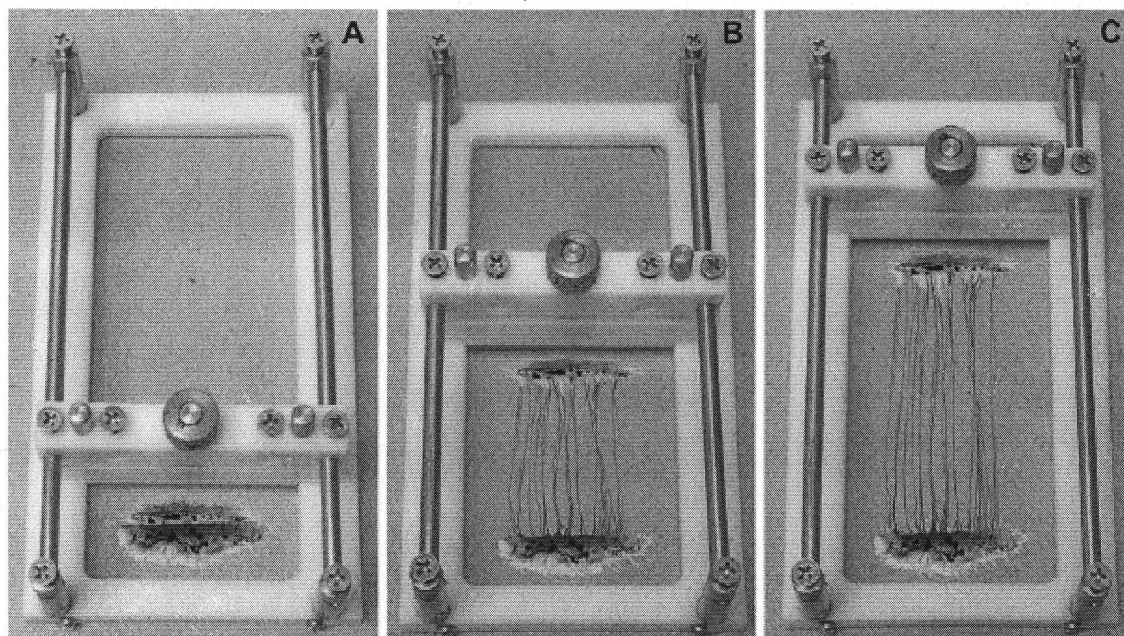
Figure 1.8 Schematic of Axon Stretch Growth. (A) Neurons are plated on two adjoining Aclar substrates and axons are allowed to grow into either culture. (B) Population of neurons are separated from the other, thereby elongating the interconnecting axons. (C) Length of axons increase as elongation proceeds [13].
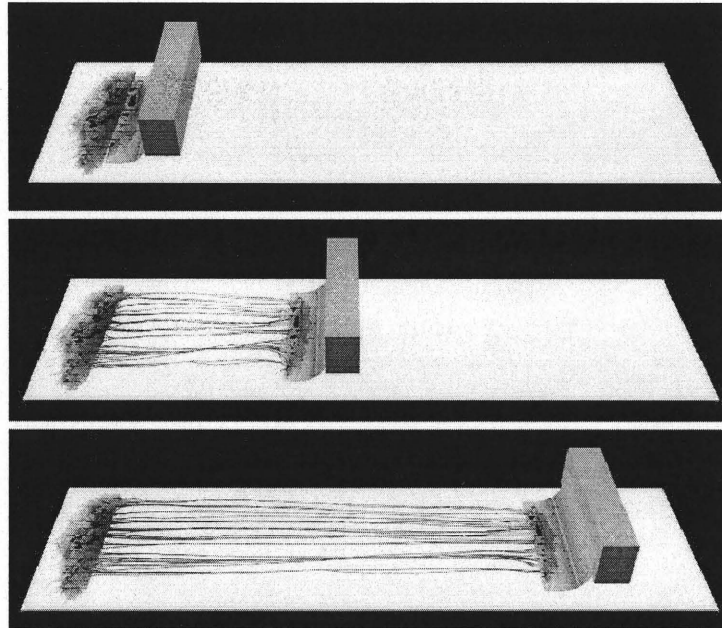
Figure 1.9 Axons stretched grown. As the towing frame moves linearly and the interconnecting axons between the two population of neurons stretch [7].

Using the device described above, axons can be stretched to a desired length of upto 10 cm in length at varying rates. To create a nerve constructs, the stretched axons are then supported by collagen hydrogel. The hydrogel protects the axons from damage during surgical manipulation and preserves the uni-axial orientation of the axons. The stretch grown axons, covered by the collagen hydrogel is then separated by cutting away from the Aclar membrane and rolled into a cylindrical structure to form a transplantable nerve construct. The nerve construct can then be transplanted into the lesions of SCI. Figure 1.10 illustrates the process described above.
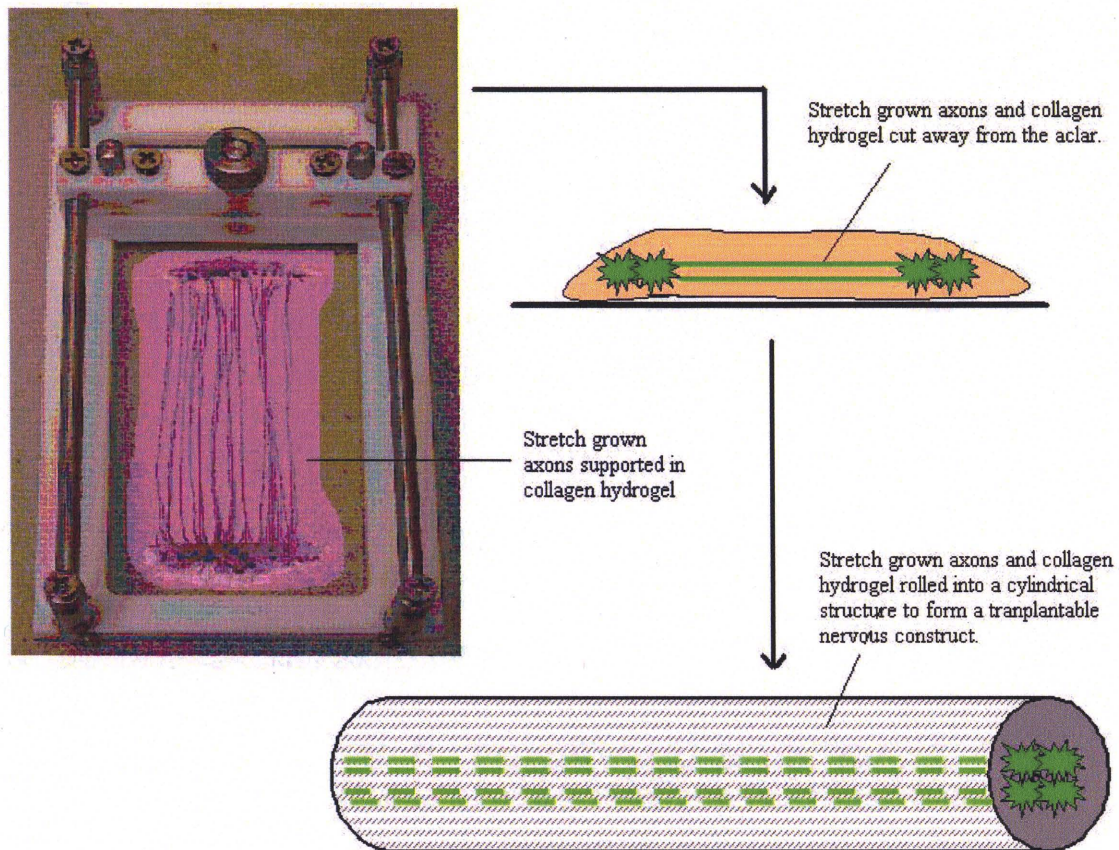
Figure 1.10 Formation of a nervous tissue construct spanned by stretch grown axons [7].

While the uni-axial axon growth achieved with the above technique is fast and efficient there still remain a few limitations to this technique that may be solved by three-dimensional (3D) axon stretch growth. Currently, the 2D axon stretch growth procedure is optimized and the stretch-growing axons from DRG cultures are at maximal density. In the current approach, axonal growth occurs in a two-dimensional (2D) plane, limiting the uniform distribution of DRG explants along the substrate interface and the number of axons that cross the interface. A higher density of neurons may yield a larger number of axon tracts available for stretch growth.

In order to form the nervous construct, the stretched axons are supported in collagen hydrogel and rolled into a cylindrical structure, as discussed above. Therefore, it poses a challenge to transform a 2D structure into a 3D configuration to fit the confines of the rat spinal cord. This process works at the expense of proper mechanical stability required for re-constructive surgical procedures. The procedure of rolling also causes damage to the stretched axons. As such, stretch growth of 3D neuron cultures can be produced to form a nerve construct that matches the rat spinal cord diameter and have better mechanical properties for constructive surgery purposes. Thus, the focus of this thesis is on the design and development of a 3D axon stretch growth device that will allow "stretching" of axons in three-dimension cultures.

1.5 Three-dimensional Axon Stretch Growth Device

The research goal of this thesis is to increase the number and density of axons in the nerve construct available for transplantation. The construct designed should fit into the small confines of the rat spinal column and should be easily handled by the surgeons. In order to achieve the goal, this thesis focuses on the modification of the 2D elongator to accommodate 3D growth of neuronal cultures. Compared to the 2D setup where axons grow across a uni-axial plane of neural culture, the 3D cultures add depth to allow axons to grow in multiple planes at the same time thus increasing the number and density of axons being stretched. The modification to the 2D axon stretch growth device includes the design of the 3D components that fit in the existing stretching frame to accommodate

3D growth of neuronal cultures. The design of the 3D components and its essential parameters are presented in details in Chapter Two.

1.6 Summary

The functional elements of the spinal cord are highlighted in this chapter. The nature and properties of the spinal cord pose a challenge for axon regeneration in the spine, over long distances, leading to motor and sensory functional loss. The success of any regeneration therapy depends on reviving functional connections by improving axon tract regeneration in the spinal cord. This chapter discusses the advantages and the disadvantages of the various approaches to treat and repair SCI. The axon stretch growth device designed by Pfister et al presents a unique insight into repairing SCI. The concept of the method and the design of the axon stretch growth device are described in details in this chapter. Although the design is fast and efficient, the few limitation (as described earlier) can be resolved by axons stretched in 3D cultures. This thesis focuses on the design of the 3D modifications and testing the essential parameters to optimize the system. The following chapter presents the design and parameters of the 3D axon stretch growth device in details.

CHAPTER 2
DESIGN OF THREE-DIMENSION AXON STRETCH GROWTH DEVICE

2.1 Introduction

The design of the 2D axon stretch growth device has been described in details in Chapter 1. We hypothesize that the number and density of axons can be increased for use in the nerve construct by stretch growing axons in 3D cultures. The goal of this thesis is to modify the 2D axon stretch growth device to accommodate axon stretch in 3D cultures. For the success of the 3D system, it is important to consider the essential parameters of the design. This chapter, thus, presents the design of the 3D axon stretch growth design and highlights the vital parameters.

2.2 Overview of the Two-dimensional Axon Stretch Growth Device

The 2D axon stretch growth device allows axons, from dorsal root ganglion (DRG) neurons, to rapidly elongate to a desired length. Interconnecting axons between two cell cultures are towed by the stepwise application of external mechanical force by means of a stepper motor and controller. This 2D system has been described in details in Section 1.4.2. Figure 2.11 shows the setup for the existing 2D stretching frame having three individual lanes. Each lane consists of separate cultures of embryonic DRG neurons. When elongated in the bioreactor by the microstepper motor and controller, each lane of axons elongates the same length in a 2D fashion.
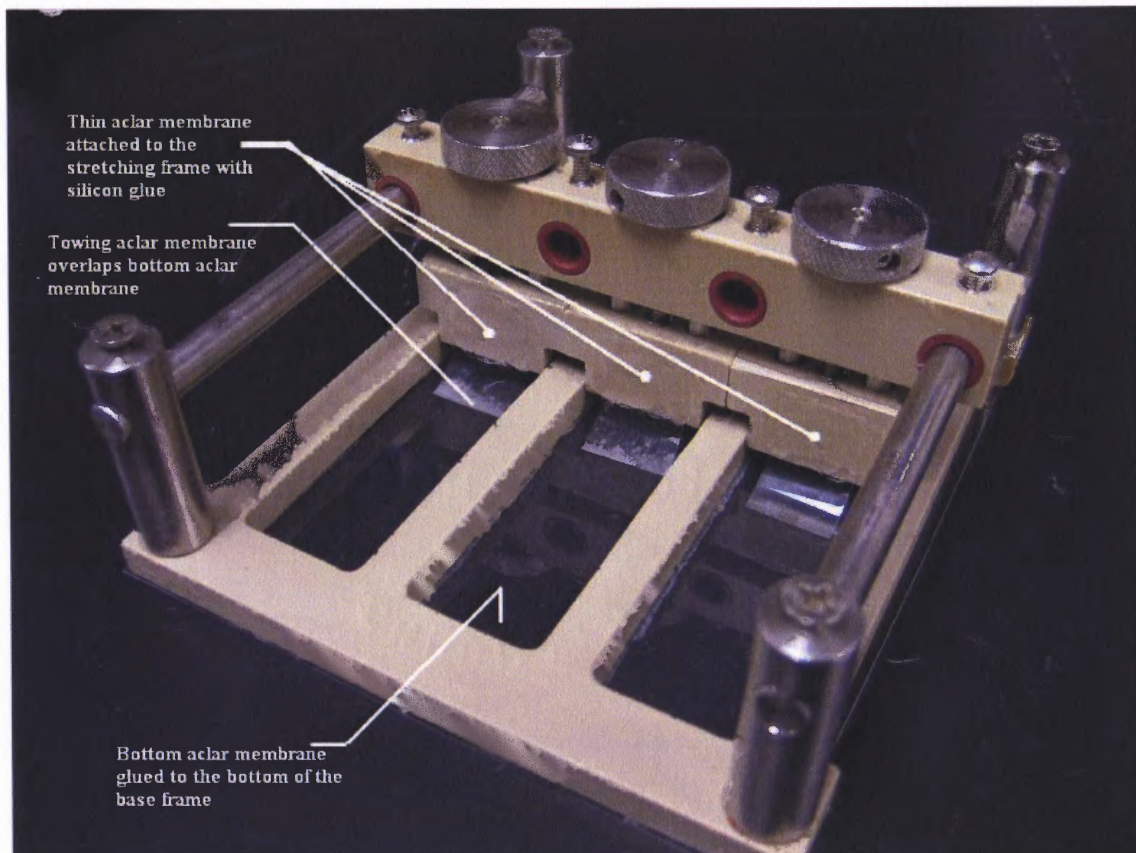
Figure 2.11 Setup of the 2D axon stretch growth device. Each lane contains a towing Aclar membrane attached to the stretching frame.

Uni-axial axonal growth in two-dimensions is fast and efficient. Currently, axon stretch growth in 2D is maximized and the DRG cultures are at maximal density. Increasing the number and density of axons, however, is required to optimize the final nerve construct formed by the stretched axons. We propose that axons stretched in 3D cultures will allow the DRG explants to be distributed more uniformly. In addition, the 3D cultures will add depth to the culture to allow axons to cross the interface in multiple planes.

As discussed earlier, the stretched axons in the 2D system are supported in collagen hydrogel and rolled into a cylindrical structure to form a 3D construct, at the

expense of proper mechanical stability for surgical purposes. Specifically, the extensive manipulation of axons in culture increases the potential of damaging the nervous tissue. The 3D cultures can solve this limitation as the final 3D culture can be matched to the geometrical confines of the rat spinal cord and thus eliminates the need to roll the 2D culture into a 3D construct. The mechanical properties of the 3D construct formed can be varied by forming a stiff hydrogel around the stretch grown axons just prior to transplantation. This Chapter thus, focuses on the design and development of the modifications made to create a 3D axon stretch growth device.

2.3 Development of the 3D Axon Stretch Growth Device

The goal of the 3D axon stretch growth device is to increase the density and total number of axons and form an effective transplantable nerve construct. However, in order to fulfill this requirement, the number of axons available for stretch growth must be increased first. The design considerations for the 3D modifications are described below:

1. *Accommodating axon growth in multiple planes*: The new 3D axon stretch growth design allows for axons to grow in multiple planes at the same time, by adding depth to the culture. The depth is added by incorporating cultures of neurons in a collagen hydrogel. Figure 2.12 illustrates the concept of axon stretch growth in multiple planes.

2. *Separation of two cultures*: Similar to the 2D setup, the 3D design requires a stationary and towing population of neurons, allowing axons to grow in-between. Thus the 3D cultures are contained in two halves.

3. *Physical barrier to constraint each half of the 3D cultures*: Since the 2D setup enables axon outgrowth in a single plane there is no need of a physical barrier to separate the cultures except for the two substrates (done by the overlapping Aclar membranes). However, because the 3D cultures consist of multiple layers of explants it is important to physically separate the two cultures yet preserve the axon outgrowth from one population of the neural culture into the other. Thus, unlike the 2D approach, a 3D culture has a thickness that must be split, hence creating a challenge to constrain each half. To accomplish this, the new design requires a physical separator for the collagen hydrogels and securing each halve of the culture at the stretching ends.
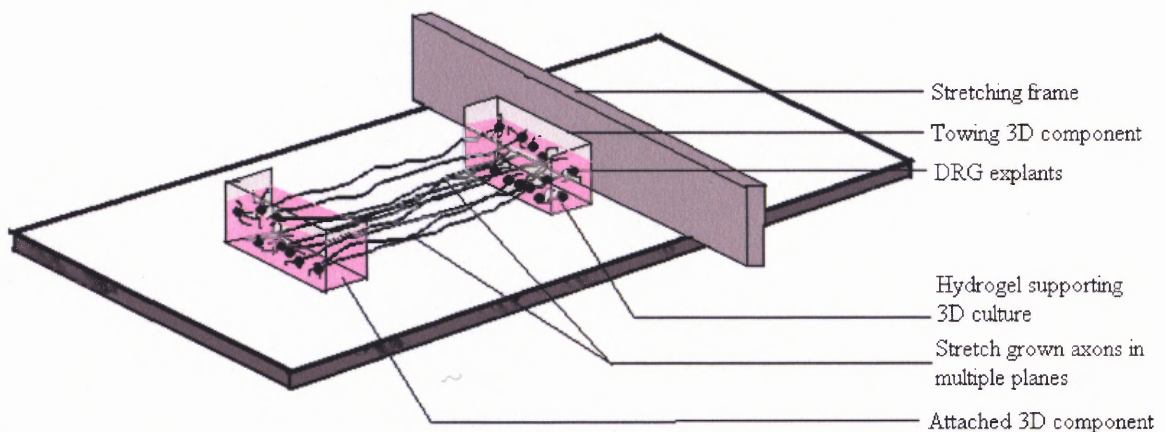
Figure 2.12 Schematic of 3D axon stretch growth mechanism.

2.4 Design Parameters of the 3D Axon Stretch Growth Device

The design of the 3D axon stretch growth device consists of two individual components designed to fit within each lane of the existing stretching frame. These components serve as a culture well to constrain the 3D cultures and to separate them into two halves during

elongation. One of the 3D components is kept stationary and the other component is allowed to move. Hence, the components are named as attached and towing component, respectively. The attached 3D component is fixed to the base frame and the towing component is fixed to the stretching frame. The components are shown in Figure 2.13, Figure 2.15 and Figure 2.17.

A Nylon mesh acts as the physical barrier separating, splitting and constraining the cultures in each component as shown in Figure 2.15 and Figure 2.17. A collagen hydrogel is used to create a 3D culture in which the rat DRG explants are suspended and grown. The two components are aligned together and the hydrogel and DRGs are plated within the two halves. In order for the 3D design to be a success it is important to discuss the essential parameters which are: (1) Dimension of the attached and towing components, (2) Choice of hydrogel and (3) Nylon mesh pore size. The following sections discuss the above criteria in further details.

2.4.1 Dimensions of the 3D Components

The 3D components are modifications of the 2D system. As such, the dimensions play an important role to make the 3D components and the existing 2D frame function as a single unit. Each of the important dimensions are discussed below:

1. The width of each component, w, (Figure 2.15 and Figure 2.17) matches the width of each lane, providing maximum surface area for DRG explants to distribute uniformly.

2. The depth of each component, d, (Figure 2.15 and Figure 2.17) is kept minimal so that DRG explants are dispersed more towards the front end, closer to the

mesh at the front. This enables axons to grow efficiently across the mesh to the population of neurons on the other half of the 3D culture.

3. The height of the components, h, (Figure 2.15 and Figure 2.17) is kept 2 mm higher that the height of the lanes of the stretching frame in order to hold the culture media inside each component, on top of the collagen hydrogel.

4. The thickness of the base of the components, t, (Figure 2.15 and Figure 2.17) is kept as minimal as possible in order to minimize the slag in the axons once stretched.
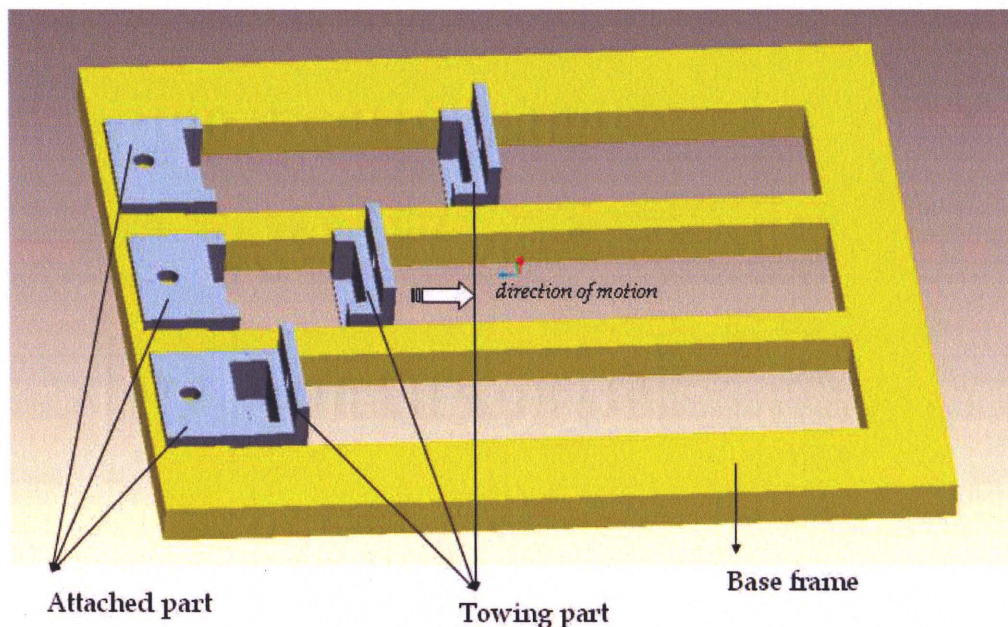
Figure 2.13 Schematic of the assembly of 3D components in the base frame.

The measurements of the components are given in Figure 2.15 (b) and Figure 2.17 (b). The 3D components are designed to fit the existing stretching frame. Thus, they act as additional attachments to the existing stretching frame requiring no alterations of the basic 2D setup. The assembly of the 3D setup includes gluing the attached 3D component to the base frame and the towing 3D component to the stretching frame with silicon glue

as illustrated in Figure 2.13 and Figure 2.23. The bottom Aclar membrane is glued to the base frame as like the 2D setup to hold and support the media and cultures. Like the 2D setup, the 3D setup can be easily autoclaved.
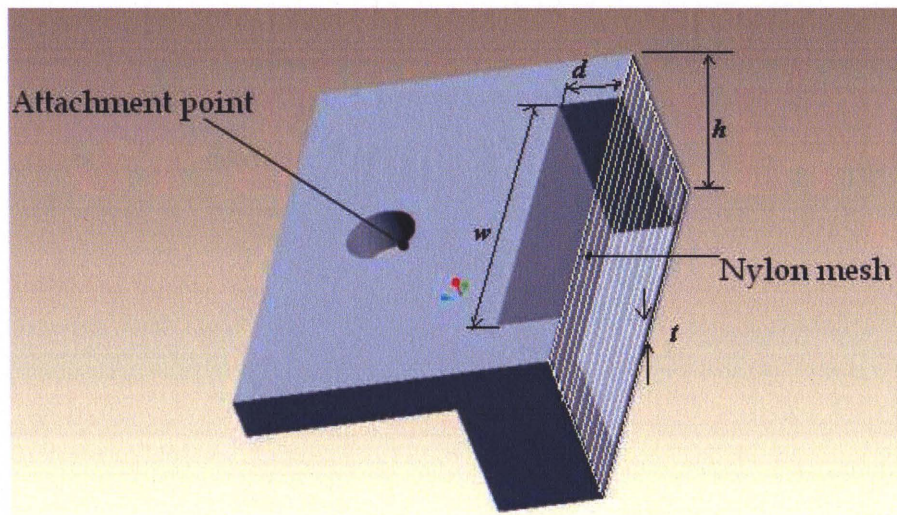
Figure 2.14 CAD drawing of the attached 3D component with Nylon mesh.
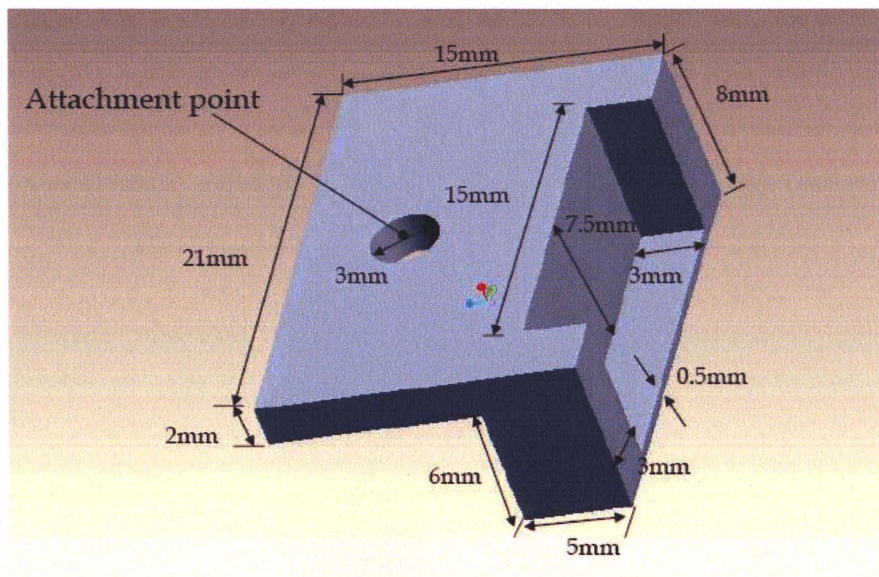
Figure 2.15 CAD drawing of the attached 3D component. Dimensions of the attached component.
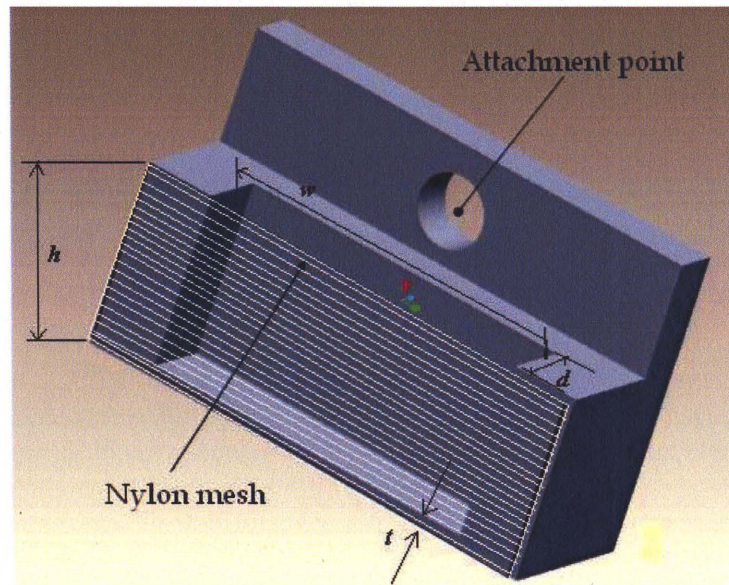
Figure 2.16 CAD drawing of the towing 3D component with Nylon mesh.
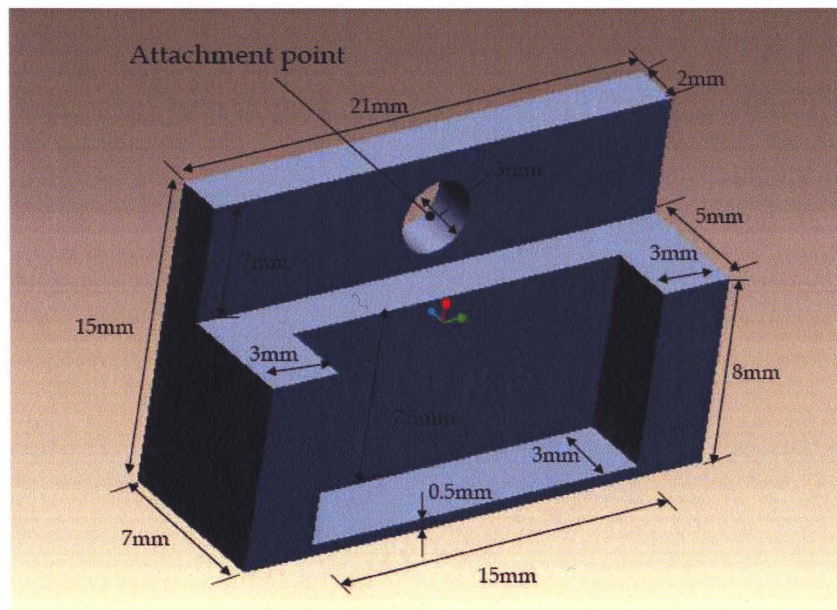
Figure 2.17 CAD drawing of the towing 3D component. Dimensions of the towing component.

2.4.2 Choice of Collagen Hydrogel for 3D Culture

Collagen based hydrogel forms the base of the 3D culture. The functions and the purpose of the hydrogel are to support the DRG explants, provide nourishment and hold the 3D cultures in place inside each component. It also acts as an extracellular matrix, encouraging axon outgrowth and uniform distribution of DRG explants throughout the culture. The hydrogel, thus, determines (1) the rate of axon outgrowth and (2) the mechanical stability. The rate of axon outgrowth, in turn, determines the time point as to start elongation after the axons have fully grown across the mesh into either side of the cultures. The mechanical stability determines the structural solidity of the 3D cultures inside the components. The goal is to obtain the most compatible hydrogel that would promote axon growth in between the two populations of DRG explants in each component and at the same time provide adequate stiffness for separating the two 3D cultures.

Lower concentration gels (0.6 mg/mL to 0.8 mg/mL) have shown to provide optimal axon outgrowth in length and rate of growth, compared to higher concentration gels (2 mg/mL to 3.2 mg/mL) [61]. However, higher concentration gels are stiffer and provide more mechanical support and structure.

In this thesis work, the above concentrations of gels are tested inside each component. Experiments have been carried out to ensure that hydrogels do not leak out through the pores of the Nylon mesh. This is important to ensure that the DRG explants stay in place inside each component and the 3D cultures stay separated. Details of the experiments are described in details in Chapter 3.

2.4.3 Nylon Mesh Pore Size

The purpose of the Nylon mesh is to act as a physical separator of the two 3D neuron cultures in each component. The pore size of the Nylon mesh, thus, plays a crucial role in holding and separating the hydrogels and allowing axon growth. Nylon meshes with different pore sizes are chosen to determine the effect of pore size on axon outgrowth and the ability to constraint the hydrogel inside each component. Here, the Nylon meshes of two pore sizes are considered: (1) *medium* pore size (30 x 30 treads per inch or 160 μm x 160 μm) and (2) *fine* pore size (104 x 104 treads per inch or 50 μm x 50 μm). Figure 2.17 shows the Nylon mesh of different pore sizes used for the design, under 4X magnification.

(a)   (b)
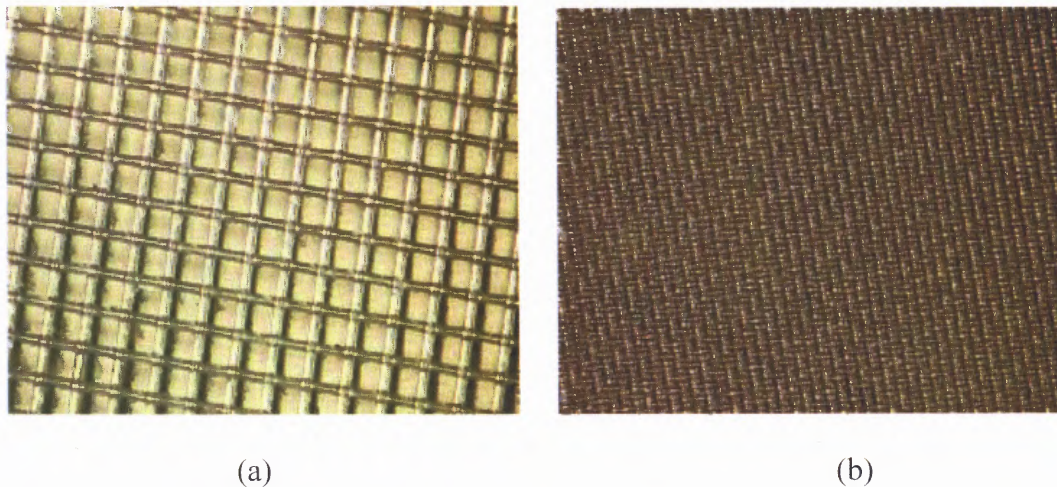
Figure 2.18 Nylon mesh pore size at 4X magnification. (a) medium pore size (160 μm x 160 μm) (b) fine pore size (50 μm x 50 μm).

The bigger the pore size of the mesh the more the tendency of the collagen hydrogel to leak out from each component and DRG explants along with it. In such a case the 3D cultures would no longer be separated by the mesh which may lead to uneven distribution of DRG explants. The bigger pore size, however, would allow more axons to

grow through the mesh because the pore sizes are much bigger than the axons posing fewer barriers for axon growth. Alternately, the smaller pore size allows less number of axons to pass through the mesh.

Thus, the Nylon mesh plays a crucial role in axon out growth. Experiments carried out to optimize the 3D design using the Nylon mesh as one of the major components is described in details in the following chapter

2.5 Setup of the 3D Axon Stretch Growth Device

The above 3D components have been built and machined by John Hoinowski, Lab Supervisor of the Biomedical Engineering Department at the New Jersey Institute of Technology. The design of the 3D components is created to scale using Computer Aided Design (CAD) Software. The components are constructed of Polyetheretherketone (PEEK) plastic because it is autoclavable and biocompatible with neuronal cultures. It also allows the hydrogel to slip out for transplantation after stretch growth. The Nylon mesh of fine and medium pore sizes is obtained from McMaster Carr. Figure 2.19 is the images of the attached component with the "*medium*" pore size Nylon mesh. The towing component with the "*medium*" pore size Nylon mesh is shown in Figure 2.20. The alignment of the two components again each other is seen in Figure 2.21.
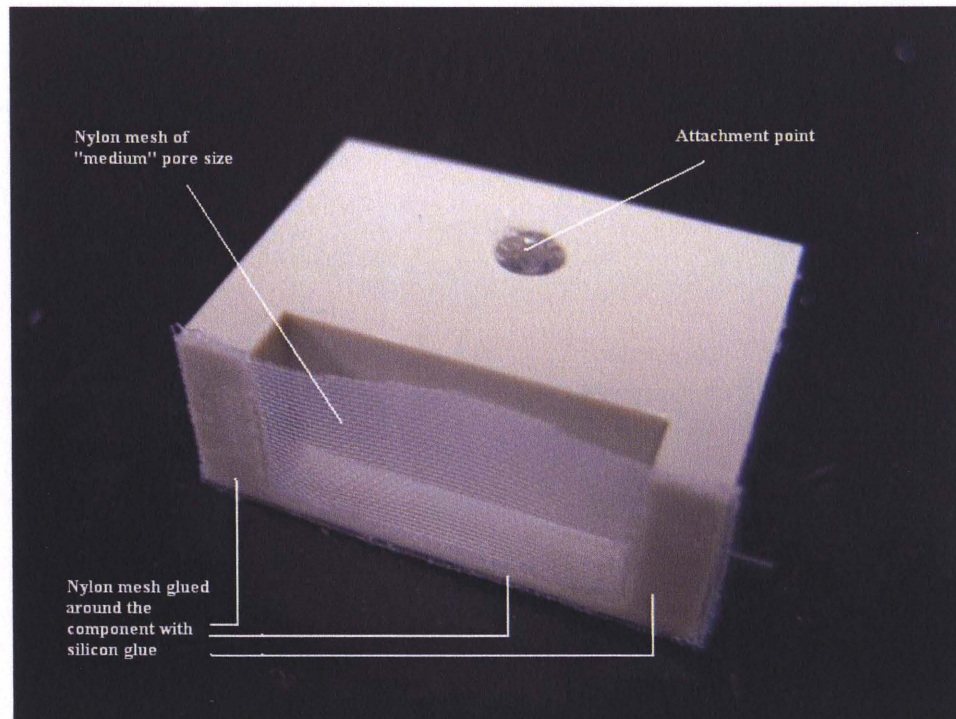
Figure 2.19 Attached component for the 3D design.
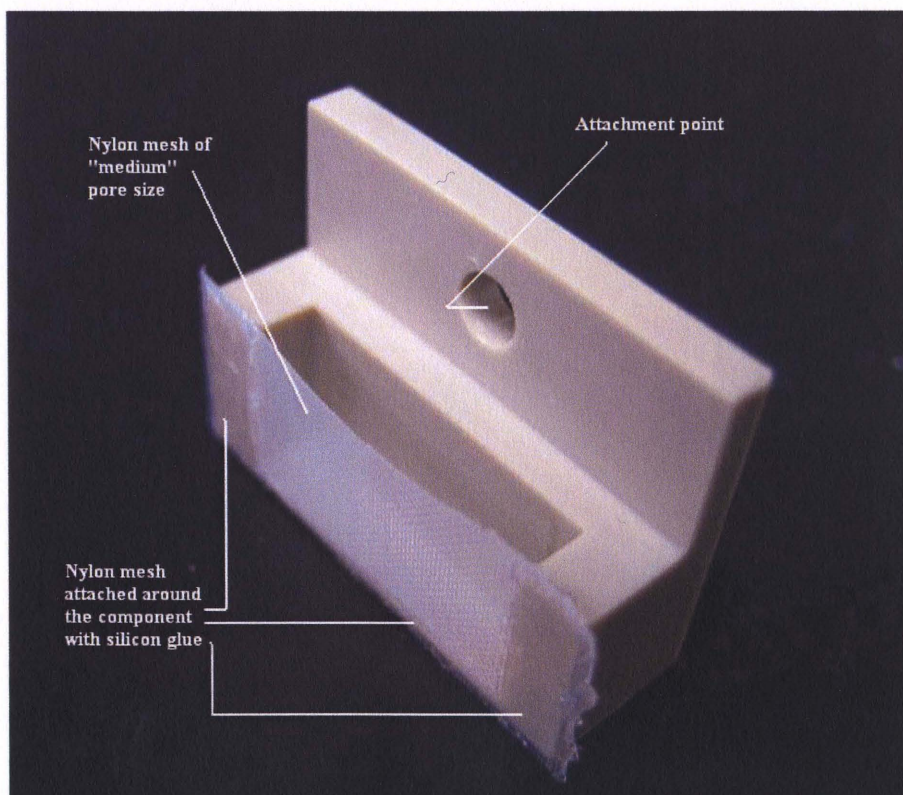
Figure 2.20 Towing component for the 3D design.
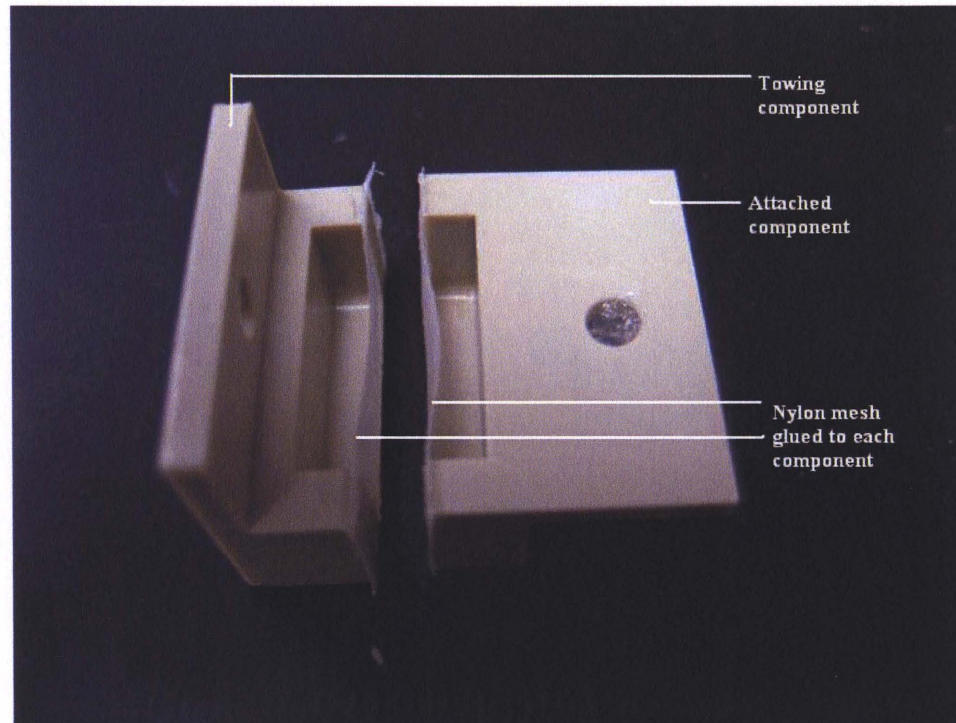
Figure 2.21 Alignment of the attached and the towing component for the 3D design.

The setup of the 3D device is shown and explained in Figure 2.23. The 3D axon stretch growth device moves in a linear fashion in each lane. Figure 2.23 (a) shows the 3D components aligned against each other. At this position the 3D cultures in each component is in direct contact with each other allowing the axons from one half of the culture to grow into the other half through the double Nylon mesh. Figure 2.23 (b) shows that as elongation starts, the 3D components gradually separate from each other. Figure 2.23 (c) shows the 3D components further apart as elongation continues.
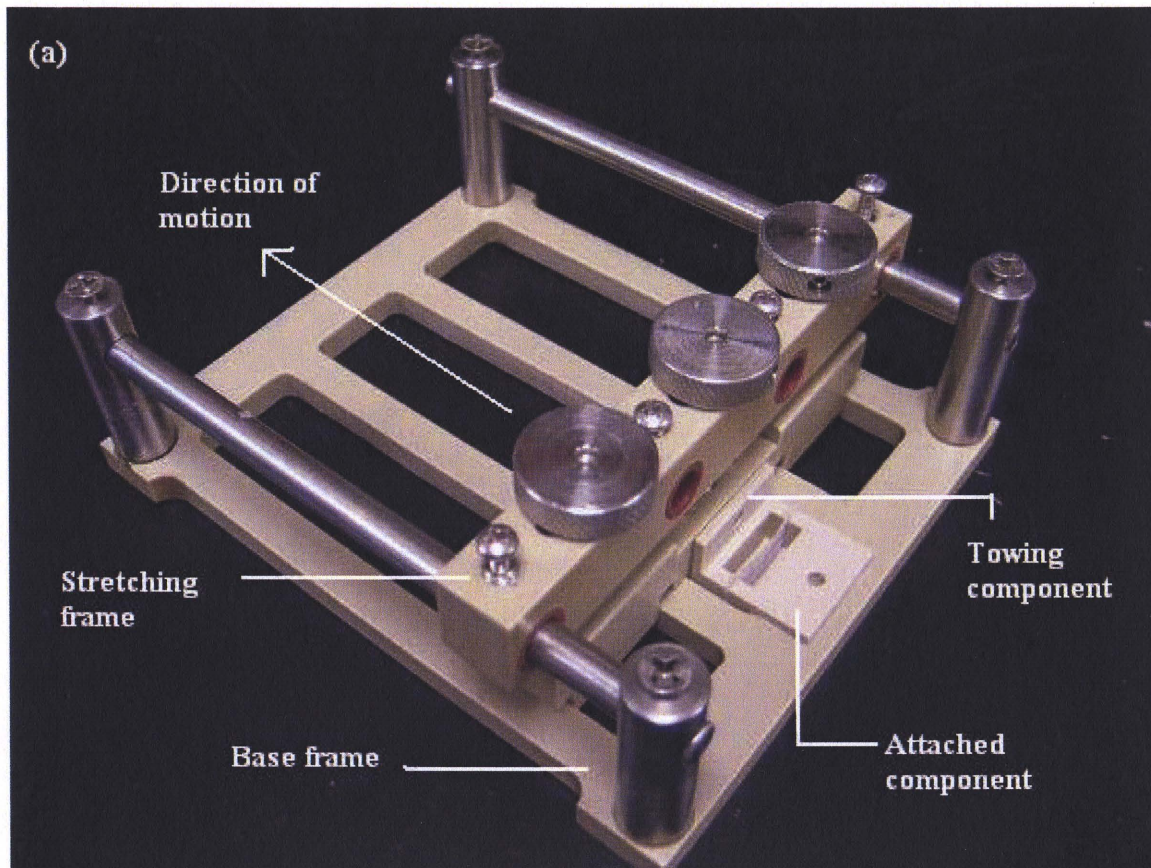
Figure 2.22 Assembly of the 3D Axon Stretch Growth Device. The two 3D components are perfectly aligned against each other in the lane of the base frame. The attached component is glued to the base frame with silicon glue and the towing component similarly glued to the stretching frame. The components contain the collagen hydrogel that forms the base of the 3D culture for the neurons. The 3D cultures are together when the two components are aligned against each. This allows the two Nylon mesh to be in contact and allows the axons to grow through the mesh into each of the adjacent 3D cultures.
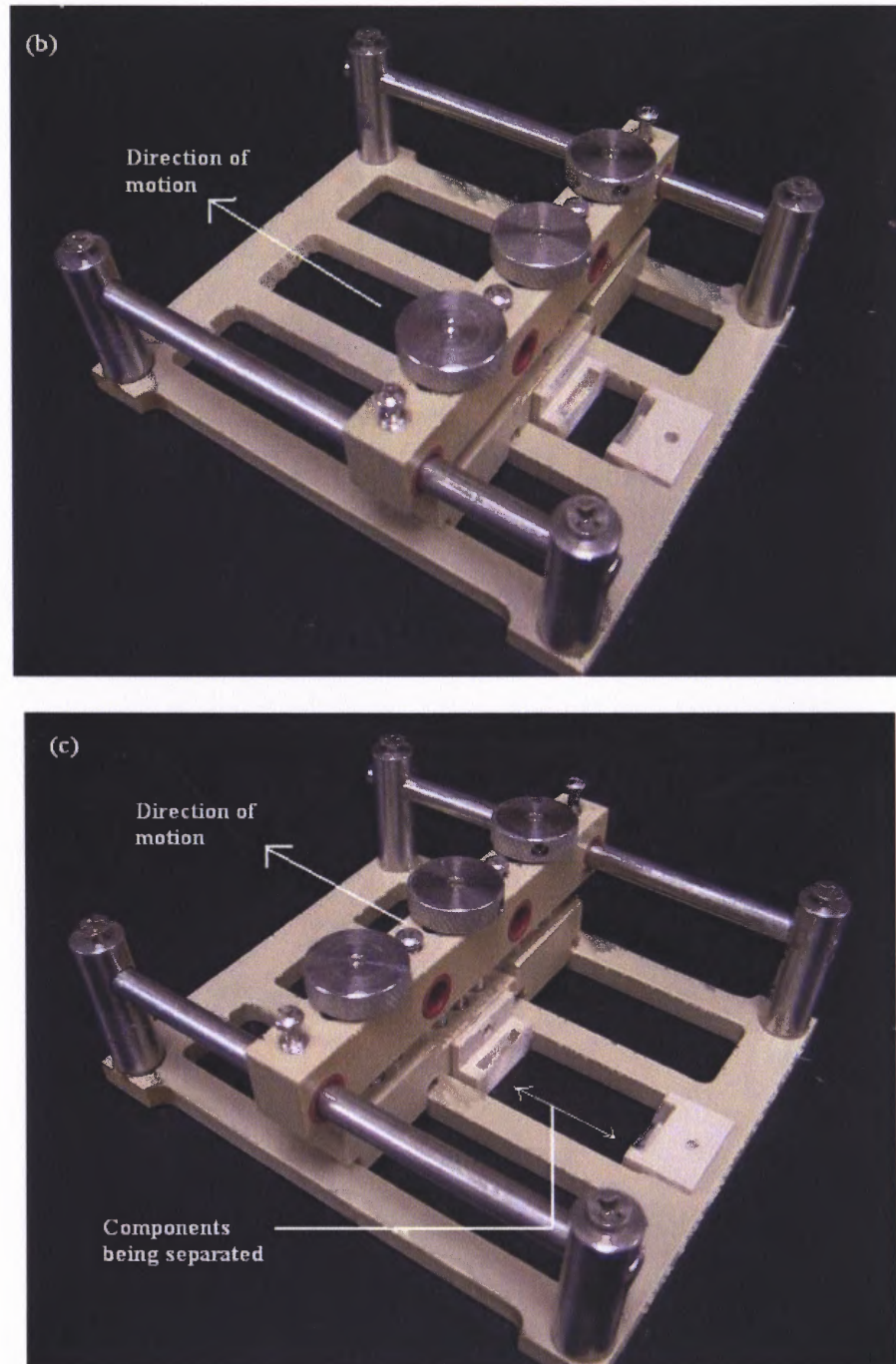
Figure 2.23 Assembly of the 3D Axon Stretch Growth Device. As the stretching frame moves uni-directionally, the attached and the towing components are separated. The 3D design mimics the concept of the 2D design, separating a population of neurons suspended in hydrogel inside each of the component and stretching the axons that grow inbetween each culture. (b) stretching begins (c) stretching continues.

2.6 Summary

The design of the 3D axon stretch growth device has been described in details in this chapter. The essential parameters of the design have been summarized and the importance of the parameters have been highlighted in the above sections. The 3D system has been built and it is seen to fit the existing frame of the 2D system. Experiments carried out to optimize the design parameters are explained in the following chapter. The next chapter also describes the experimental protocol for the 3D device and the results obtained.

CHAPTER 3

EXPERIMENTAL PROTOCOL AND RESULTS

3.1 Introduction

The design of the 3D axon stretch growth device has been discussed in Chapter 2. The essential parameters to accomplish axon stretch growth of 3D cultures are: (1) the dimension of the attached component and the towing component, (2) the choice of hydrogel, and (3) the pore size of the Nylon mesh. The attached and towing components are made to the specifications discussed in the previous chapter. These components have been easily assembled into the existing axon stretch growth bioreactor and visual alignment is achieved as shown in Figure 2.21 and Figure 2.23. This modified system has been used to identify the optimal hydrogel and Nylon mesh pore size for 3D stretch growth. Cultures of rat embryonic dorsal root ganglia (DRG) neurons are used in all experiments. This chapter focuses on the description of the experimental setup to test the parameters and the results obtained are described in Section 3.2. The chapter also provides the experimental protocol for the 3D axon stretch growth device and explains the observations in Section 3.3.

3.2 Experimental Set-up of Essential Parameters and Observations

3.2.1 Determination of Optimal Hydrogel

A hydrogel, made from type 1 collagen from rat tail, is used to physically suspend DRG neurons in a 3D culture. The mechanical properties of the collagen hydrogel can be easily adjusted by varying the concentration of collagen in the hydrogel. The preferred protein for DRG neurons is collagen because it supports DRG growth in both 2D and 3D culture conditions. Type 1 collagen has been shown to not cause an adverse reaction when implanted *in vivo* because it is highly biocompatible and thus, supports cell migration, proliferation, cell adherence, and cell differentiation. Collagen, being natural, does not cause an adverse reaction when implanted *in vivo* and does not degrade into toxic components inside the body [61].

The purpose of the hydrogel is to provide an extracellular matrix like scaffold for 3D culture. The hydrogel confines the DRG explants in 3D, holds the 3D cultures in place inside each component of the axon stretch growth system, and supports DRG axon growth throughout the gel. The goal is to identify the optimal properties of the hydrogel that will (1) allow rapid axon outgrowth to bridge the two populations of DRG explants within each component and (2) provide adequate stiffness to hold the cultures in place during separation of the 3D culture

Lower concentration collagen hydrogels (0.6 – 0.8 mg/mL) are less stiff compared to the hydrogels having a higher concentration (2.0 – 4.0 mg/mL) of collagen. While stiffer gels are easier to work with and manipulate, lower concentration gels allow for more rapid axon outgrowth than the higher concentration gels [61]. In order to achieve optimal axon outgrowth and mechanical stability for the 3D design, in this work,

collagen concentrations of 0.8 mg/mL, 2.0 mg/mL and 3.2 mg/mL are tested for each of the 3D components. The experimental set-up and the observations are discussed below.

Collagen hydrogel is made according to the standard protocol of Pfister et al [13]. Each 3D component of the axon stretch growth device can hold upto 250 μL of hydrogel. In total, 500 μL of hydrogel solutions of 0.8 mg/mL, 2.0 mg/mL and 3.2 mg/mL collagen hydrogel is made from measured amounts of 10X MEM, sterilized cell culture water, 1M concentration of NaOH, and collagen stock solution obtained from Becton, Dickinson and Company (BD). All the ingredients are mixed in specific proportions on ice to prevent the hydrogel from polymerizing. The ingredients and proportions to make 500 μL of collagen hydrogel is given in Table 3.1. While the hydrogel mixture is still in the liquid state, 250 μL of the solution is pipetted in each of the 3D components.

Table 3.1 Proportion of Ingredients for Collagen Hydrogel

500 μL of collagen hydrogel	0.8 mg/mL	2.0 mg/mL	3.2 mg/mL
10 X MEM	50 μL	50 μL	50 μL
Sterilized Water	348.5 μL	196 μL	44 μL
1M NaOH	6 μL	10 μL	11 μL
Collagen stock solution (4.0 mg/mL)	100 μL	250 μL	400 μL

Lower concentration collagen hydrogels require more time to polymerize and are less viscous compared to higher concentration gels. For this design, the hydrogel must adhere to the Nylon mesh without leaking out before polymerizing. Each hydrogel concentration is examined and monitored to see if the hydrogel solutions seep out

through the Nylon mesh during the course of pipetting and polymerizing.
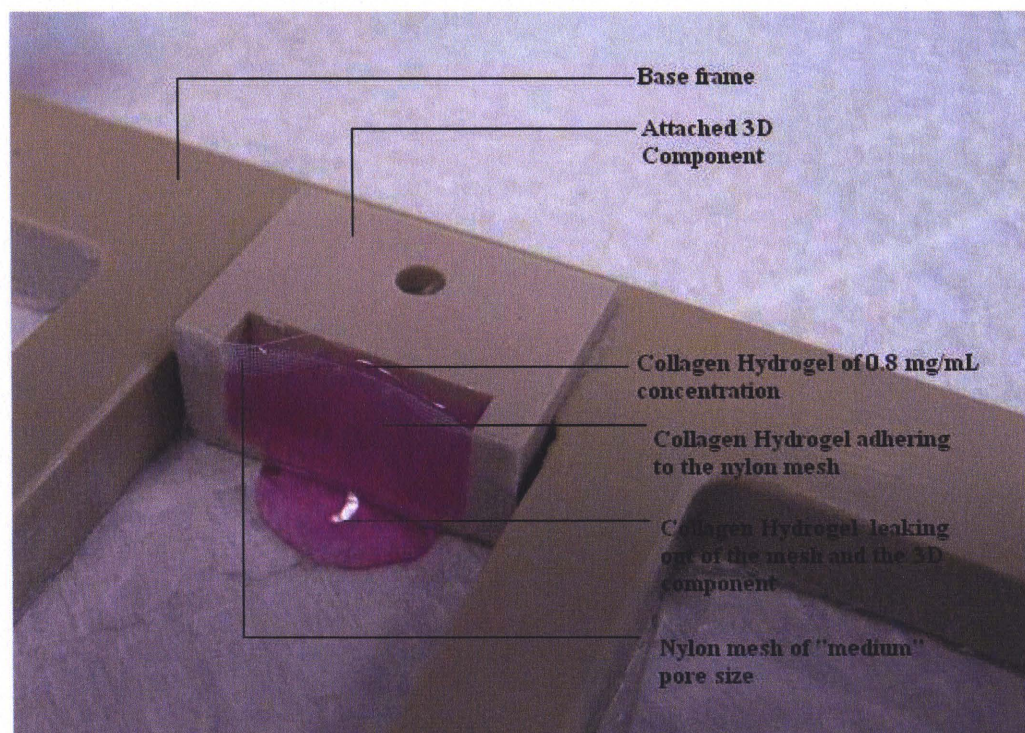
Figure 3.24 0.8 mg/mL concentration of collagen hydrogel is pipetted into the attached 3D component. It is seen that during polymerization, the hydrogel leaks out through the Nylon mesh of "*medium*" pore size.

Figure 3.24 shows 0.8 mg/mL collagen hydrogel solution inside the attached 3D component. During the course of polymerization, the hydrogel, being less viscous, is observed to leak out of the Nylon mesh. This shows that the lower concentration collagen hydrogel lacks the mechanical stability required for suspending and containing the DRG neurons inside the 3D components. If leak occurs, as shown in the figure, the two 3D cultures cannot be formed and the cultures will no longer be separate.

Figure 3.25 shows the hydrogel containing a higher concentration of collagen (2.0 mg/mL and 3.2 mg/mL). The higher concentration collagen hydrogels require less time to polymerize and the higher viscosity of the gel is observed to retain its structure inside each 3D component. As seen in the image, the hydrogel adheres to the mesh but does not

leak through. This allows the two 3D components to be in contact with each other and encourage axon outgrowth through the double layer of mesh, yet conserve the separation and the structural stability of the 3D cultures.
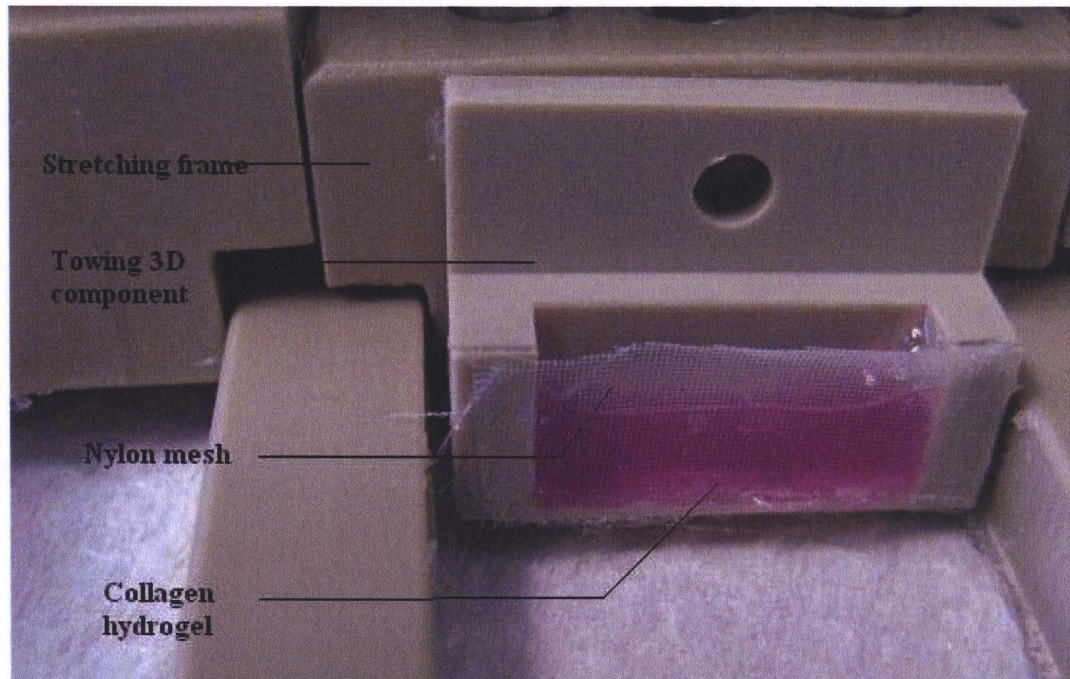
Figure 3.25 2.0 mg/mL and 3.2 mg/mL concentration of collagen hydrogel is pipetted into the towing 3D component. It is seen that the hydrogel retains is structure and does not leak out through the Nylon mesh of "*medium*" pore size.

From the above tests, it is concluded that higher concentration collagen hydrogel best suits the purpose for the 3D design, as it retains its structure inside each component. The collagen hydrogel is able to suspend the DRG neurons and provide adequate mechanical stability. Henceforth, the experiments conducted in the later sections involve the use of 2.0 mg/mL and 3.2 mg/mL concentration of collagen hydrogel.

3.2.2 Choice of Nylon Mesh Pore Size

The Nylon mesh acts as a physical separator of the two 3D neuron cultures in each component. The pore size of the Nylon mesh plays a crucial role in holding and separating the hydrogels and allowing axon growth. Nylon meshes with pore sizes of 30 x 30 treads per inch or 160 μm x 160 μm ("medium" pore size), and 104 x 104 treads per inch or 50 μm x 50 μm ("fine" pore size), are chosen so as to determine the effect of pore size on axon outgrowth. The bigger pore size allows more axons to grow through the mesh. The converse is true for the smaller pore size of the Nylon mesh. The outgrowth of axons will in turn determine the time point, i.e. time required to start the elongation process. This corresponds to the time when most axons have grown across each mesh into either half of the 3D culture. The experimental setup to test this parameter and the results obtained are discussed below.

To test the ability of axons to growth through the Nylon mesh, the experimental set up includes gluing a double layer of Nylon mesh in each well of a 24-well tissue culture plate. The double layer mimics the setup of the actual 3D components: one of the attached components and one of the towing components. In order for the axons to grow to either population, the axons have to grow through both layers of mesh.

In order to form the double layer, Nylon mesh of each pore size is cut to match the diameter of each well. To ensure that the double mesh is sturdy and vertically in place across each well, rectangular pieces of thin glass are glued on either side of the cut pieces of the Nylon mesh, as shown in Figure 3.26. Warped Nylon mesh inside the well cast shadows while imaging under the phase contrast microscope making it difficult to image

the axons that grow through the mesh. For this reason, the glass pieces help the Nylon mesh to be vertical.
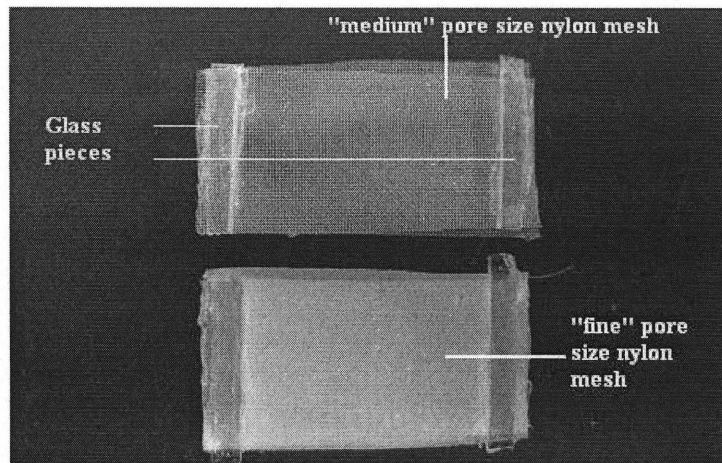
Figure 3.26 Double layer of Nylon mesh both "*medium*" and "*fine*" is secured with glass pieces on either side for more stability.
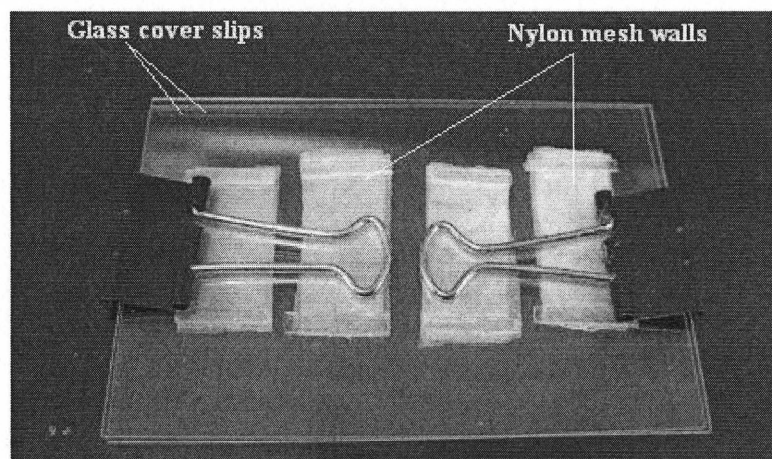
Figure 3.27 Nylon mesh walls secured in between two glass cover slips to prevent from warping during the sterilization procedure.

The Nylon mesh walls are then autoclaved in between two cover slip glasses secured together (Figure 3.27). This prevents the Nylon mesh walls from further warping once exposed to heat and pressure inside the autoclave. After sterilization, the Nylon mesh walls are glued on the inner walls of each well with silicon glue inside sterilized hood. The pieces of glass on the mesh walls also help to secure the glue firmly in position. Figure 3.28 shows the Nylon mesh walls glued inside each well. The 24-well plate is then let to dry inside the hood overnight.
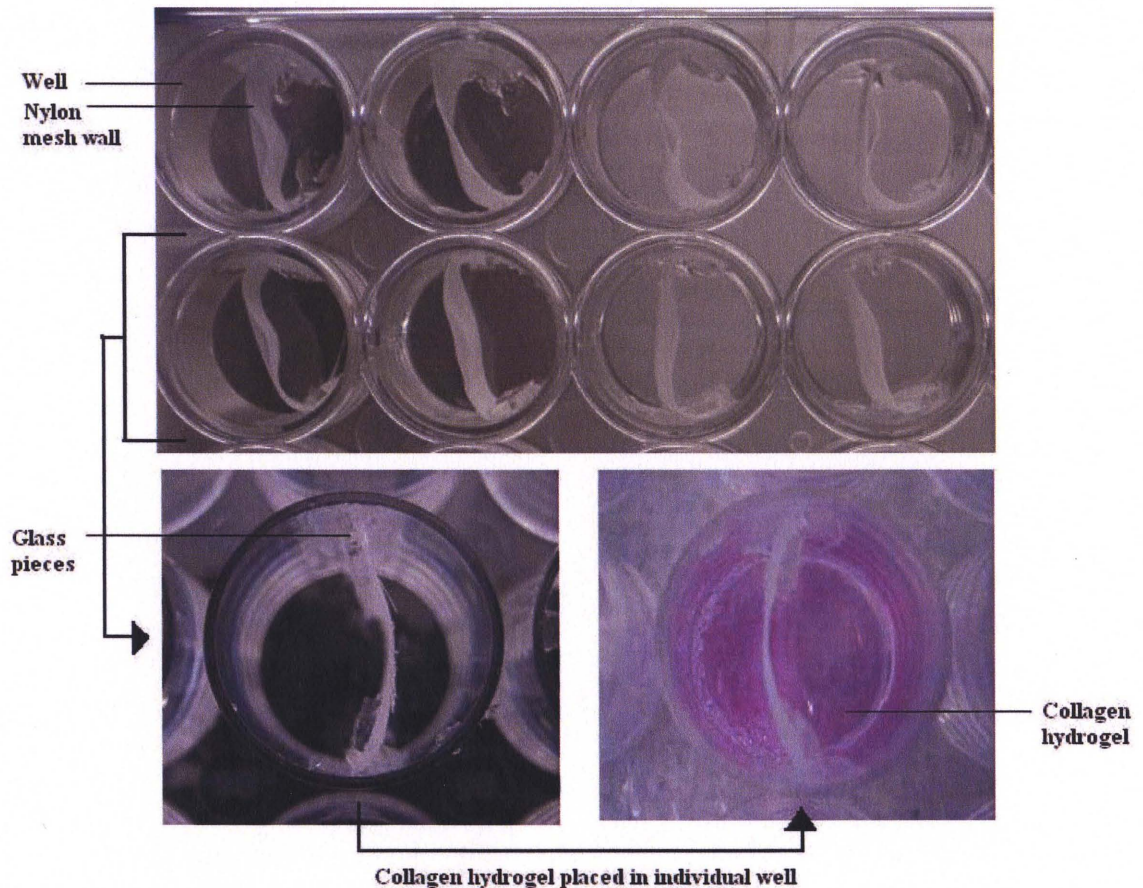
Figure 3.28 Nylon mesh walls are secured with silicon glue in each well of a 24-well plate cell culture dish. After the glue dries, collagen hydrogel is pipetted in each well.

Often the edges of the Nylon mesh walls are not even. This results in a gap between the bottom of the well and the bottom edge of the mesh wall. In such a case, when DRG explants are suspended in the hydrogel, axons can grow through the bottom gap and not through the Nylon mesh. This can result in erroneous data. In order to overcome this problem an initial layer of 500 μL collagen hydrogel is pipetted in each well. This allows the bottom gap to be filled with hydrogel. Once the hydrogel polymerizes, DRG explants are selectively plated on the layer, close to the Nylon mesh wall.
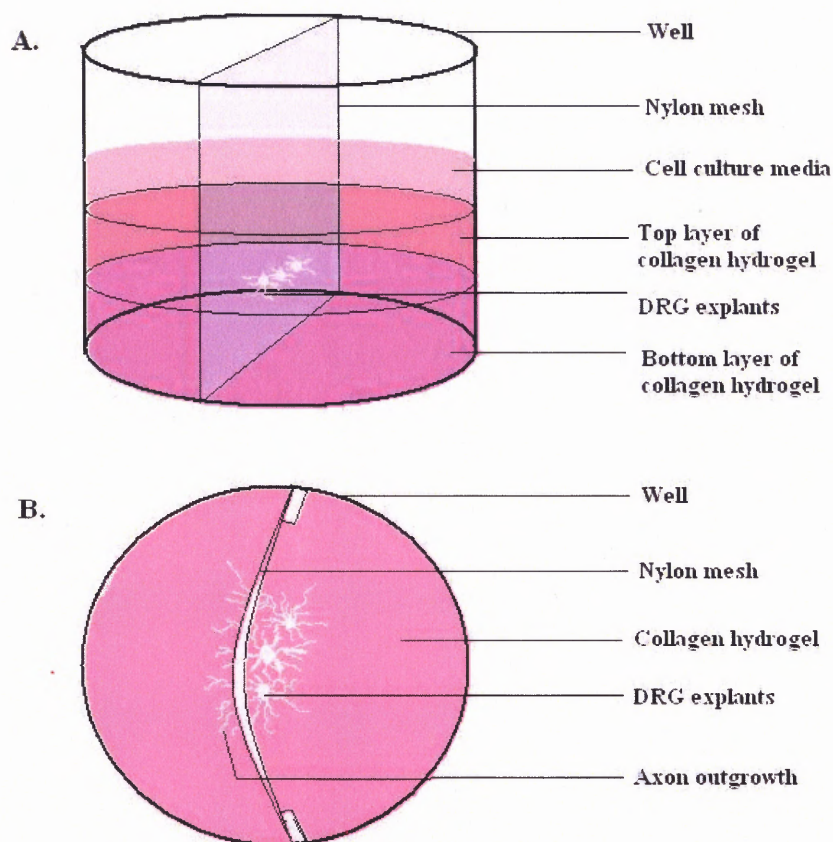
Figure 3.29 Schematic of the procedure of plating the DRG neurons in each well. (A) DRG explants are "sandwiched" in between two layers of collagen hydrogel. (B) Top view of the culture well.

Explants are plated only on one side of the mesh wall to make sure axons that do grow through the mesh are originated from the DRG neurons plated on the other side. This also helps minimize inconsistent data. Another 400 μL of hydrogel is pipetted on top of the DRG explants and allowed to polymerize. In this way the DRG are "sandwiched" in between two layers of hydrogel. Cell culture media is then placed in each well once the hydrogels have completely polymerized. The cultures are then incubated and axons are allowed to grow in culture. Figure 3.29 is a schematic of the procedure explained above.

Experiments are carried out using 2.0 mg/mL and 3.2 mg/mL collagen concentration hydrogel with both "*medium*" and "*fine*" pore size of Nylon mesh. The cell cultures in each well with the Nylon mesh are imaged using a Phase Contrast Light Microscope (PCLM). Phase contrast images are obtained for specific time points of 2 days, 5 days, 7 days, 9 days, 14 days and 21 days to observe the axon outgrowth behavior, and the time it takes for axons to grow across the double layer Nylon mesh of mentioned pore sizes. In this section, two samples of each case are imaged and discussed.

Figure 3.30 and Figure 3.31 (a) and (b) show the phase contrast images for the experimental setup with "*medium*" pore size Nylon mesh in 2.0 mg/mL collagen hydrogel. Figure 3.30 shows the axon outgrowth from the DRG explants at day 2. Axon outgrowth on day 2 is not sufficient to reach the Nylon mesh. However, on day 5 (Figure 3.31 (a)), axons are seen to just cross through the mesh, whereas on day 7 (Figure 3.31 (b)), the axon length, and number through the mesh, is more as compared to that on day 5.
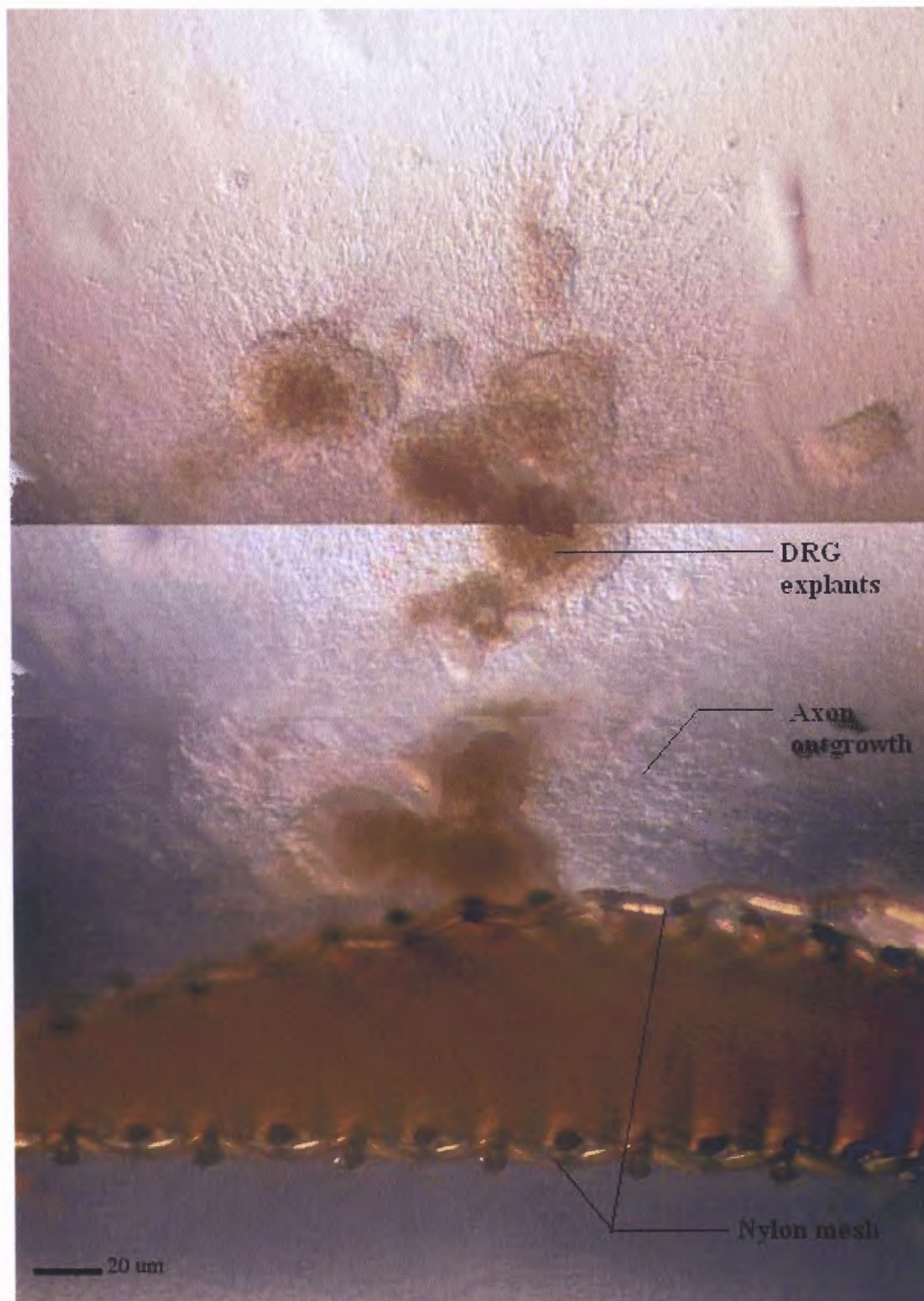
Figure 3.30 Day 2: DRG outgrowth through Nylon mesh of "*medium*" pore size in 2.0 mg/mL collagen concentration hydrogel.
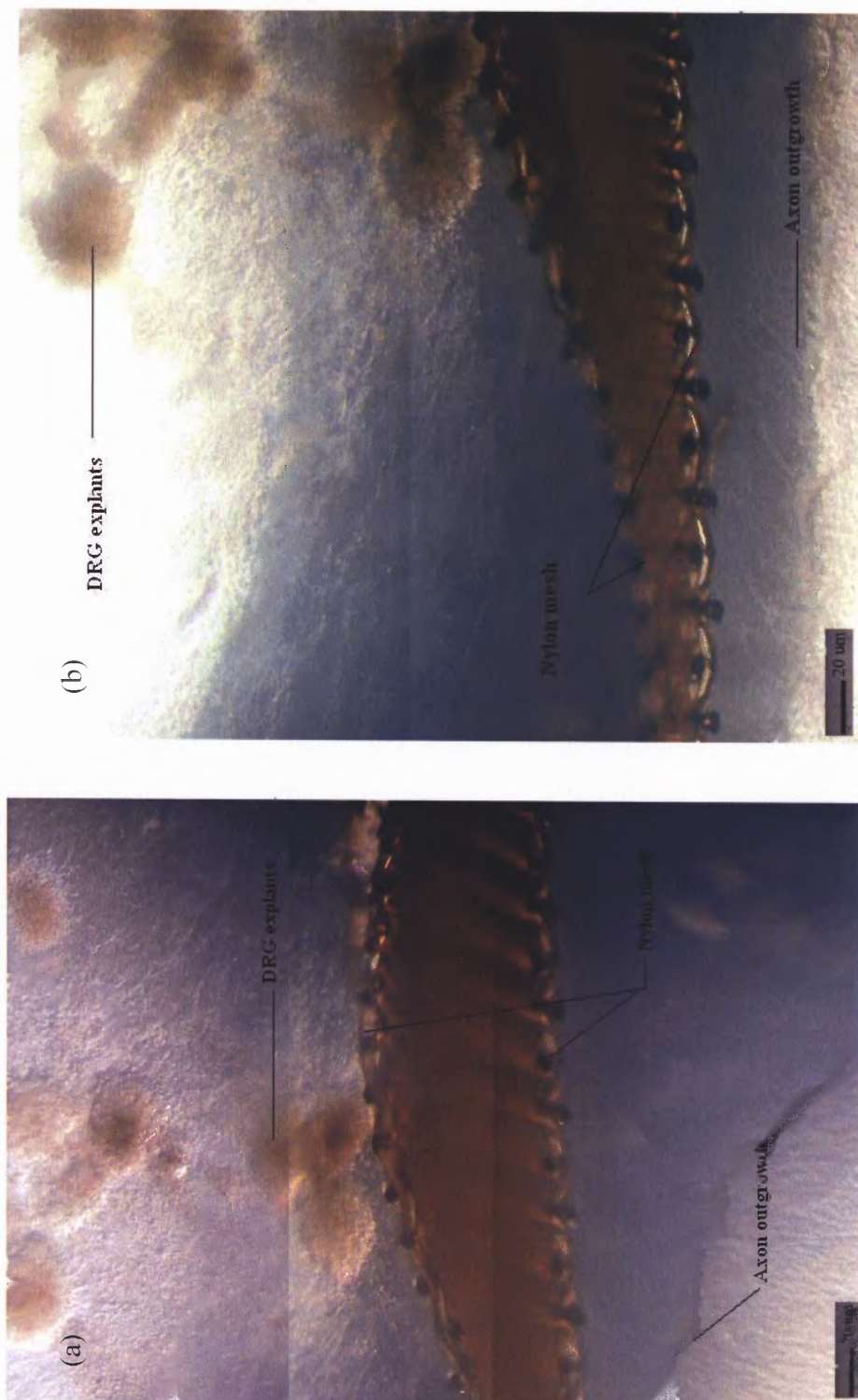
Figure 3.31 DRG outgrowth through Nylon mesh of "*medium*" pore size in 2.0 mg/mL collagen concentration hydrogel. (a) Day 5: few axons grow through the mesh (b) Day 7: number of axons growing through the mesh increase.

Figure 3.32 and Figure 3.33 (a) and (b) are the phase contrast images of the another experimental sample with "*medium*" pore size Nylon mesh and 2.0 mg/mL collagen hydrogel. Figure 3.32 shows the axon outgrowth from the DRG explants at day 2, which is not long enough to reach the Nylon mesh. On day 5 (Figure 3.33 (a)) axons do grow through the mesh and on day 7 (Figure 3.33 (b)) the axon length and number is more as compared to that on day 5.
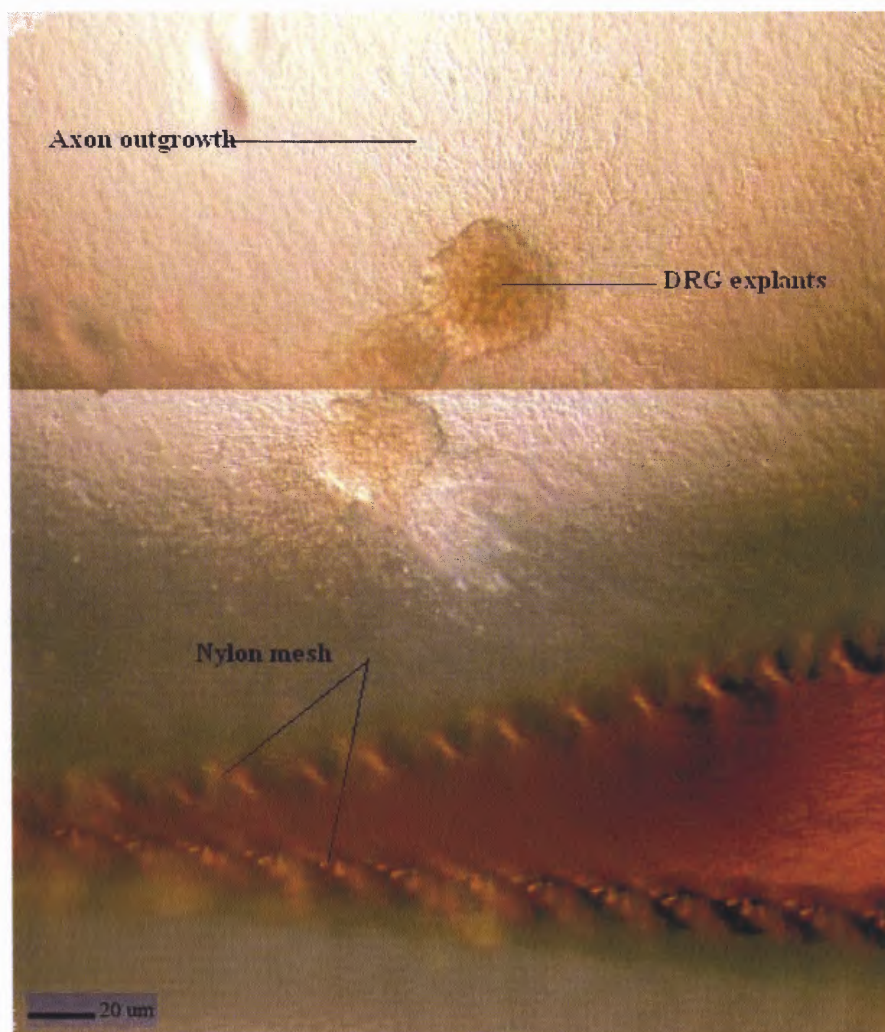
Figure 3.32 Day 2: DRG outgrowth through Nylon mesh of "*medium*" pore size in 2.0 mg/mL collagen concentration hydrogel.
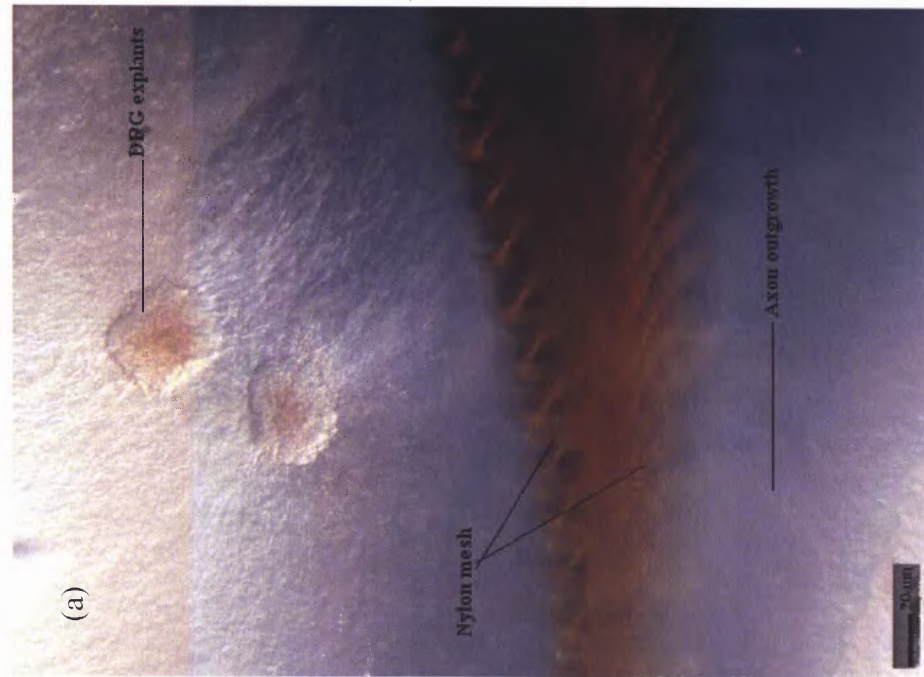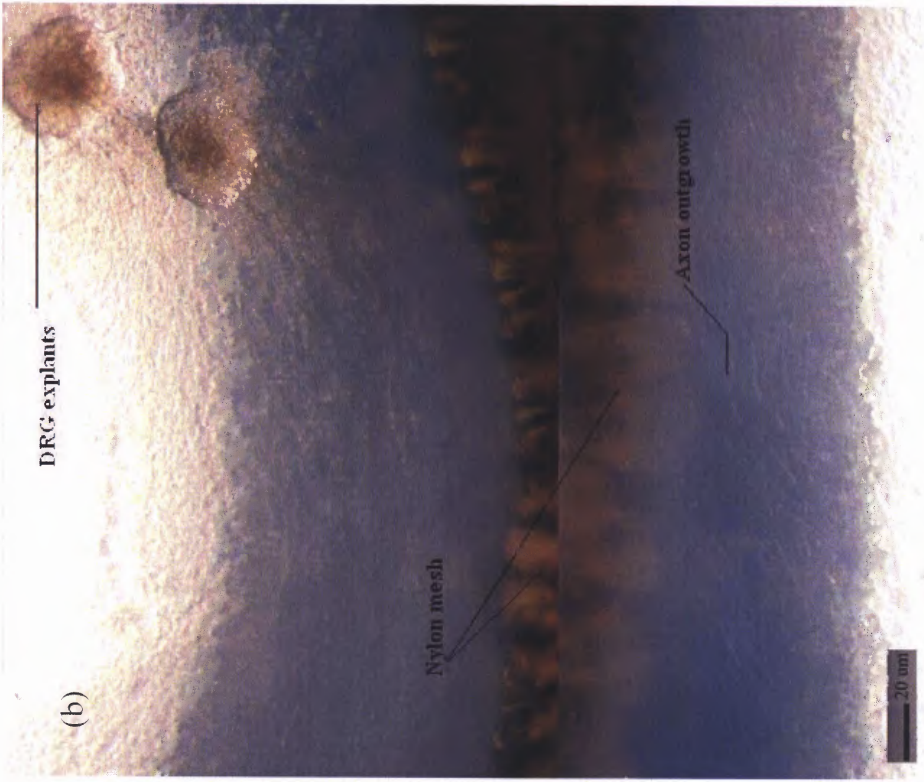
Figure 3.33 DRG outgrowth through Nylon mesh of "*medium*" pore size in 2.0 mg/mL collagen concentration hydrogel. (a) Day 5: few axons grow through the mesh (b) Day 7: number of axons growing through the mesh increase.

Figure 3.35, Figure 3.35 (a) and (b) and Figure 3.36 are the images of the first sample of experimental setup with "*medium*" pore size Nylon mesh and 3.2 mg/mL collagen hydrogel. In Figure 3.35 and Figure 3.35 (a) it is seen that on day 2 and on day 5, not many axons are seen to reach or grow through the Nylon mesh. The 3.2 mg/mL collagen hydrogel has a higher concentration of collagen and hence it is stiffer as compared to the 2.0 mg/mL collagen hydrogel hindering the rate of axonal outgrowth. When compared to the observations obtained from the experimental setup with 2.0 mg/mL collagen hydrogel, it is seen that axons require a longer amount of time to grow an equal length through the Nylon mesh, in the 3.2 mg/mL concentration of collagen hydrogel (Day 9 instead of Day 7). This is shown in Figure 3.36.
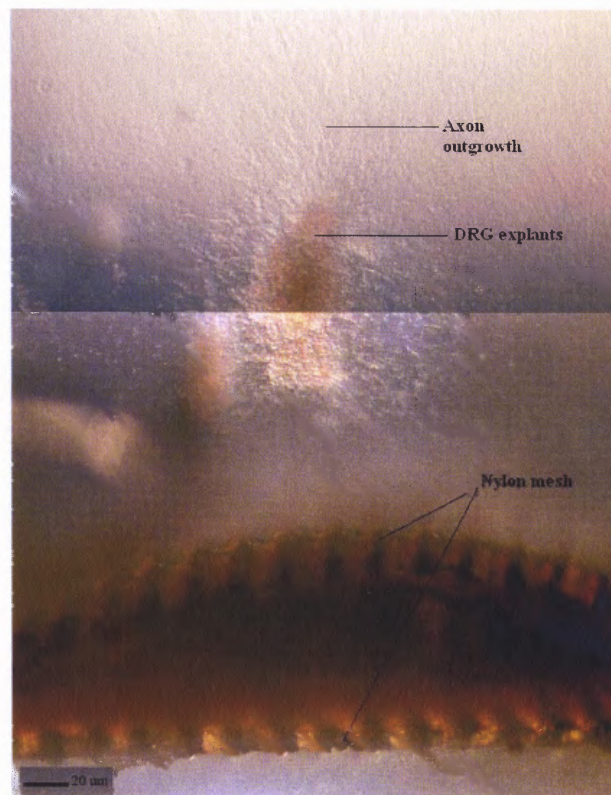
Figure 3.34 DRG outgrowth through Nylon mesh of "*medium*" pore size in 3.2 mg/mL collagen concentration hydrogel on Day 2.
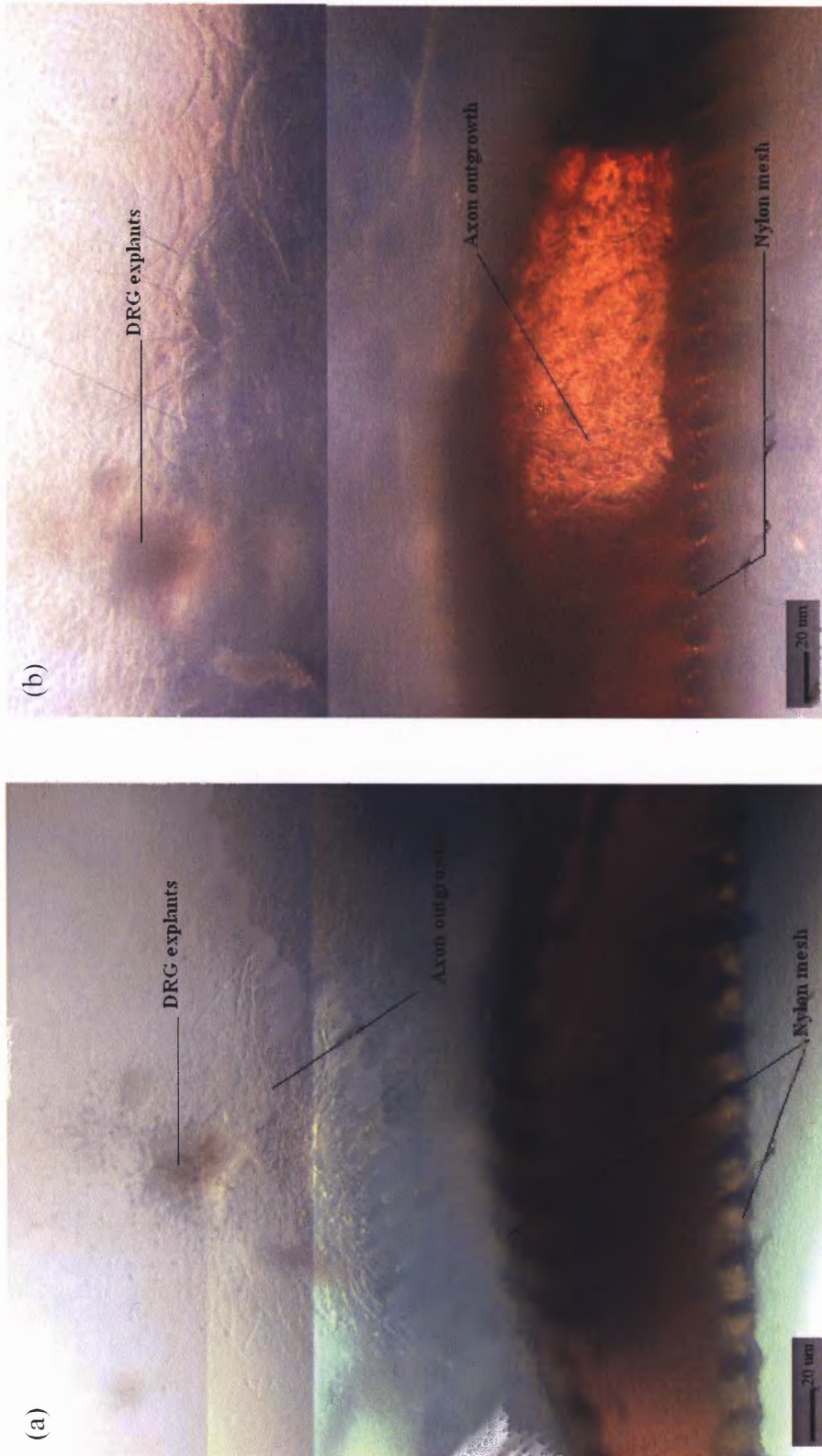
Figure 3.35 DRG outgrowth through Nylon mesh of "*medium*" pore size in 3.2 mg/mL collagen concentration hydrogel. (a) Day 2: axon outgrowth from DRG explants (b) Day 5: continued growth of axons.
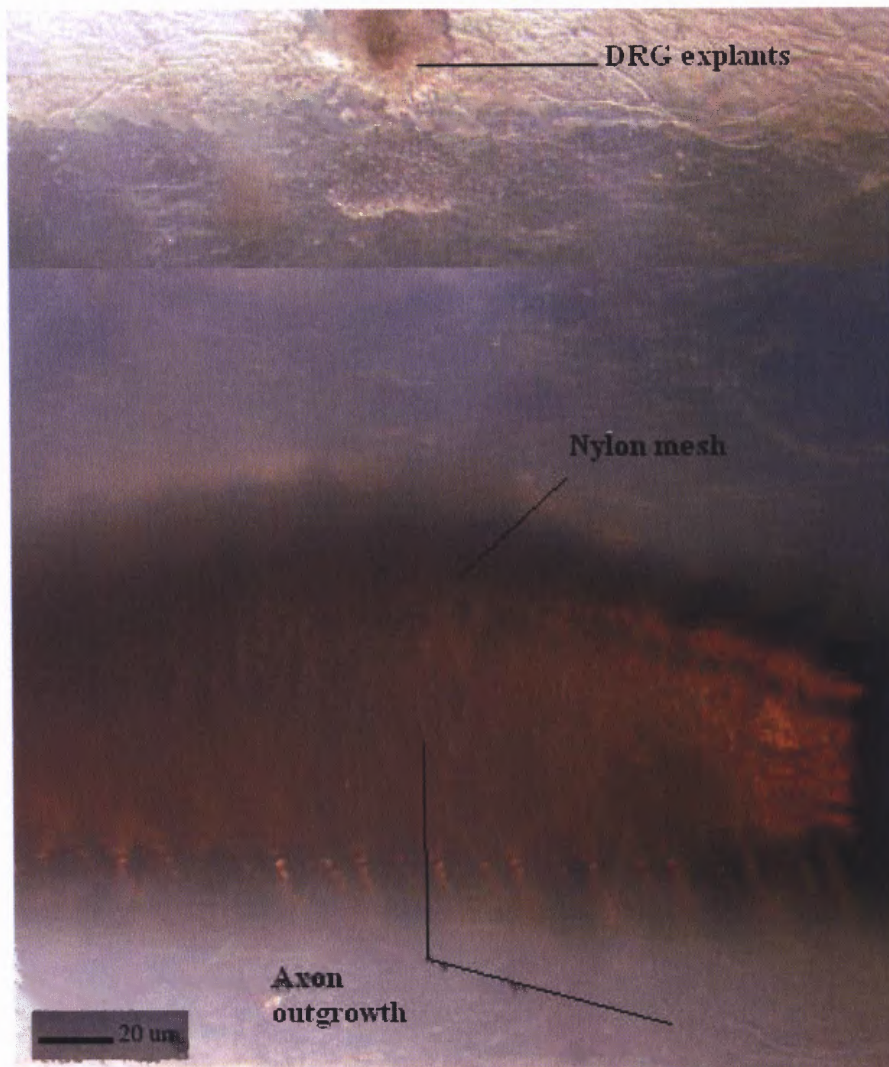
Figure 3.36 DRG outgrowth through Nylon mesh of "medium" pore size in 3.2 mg/mL collagen concentration hydrogel. Day 9: number of axons growing through the mesh increase.

Figure 3.37 (a) and (b) and Figure 3.38 (a) and (b) show another observation with "*medium*" pore size Nylon mesh and 3.2 mg/mL collagen hydrogel. Similar to the above experiment, these images confirm the observation that axons take longer to grow through the mesh to the other side. On day 9 the axons are seen grow across the Nylon mesh.
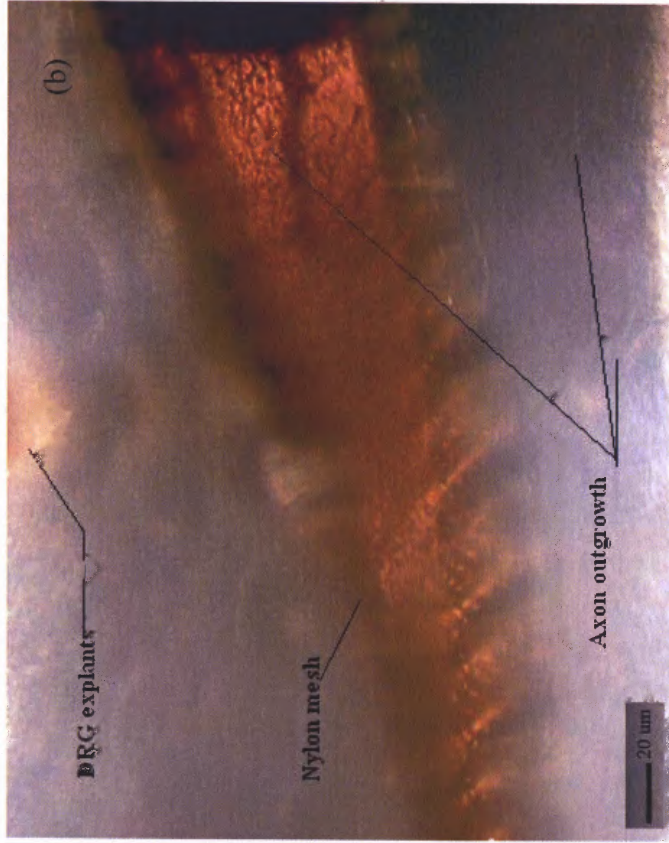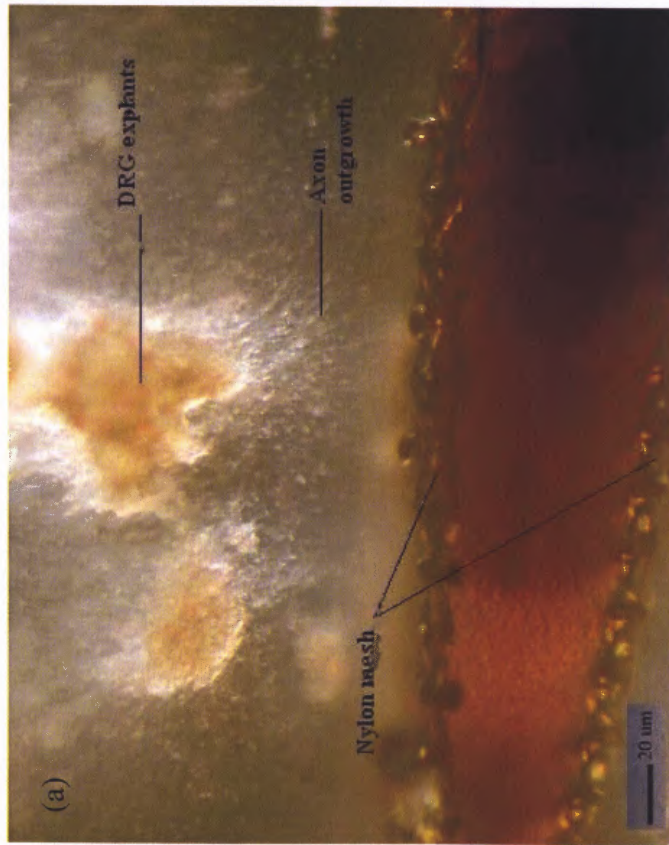
Figure 3.37 DRG outgrowth through Nylon mesh of "medium" pore size in 3.2 mg/mL collagen concentration hydrogel. (a) Day 2: axon outgrowth from the DRG explants (b) Day 9: number of axons growing through the double mesh increases.
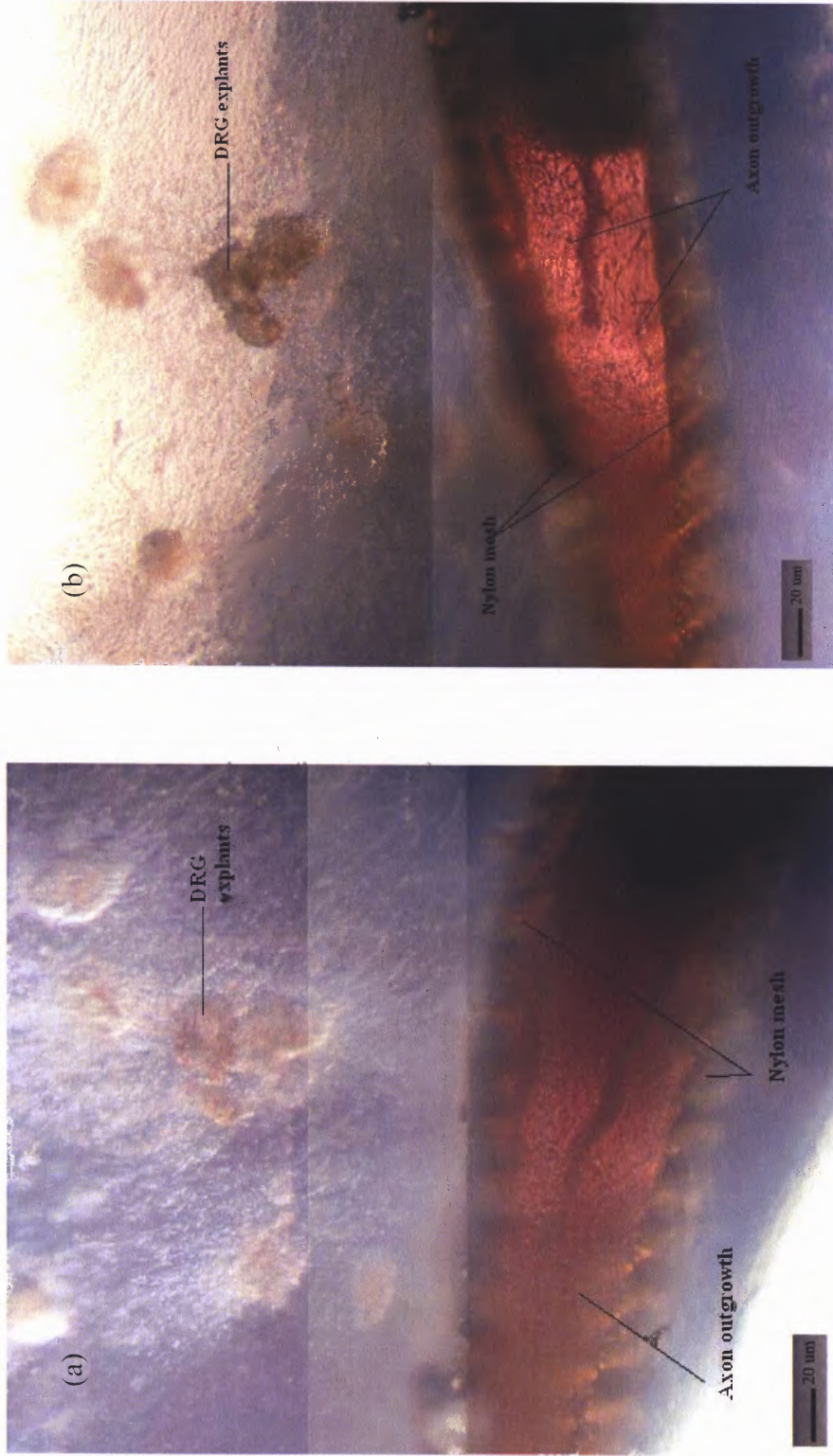
Figure 3.38 DRG outgrowth through Nylon mesh of "medium" pore size in 3.2 mg/mL collagen concentration hydrogel. (a) Day 5: continued growth of axons through the mesh (b) Day 7: number of axons growing through the mesh increase
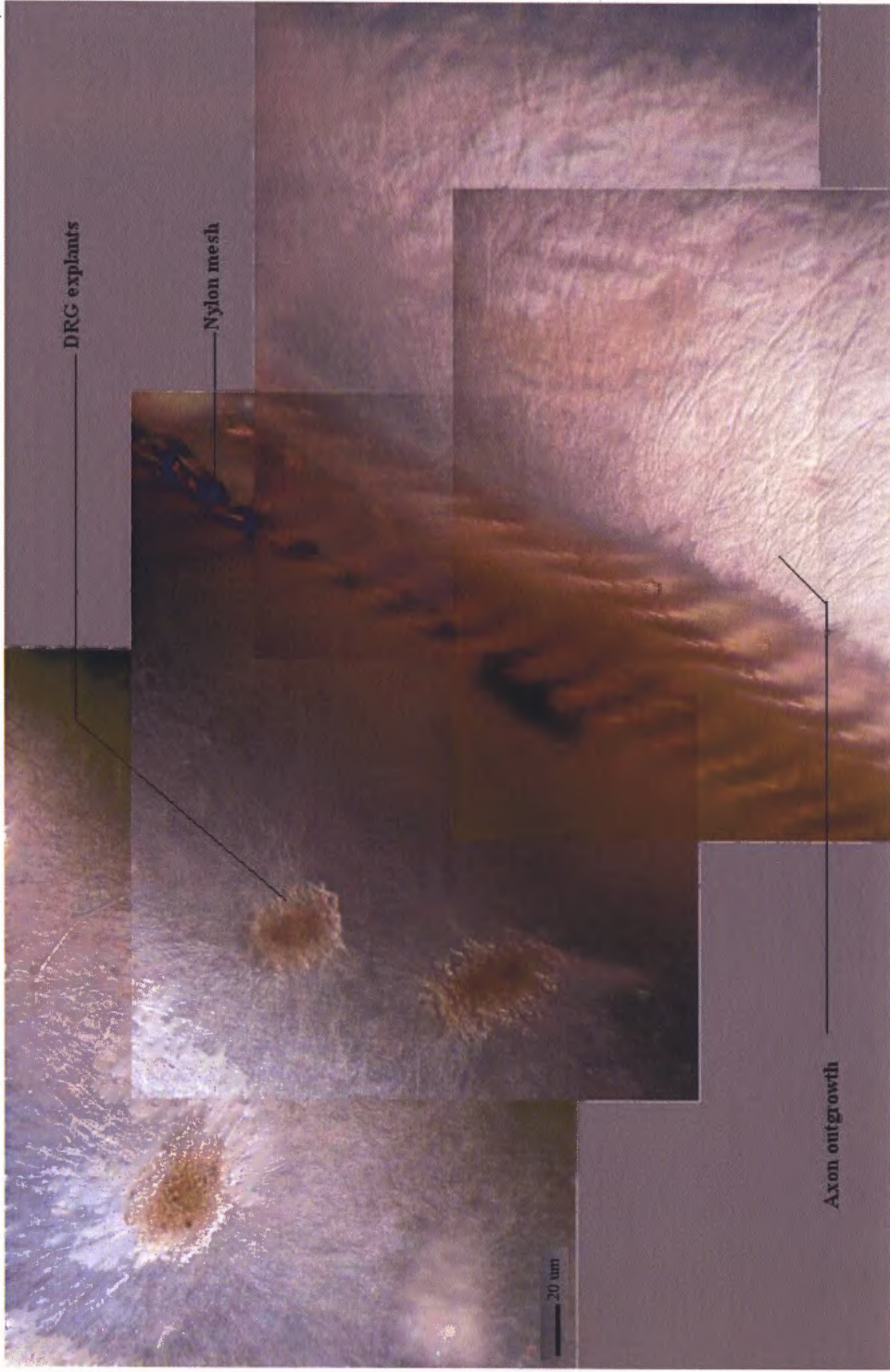
Figure 3.39 Day 14: axon outgrowth through the Nylon mesh of "medium" pore size in 2.0 mg/mL. The density of axons on either side of the mesh is comparable.

Figure 3.39 is the image showing axon outgrowth through "*medium*" pore size Nylon mesh in 2.0 mg/mL at day 14. It is seen that the "*medium*" pore size Nylon mesh allows most axons to grow through the mesh. Observations reveal that the axons that do grow through the mesh have similar lengths on either side of the mesh. This confirms that the "*medium*" Nylon mesh size does not hinder axon growth through it.

Figure 3.40 Day 21: axon outgrowth through the Nylon mesh of "*medium*" pore size in 3.2 mg/mL. The density of axons on either side of the mesh is comparable.

Similarly, Figure 3.40 shows axon outgrowth through "*medium*" pore size Nylon mesh in 3.2 mg/mL at day 21. The density of axons on either side of the mesh is seen to be comparable. However, in the stiffer gel (3.2 mg/mL concentration of collagen hydrogel), the rate of axon outgrowth is slower.

Figure 3.41 is the image of experimental setup with "*fine*" pore size Nylon mesh and 3.2 mg/mL collagen hydrogel on day 7. As seen from the figure, very few axons are visible to grow through the double layer of Nylon mesh. Figure 3.42 shows the images for the experimental setup with "*fine*" pore size Nylon mesh and 2.0 mg/mL collagen hydrogel on day 14. Unlike the "*medium*" pore size Nylon mesh, the "*fine*" pore size of the mesh allows fewer numbers of axons to grow through. Also, observations reveal that the density of axons on either side of the mesh is not comparable: axons density on the opposite side of the mesh is much less than that on the side of the DRG explants.
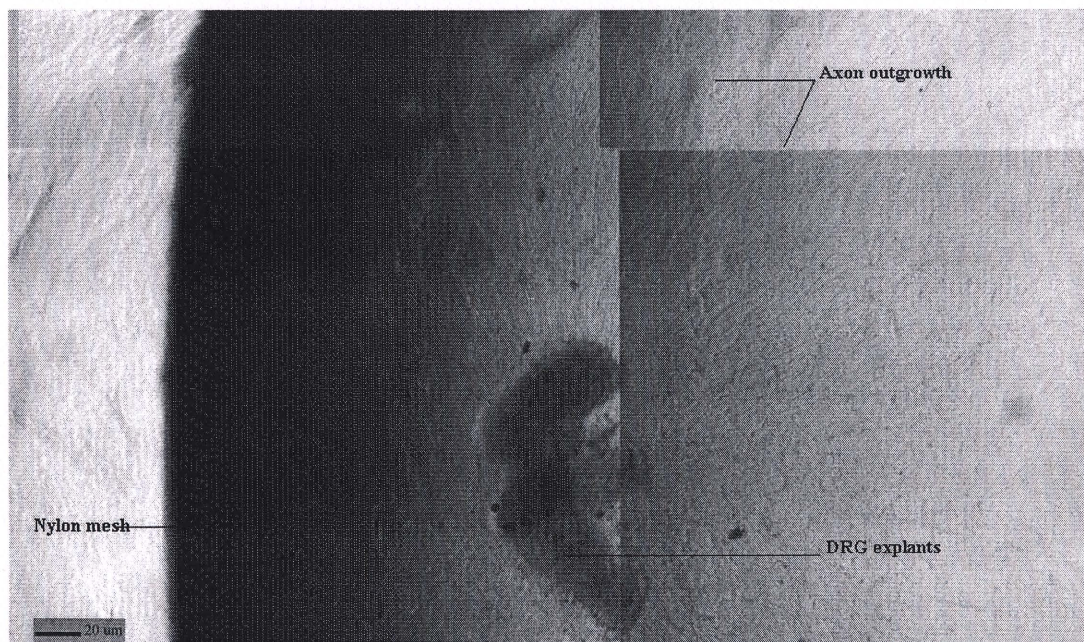
Figure 3.41 Day 7: axon outgrowth through the Nylon mesh of "*fine*" pore size in 3.2 mg/mL.
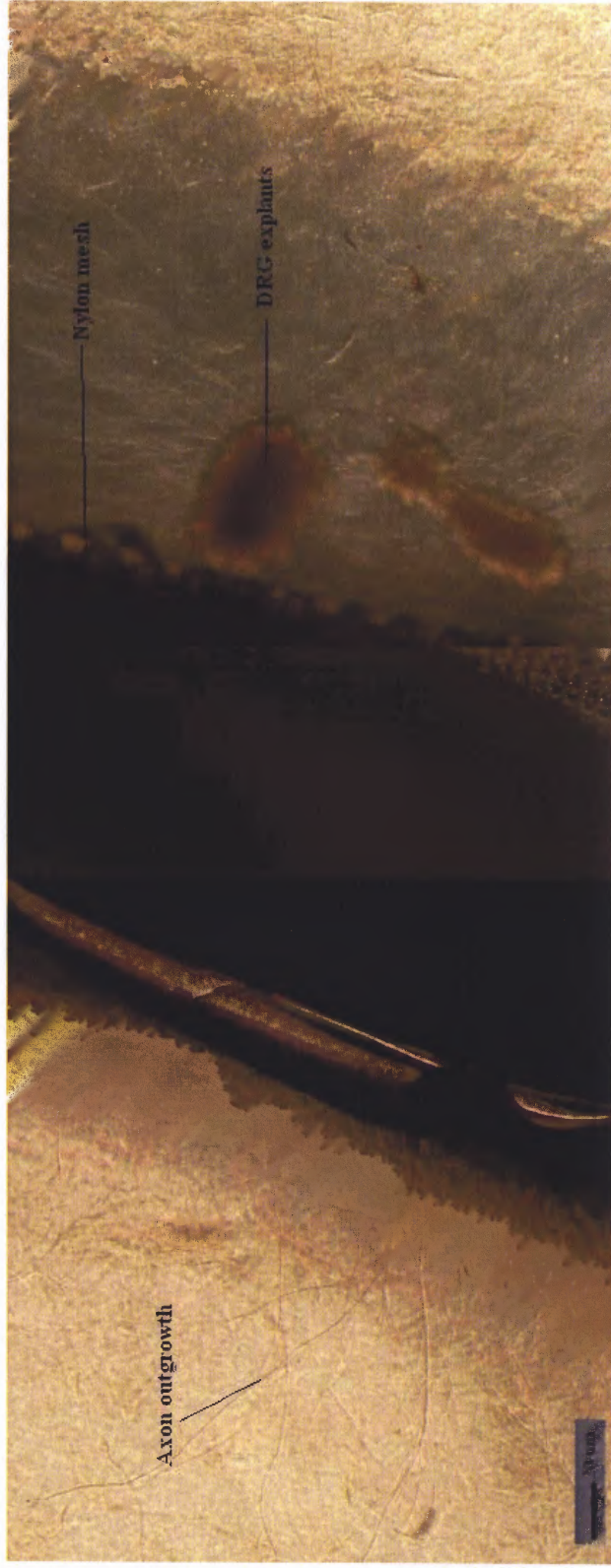
Figure 3.42 Day 14: Axon outgrowth through the Nylon mesh of "*fine*" pore size in 2.0 mg/mL.

Phase contrast microscopy is sensitive to light and shadows. The bending of the Nylon mesh walls in the wells, often times, result in shadows being cast upon the hydrogel. This makes it difficult to image and track the axons growing through the Nylon mesh. In order to overcome this problem. Green-fluorescent Calcein AM is used to stain the cells. This fluorescent stain has an excitation and emission maxima of about 494 nm and 517 nm respectively which is comparable to many other commonly used green-fluorescent

dyes. Calcein AM is retained in cells having intact membranes and does not stain dead cells. This property allows calcein to be used for fluorescence-based assays for cell viability [62]. Calcein is used to stain the cells in each well and fluorescent images of the live axons are obtained to track their growth direction through the mesh.

Calcein AM is obtained from Molecular Probes. The experimental set-up for the calcein stain sample follows the same protocol as discussed above. The DRG explants are allowed to grow in each well with the Nylon mesh walls. On day 5, the cultures are stained with calcein AM according to the standard protocol attached with the product description from Molecular Probes [62]. Staining with calcein AM renders a better image compared to the phase contrast images and the effect of pore size on axon outgrowth is clearly visible. Figure 3.43 and Figure 3.44 are the fluorescent images of axon outgrowth through the "*medium*" pore size mesh in 2.0 mg/mL collagen concentration hydrogel on day 5 and day 7, respectively. It is evident from the images that almost all of the axons from the DRG explants grow through the Nylon mesh of "medium" pore size. The densities of axons on either side of the mesh are also comparable.

Figure 3.45 (a) and (b) are the calcein stained images of the DRG neurons and axons. The figures show similar axon outgrowth on a second sample with "*medium*" pore size mesh in 2.0mg/mL collagen hydrogel. The density of axons on either side of the Nylon mesh is seen to be comparable showing the "*medium*" pore size allows most axons to grow through the mesh
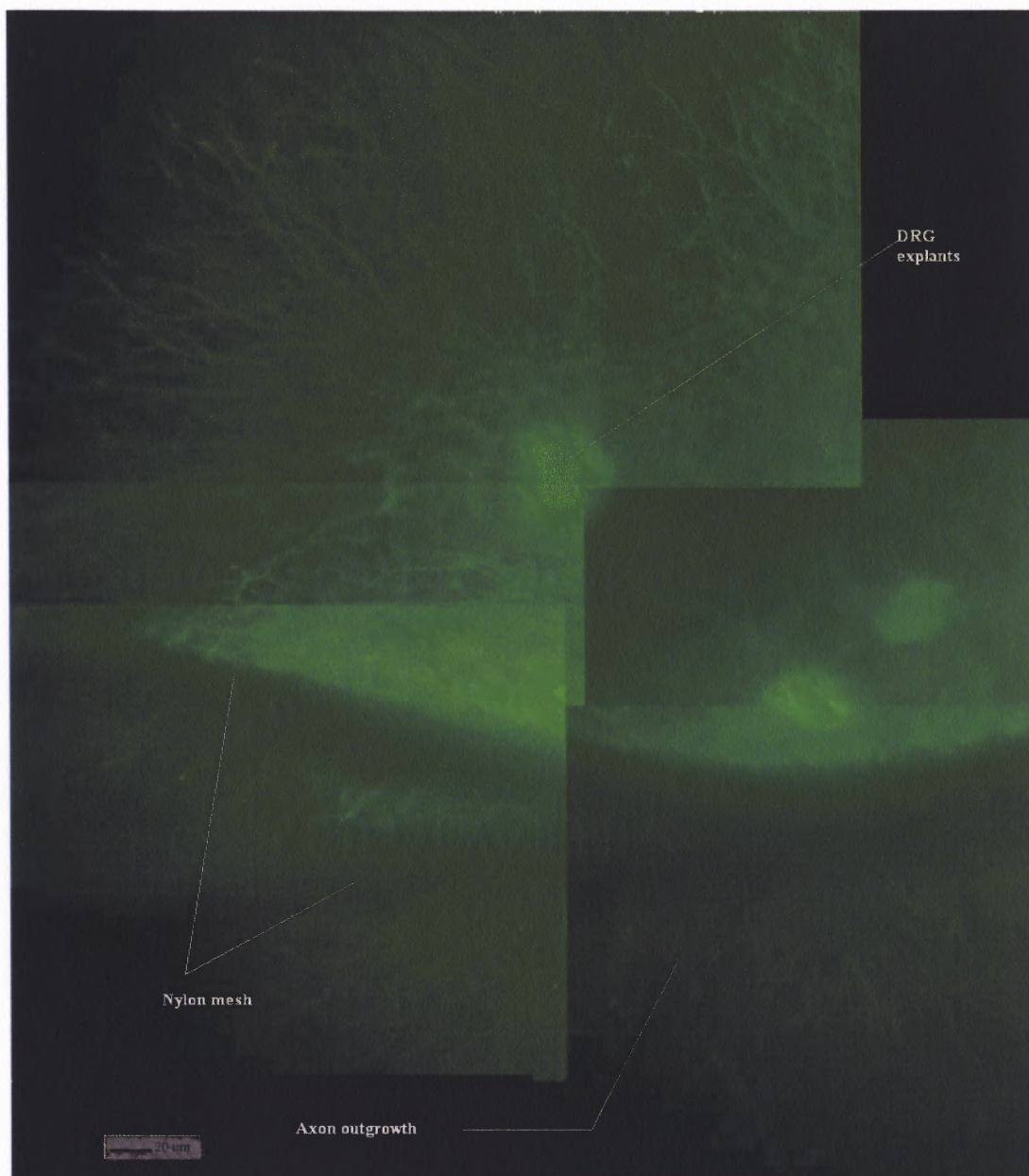
Figure 3.43 Day 5: axon outgrowth through "medium" pore size of Nylon mesh in 2.0 mg/mL collagen concentration hydrogel. Axon length and density is comparable on either side of the mesh showing that the medium pore size of the mesh does not hinder axon outgrowth.
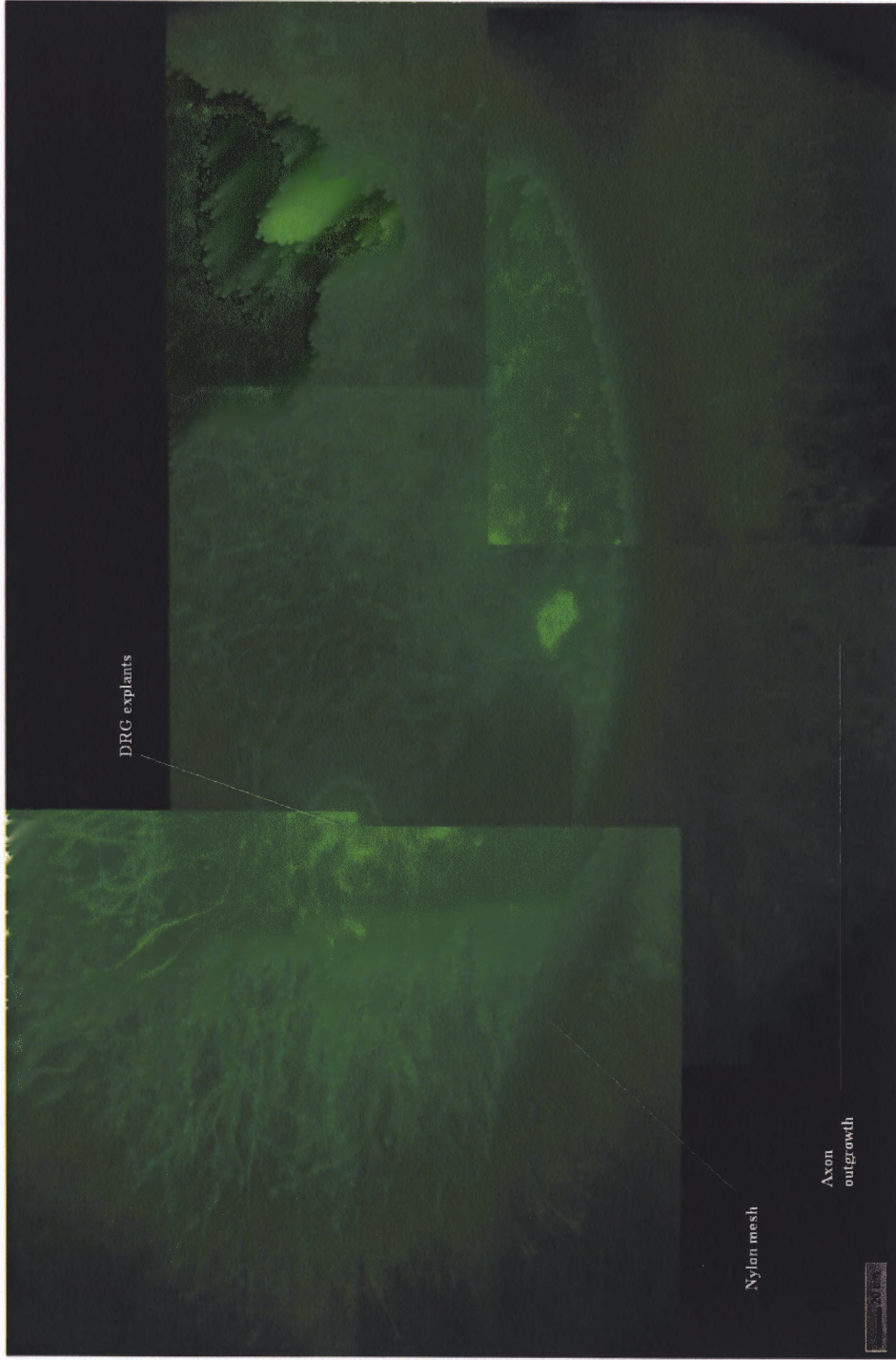
Figure 3.44 Day 7: axon outgrowth through "medium" pore size of Nylon mesh in 2.0 mg/mL collagen concentration hydrogel. Axon length increases on day 7 and density of axons is comparable on either side of the mesh.
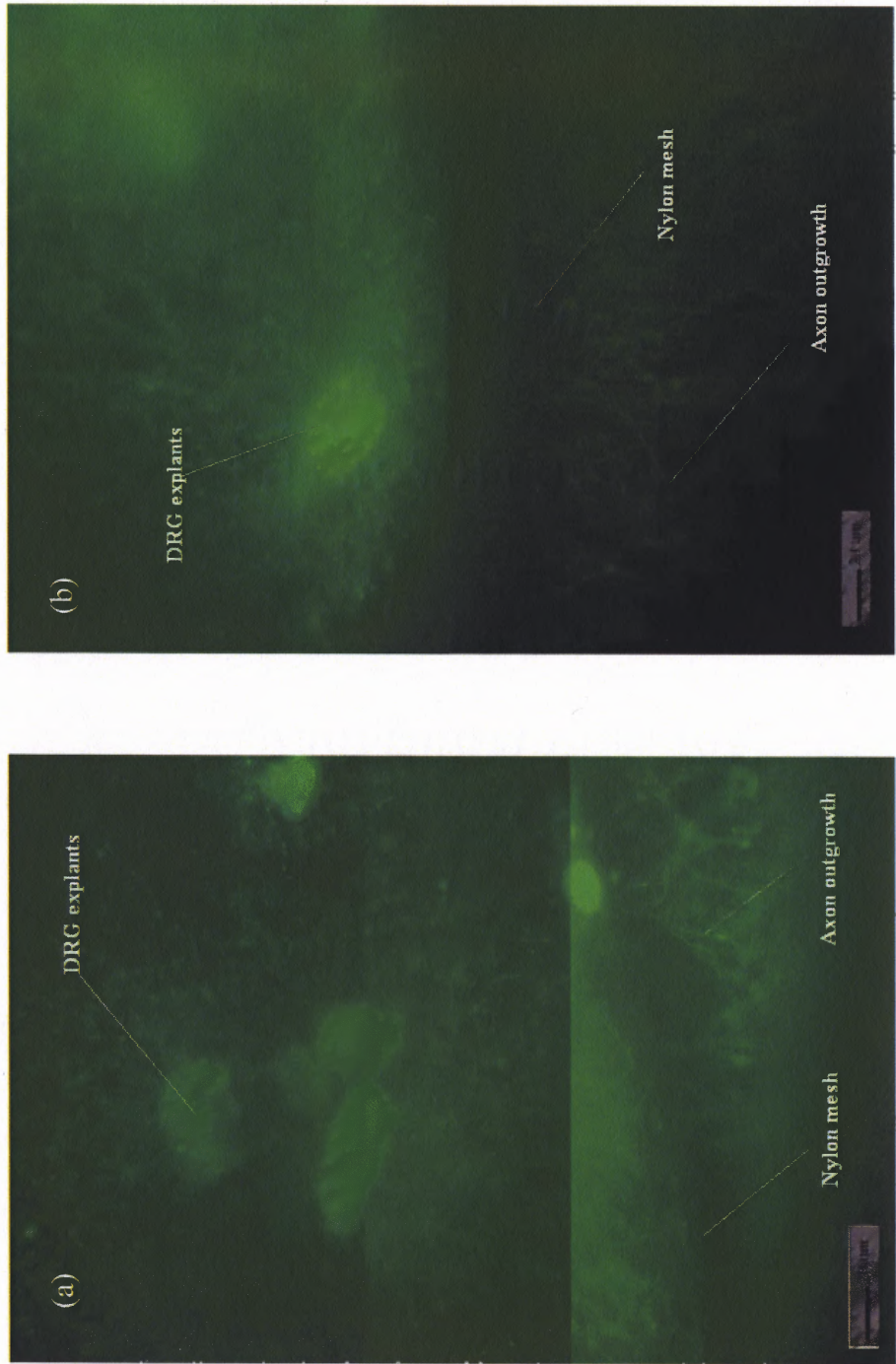
Figure 3.45 Axon outgrowth through "medium" pore size of Nylon mesh in 2.0 mg/mL collagen concentration hydrogel (a) Day 5: axon outgrowth through the Nylon mesh. (b) Day 7: axon length increases on day 7.

Figure 3.46 shows axon outgrowth through "fine" pore size Nylon mesh in 2.0mg/mL collagen hydrogel. The number of axons growing through the fine mesh size is less compared to that of the medium pore size. Hence observations reveal that the fine pore size hampers axon outgrowth through the mesh.
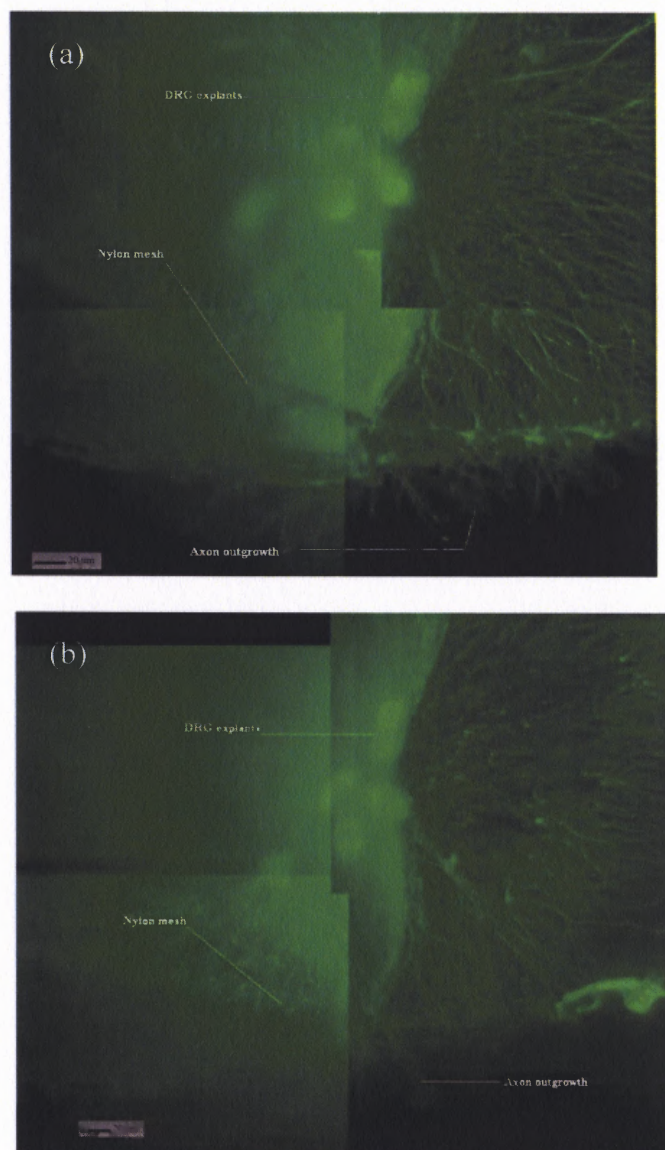
Figure 3.46 Axon outgrowth through "fine" pore size of Nylon mesh in 2.0 mg/mL collagen concentration hydrogel (a) Day 5 (b) Day 7. It is seen that the fine pore size of the mesh hinder axon outgrowth.

Figure 3.47 shows axon outgrowth through the "medium" pore size mesh in 3.2mg/mL on collagen hydrogel on day 14. The image shows that the medium pore size allows almost all axons to grow through the mesh.
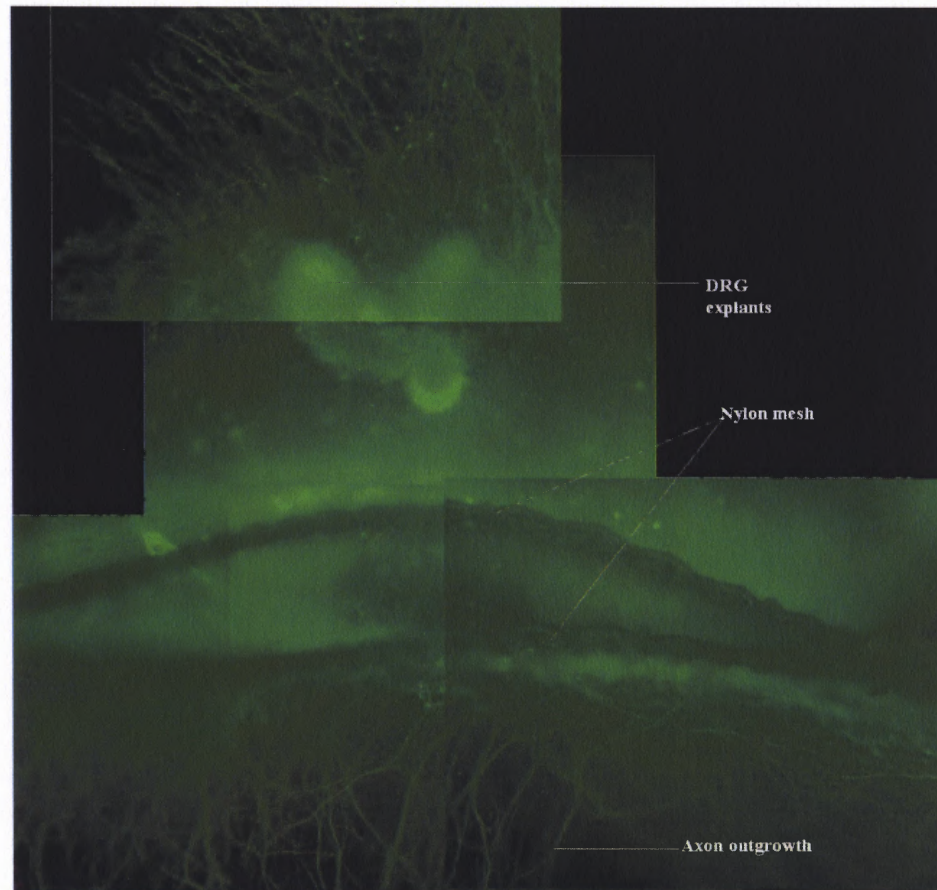
Figure 3.47 Axon outgrowth through "medium" pore size of Nylon mesh in 3.2 mg/mL collagen concentration hydrogel on Day 14.

The above images presented in this section render a clear view of the effect of the concentration of the collagen hydrogel and of the pore size of the Nylon mesh on axon outgrowth. As discussed earlier, collagen hydrogel concentration determines the rate of axon outgrowth and defines the mechanical stability of the 3D cultures in each 3D component. The Nylon mesh pore sizes, on the other hand, determine the number and

density of axons growing in between each pair of 3D components. The time point of axon outgrowth is important as it determines the point when to start the elongation process once axons are fully grown in between each 3D component. Both, the concentration of the collagen hydrogel, and the pore size of the Nylon mesh, determine the time point.

Collagen hydrogels with concentrations of 2.0mg/mL and 3.2 mg/mL are tested with the "*medium*" and "*fine*" pore size mesh. Visual observation of the collagen hydrogel concentration does not appear to affect the number of axons growing through the Nylon mesh. From the observations discussed in Section 3.2.1, both the 2.0 mg/mL and 3.2 mg/mL concentrations of collagen hydrogel work best in the 3D components while providing structure and stability. However, observations discussed in Section 3.2.2, show that the rate of axon growth through the mesh is slower in the stiffer hydrogel (3.2 mg/mL collagen concentration) when compared to the less stiff one (2.0 mg/mL). The 3D axon stretch growth device calls for both fast and optimal axon outgrowth through the Nylon mesh in each component in order to generate a continuous "flow" of axons in between the two 3D neuron cultures. Hence, the 2.0 mg/mL collagen concentration of hydrogel meets all requirements for the design. As seen from the phase contrast and the fluorescent images, 2.0 mg/mL collagen hydrogel encourages a good rate of axon growth through the Nylon mesh of either pore size, allowing the elongation process to start at day 7.

The Nylon mesh pore size has an evident effect on the number and density of axons growing through the mesh. Images presented in this section exhibit that the "*fine*" pore size of the Nylon mesh obstructs the number of axons growing through the mesh and so the density of axons on the opposite side of the mesh remains a lot less than that

compared to the density around the DRG explants. The *"medium"* pore size however, allows almost all axons to grow through the mesh resulting in an equal density of axons on either side of the mesh. Hence, for the 3D design purpose, the *"medium"* pore size Nylon mesh optimizes the density of axons.

The time required for axons to fully grow in between the two 3D cultures is an important parameter as it determines when to start the elongation process. From the images and observations done in Sections 3.2.1 and 3.2.2, it can be concluded that the time it takes for all the axons to completely grow through the mesh is 7 days. Axons from the DRG explants close to the mesh grow through within a period of 5 days. However, in order for the axons (originating from the DRG explants further away from the mesh) to cross the mesh, a period of one week is required. In all the images presented here, it can be seen that on day 7 the number and density of axons growing through the Nylon mesh is optimal for the 2 mg/mL collagen concentration hydrogel. In the 2D axon stretch growth device, there is no hydrogel to suspend the neurons. The neurons grow in a 2D plane on the extra cellular matrix of collagen. Thus the 2D setup allows the elongation process to start on day 5 after the axons have fully grow into either 2D cultures In the 3D setup, the use of the hydrogel is crucial, as emphasized earlier. The growth of axons in a hydrogel thus, decreases the rate of axon outgrowth because axons grow three dimensionally in multiple planes. Also the hydrogel being stiffer delays axon growth rate. Hence, elongation process for the 3D design is determined on day 7 versus day 5 for the 2D setup.

3.3 Experimental Set-up of the 3D Axon Stretch Growth Device

This section describes the experimental protocol for the 3D axon stretch growth device. The setup of the device uses the optimized parameters that have been discussed in the earlier sections. The setup of the 3D axon stretch growth device is similar to the 2D setup. The device along with its 3D components are cleaned with soap and thoroughly rinsed with sterilized reverse osmosis (RO) water and dried in a biological safety cabinet. The Nylon mesh is cut to the size of the each 3D component. Next, a thin and even layer of silicon glue is "painted" around the front edges of the component. A uniform thin layer of glue is crucial because the thickness of the glue around the edges would result in a gap in between the attached and the towing component when brought together and aligned against each other in the stretching frame. Once the hydrogel is pipetted in the components, as discussed below, this gap may hinder the hydrogel of the two components to be in close contact with each other, thus disrupting the continuous path for axon outgrowth.

The cut pieces of the Nylon mesh are firmly set in place on top of the glue around the edges of the components. The bottom plane of the components is extremely thin (approximately 5 mm as seen in Figure 2. 9) and as such, extra caution is taken to ensure that the Nylon mesh is firmly in place on the front. If the Nylon mesh is not securely glued to the bottom of the component then it can come off during the elongation process, causing the 3D culture to leak out as shown in Figure 3.48. Figure 2.18 and 2.19 show the Nylon mesh glued around the edges of each of the components. Once the Nylon mesh is glued, the attached component is glued with silicon glue to the base frame and the towing

component glued to the stretching frame and dried overnight. Figure 2.21 shows the components glued to the frame.
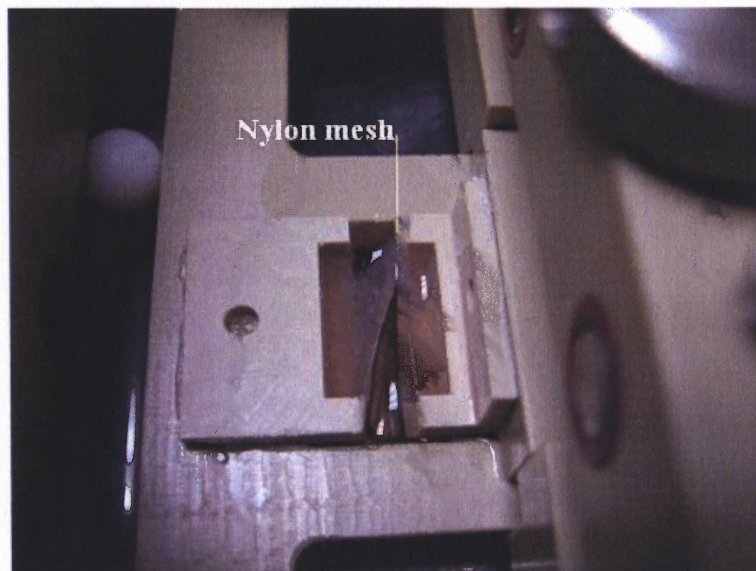
Figure 3.48 Nylon mesh can come apart if not secured with glue around the bottom edge of the component.

After the glue is dry, the device is sterilized in the autoclave and dried under sterilized hood while the thick Aclar membrane is glued on the bottom of the base frame, similar to the 2D setup, following the protocol of Pfister et al [13].

Before plating the DRG explants in the components, an initial coating of collagen hydrogel is placed in between the two components. This is done to ensure that there are no visible gaps in between the Nylon mesh of the two components. The components are viewed under the microscope to help fill the gap with the hydrogel. Figure 3.49 (a) shows the gap, under 4X magnification that usually results when the components are brought together, as a result of the thickness of the glue and the mesh for each component. Testing has shown that this gap leads to the failure of axons to grow through the mesh into either side of the 3D cultures. In such a case, axons of the 3D cultures are not

connected and elongation of this setup would yield no stretched axons. As a solution to this problem, the initial coating of hydrogel fills the gap in between the components forming a continuous path for the axons to grow from one 3D culture to the other. Figure 3.49 (b) shows the gap between the components being filled with hydrogel. Experiments have shown that approximately 200 μL of collagen in hydrogel is needed to fill the gap. Once the gap is filled the hydrogel is let to polymerize inside the incubator.

Gap in between components

Gap filled with hydrogel

(a)   (b)
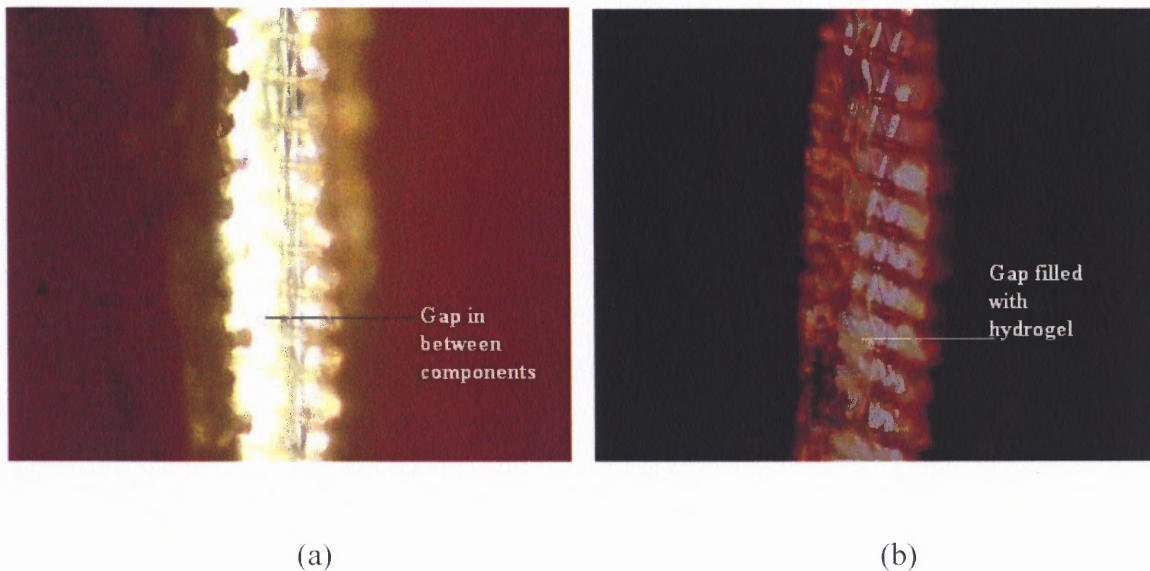
Figure 3.49 (a) "gap" between the two 3D components. (b) "gap" is filled with collagen hydroge to ensure completely contact in between each component.

Primary cultures of embryonic dorsal root ganglion (DRG) neurons are the source of axons for both 2D and 3D setup. The DRG isolation procedure and media preparation and elongation process follow the standard protocols as previously described by Pfister et al. [13]. The DRGs are obtained from 15 day old embryos (E15). E15 is chosen because on that day the embryos have more structure and are easier to handle and the DRG neurons can be obtained without trouble from the sides of the spinal cord. The DRG explants are collected and suspended in L15 cell culture media. L15 culture media allows

working with cells at room temperature without disturbing the pH level. Imbalance in pH in culture media may be harmful to the cells.

Each 3D component allows 250 μL of collagen hydrogel to be pipetted in. Hence in total of 500 μL of collagen hydrogel of, 2.0 mg/mL is made according to the protocol described in section 3.2.1. DRG explants are centrifuged to a pellet at the bottom of the tube and the supernatant of L 15 culture media is removed. Then the DRG explants are resuspended in the collagen hydrogel mixture and pipetted up and down to disperse the pellet. Next, 250 μL of the collagen hydrogel mixture and the DRG explants is pipetted in each of the component which is in close contact with each other. The 3D setup is then placed inside the bioreactor and incubated until the hydrogel polymerizes. Next cell culture media is placed on top and around the 3D components so as to fill the lane of the base frame and incubated. Growth media consists of Neurobasal Medium (Invitrogen), supplemented with B27 supplement, 1% fetal bovine serum (FBS), L-glutamine, 20 % concentration glucose, and 10ng/ml nerve growth factor (NGF) (Becton Dickinson). Mitotic inhibitors (MI) are used to inhibit the elimination of non-neuronal cells and Penicillin/Streptomycin to prevent bacterial growth.

Observation reveals that the *"medium"* pore size Nylon mesh allows the culture media to seep out of the components resulting in less media to be retained on top of the hydrogel. Hence, by pipetting 1 mL of media on top of the cultures every day and surrounding the cultures with media in the lane, ensures that the DRGs get adequate nourishment.

The time point to start the elongation process is decided based on the experiments discussed in Section 3.2.2. Once the axons have fully grown into either side of the 3D

components after a duration of 7 days, elongation of the 3D setup is begun by the stepper motor and controller.

Tests of the 3D axon stretch growth device have been carried out using 3D axon stretch growth device. For the particular test shown below, the concentration of collagen used was 2.0 mg/mL and DRGs from three rat embryos' spinal cord. The 2D setup also utilizes DRGs from three rat embryos' spinal cord for each lane and hence the number of DRGs was kept consistent for the 3D setup as well. Elongation process was started on day 7. Stretching occurred at a rate of 1 mm/day for 10 days. Using the optimized parameters as discussed earlier, axons was stretched to 1 cm in length. This shows that the 3D components have been successful in stretching axons in the 3D cultures in the fashion discussed above. Figure 3.50 and Figure 3.51 are the images of the 3D stretch grown axons.

For another experiment axons were stretched to a length of 6 mm at a rate of 1 mm/day. 3.2 mg/mL collagen hydrogel was used as the base of the 3D cultures, culturing DRG explants from three rat embryo spines. The images of axon growth through 3D cultures are shown in Figure 3.52 (a) to (d) and in Figure 3.53 (a) and (b). Figure 3.52 (a) to (c) are the phase contrast images of the stretched axons. The figures show that axon stretch occurs in multiple planes. Figure 3.52 (d) and Figure 3.53 (a) and (b) are the fluorescent images of the same set of axons, stained with calcein.
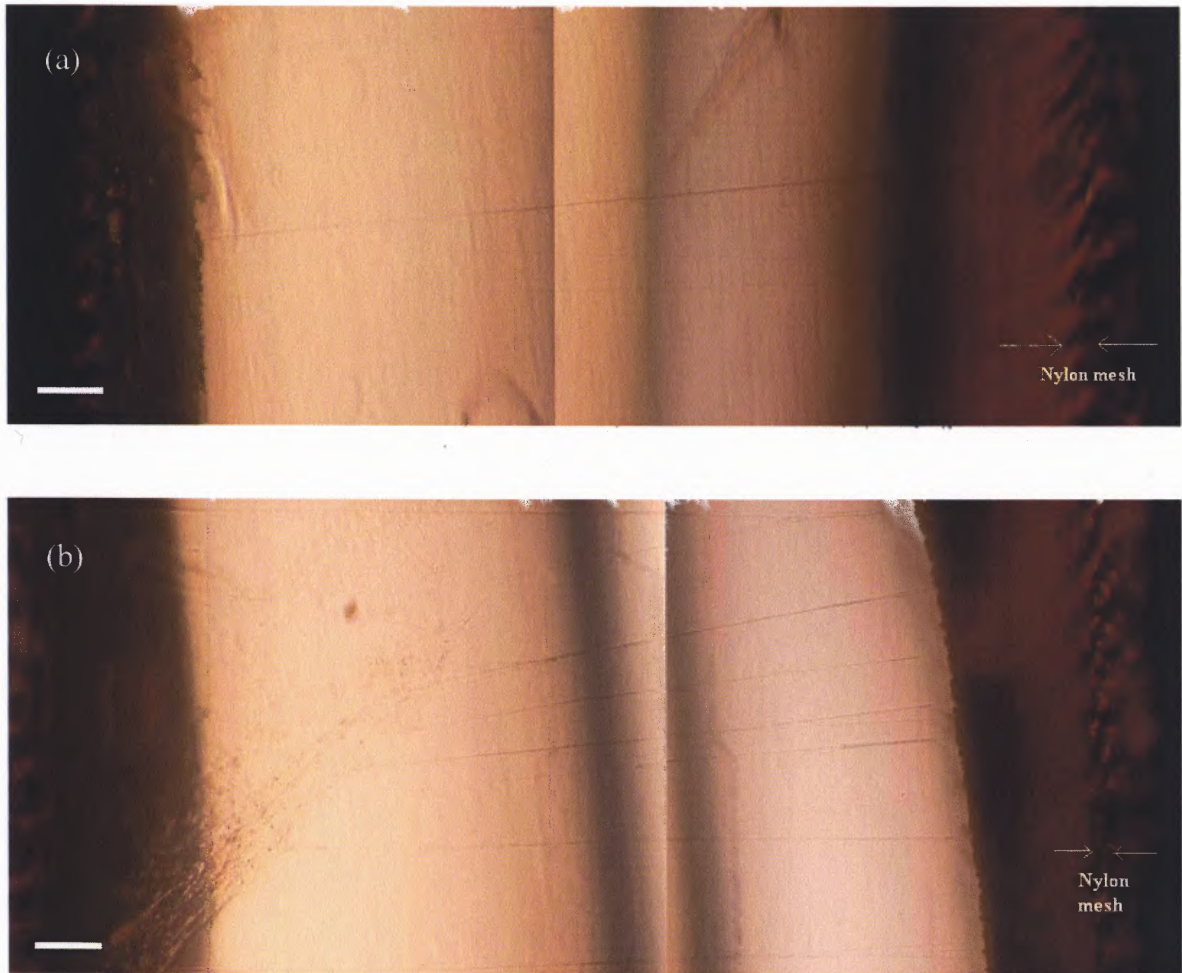
Figure 3.50 Axons stretched using the 3D axon stretch growth device. Here axons have been stretched to a length of 1 cm at a rate of 1 mm/day. Axons are seen to grow through the Nylon mesh. Images are taken at multiple planes. This shows that 3D axon stretch growth device is successful in stretching axons in 3D cultures.
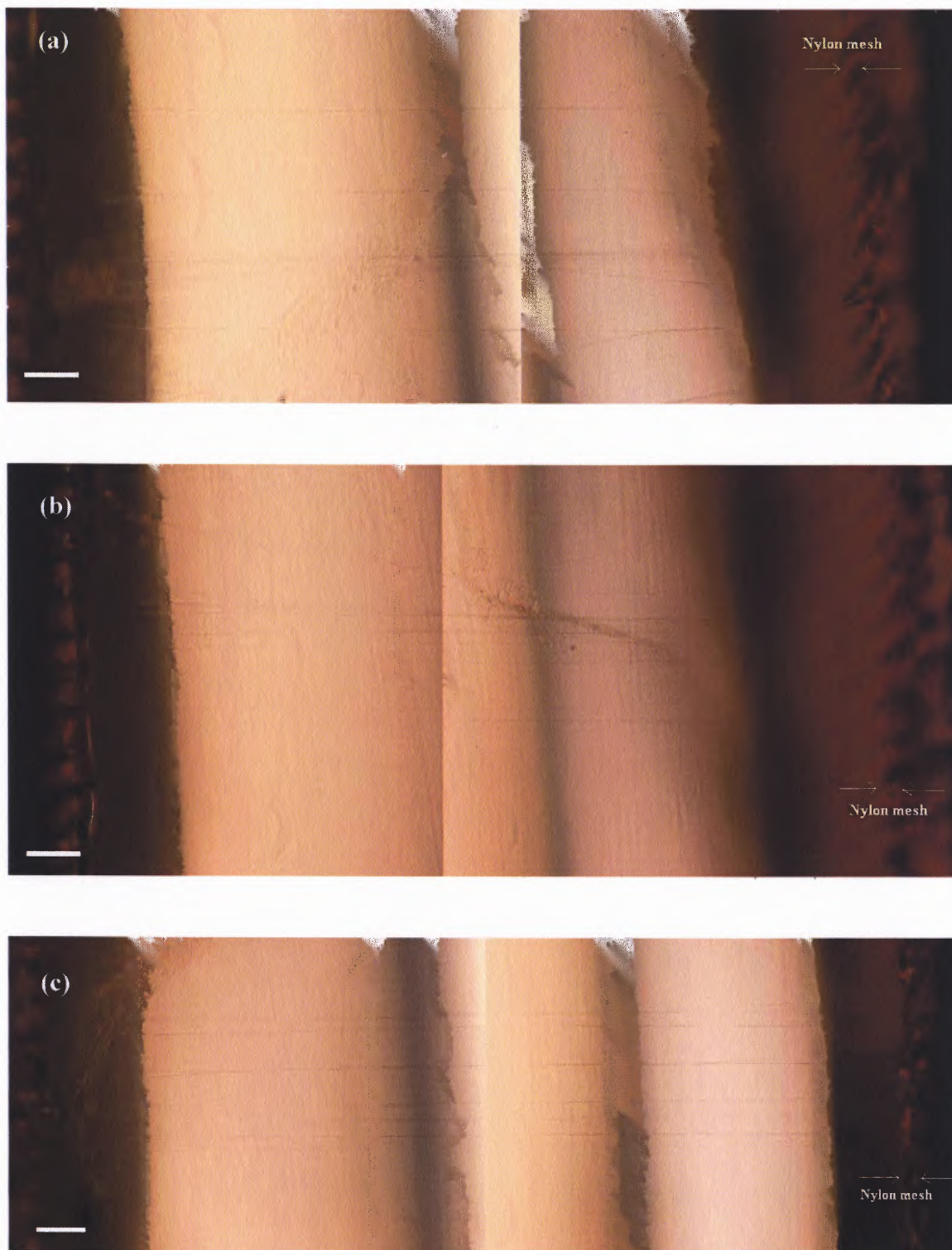
Figure 3.51 Axons stretched using the 3D axon stretch growth device.
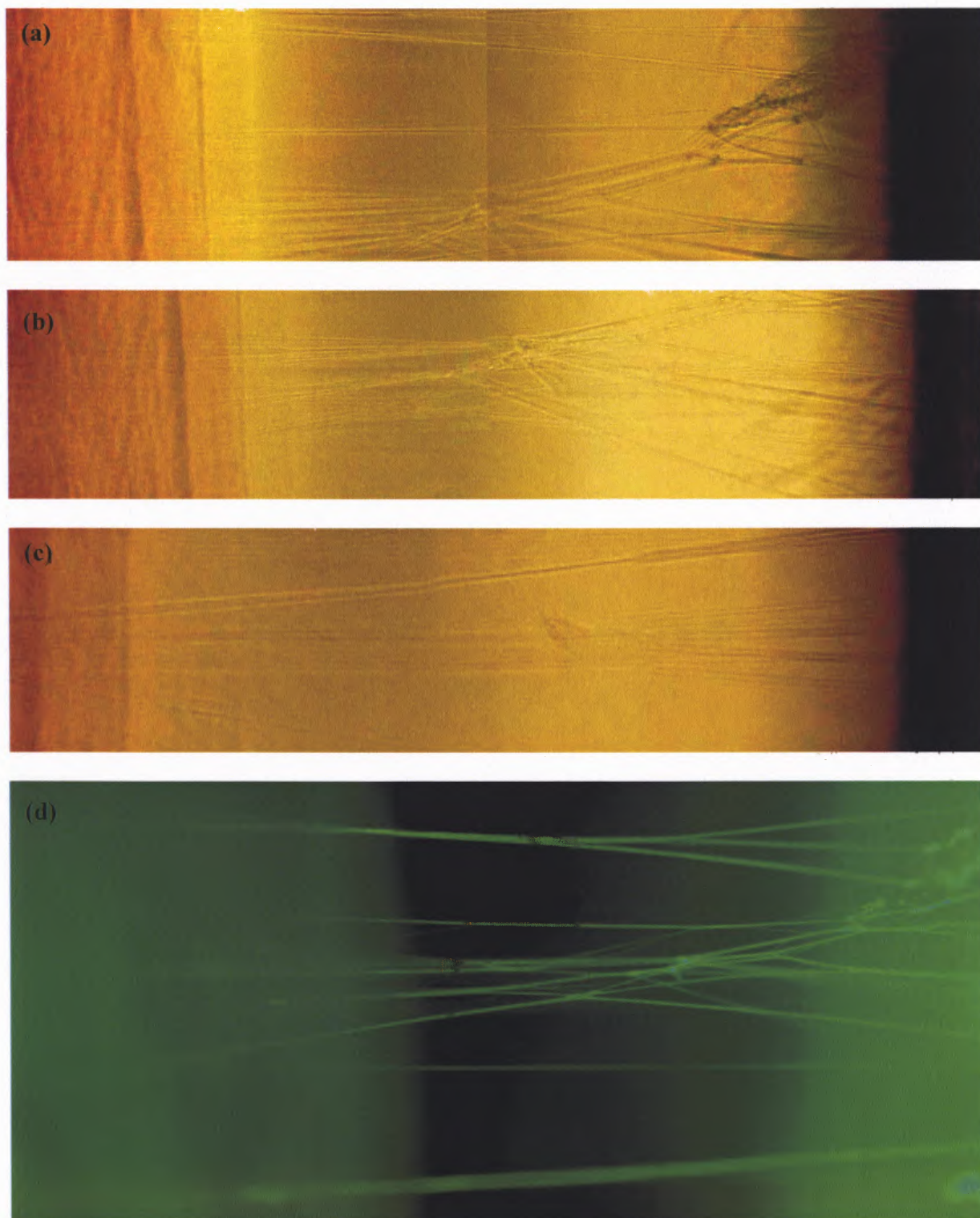
Figure 3.52 Axon stretch growth in 3D cultures. (a), (b), (c) Phase contrast images of axons stretched using the 3D device, under 10X magnification, stretched to a length of 6 mm. (d) Axons grown in 3D cultures, stained with Calcein. Axons are seen to grow in multiple planes.
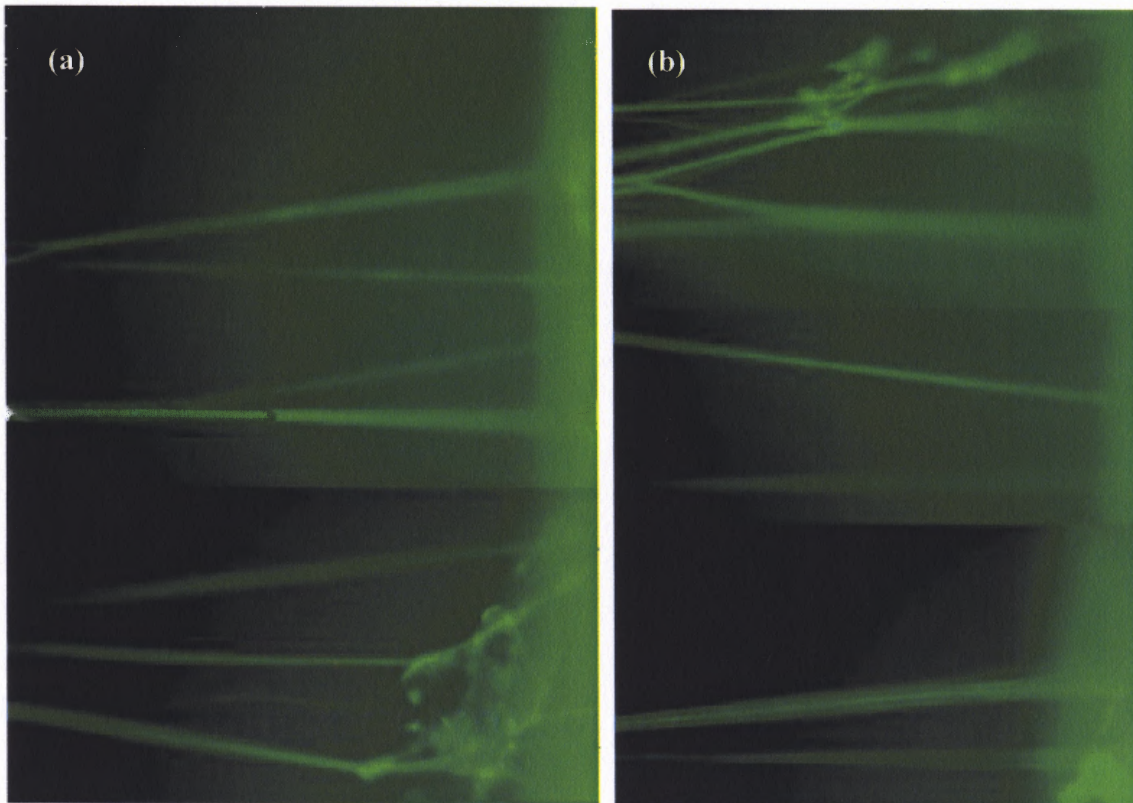
Figure 3.53 (a), (b) Axons stretched in 3D cultures stained with Calcein. Axons are seen to grow in multiple lanes across the Nylon mesh.

3.4 Summary

This chapter discusses the important parameters of the 3D design. The experimental set up for testing the parameters and observations obtained are discussed in detail in here. It can be concluded that in order to optimize the 3D axon stretch growth design, we should use 2.0 mg/mL concentration of collagen hydrogel because it retains its structure and contains the 3D culture in each 3D component. This hydrogel concentration does not hinder the rate of axon outgrowth. "*Medium*" pores size Nylon mesh optimizes the number and density of axons growing through the mesh. The optimized parameters

determines the elongation process to start on day 7 when all the axons are fully grown across both mesh for each component into either 3D neuron cultures.

Using the above optimized parameters axons have been stretched to a length of 1 cm at a rate of 1 mm/day for 10 days. The preliminary testing has shown the success of the 3D axon stretch growth design.

The next chapter discusses the quantification method used to measure the cross sectional area of the axon bundles stretched and grown using the current 2D device. The chapter focuses on the use of confocal microscopy, and Nikon EZ-C1 FreeViewer software for the purpose of quantifying axon bundles.

CHAPTER 4

QUANTIFICATION OF AXONS STRETCHED IN TWO-DIMENSION

4.1 Introduction

As discussed earlier in Chapter 3, the essential parameters of the 3D axon stretch growth device have been tested. Using the chosen parameters, the 3D axon stretch growth device has achieved axon stretch growth using 3D cultures. However, for 3D cultures to be useful, the number of and axon bundle density of stretch-growing axons must be better compared to 2D cultures. Such a comparison requires an understanding of the axon profile (thickness) and cross-sectional area of axon bundles grown in 2D cultures. As a result, in this chapter, a quantification method used to understand the profile of axon bundles stretched using the 2D system is discussed. The quantification method uses the confocal microscope to calculate the cross-sectional area of axon bundles. It can also be used to analyze the effect of the rate of stretch growth on axon bundle cross-sectional area. The preparation of the samples is discussed in Section 4.2 and the quantification of axon bundle thickness is discussed in Section 4.3. The chapter also provides description of the calculation method and the software used to validate the data obtained.

4.2 Preparation of Samples

Confocal microscopy has proved to be a powerful imaging tool to quantify axon outgrowth in various hydrogels and scaffold materials. Confocal microscopy eliminates light collected from out of focus planes that degrades image quality, thereby offering an advantage over other conventional techniques. Confocal microscopy also provides the ability to collect serial optical sections from thick specimens to create 3D renderings. The work discussed in this chapter takes advantage of this 3D scanning ability. The work is carried out on the Confocal Microscope (NIKON) to measure of the cross sectional area of the axon bundles stretched using the 2D axon stretch growth device. The samples preparation of stretch grown axons is mentioned below.

The axons are stretched in 2D using the existing 2D axon stretch device. Stretch-grown axons are then fixed with 4% paraformaldehyde (PFA) and treated with 0.1% Triton X and 4% normal goat serum (NGS) in PBS at room temperature according to the standard protocol of immunocytochemistry by Pfister et al. [13]. Immunocytochemistry is a method that uses antibodies to target antigenic receptors on the cell membranes. Primary antibodies in 4% NGS, and 0.1% Triton X in PBS are applied to the fixed axons. The primary antibodies used are: *SMI-31*, Sternberger Monoclonals, in a dilution of 1:1000 specific to phosphorylated state of neurofilament fragment, and *SMI-62*, Sternberger Monoclonals, in a dilution of 1:1000 specific to assembled forms of tubulin. Next, the axons are treated with fluorescent secondary antibodies, IgG 488 Goat anti Mouse (GαM) obtained from Molecular Probes, Eugene, OR.

After being marked with fluorescent antibodies, the Aclar membrane containing the 2D stretched axons is cut away from the base frame and mounted in between glass

cover slips with mounting media. The mounting media preserves the fluorescence and prevents the fixed axons from drying. This sample of stretched, labeled and preserved axons are then viewed and imaged under the confocal microscope.
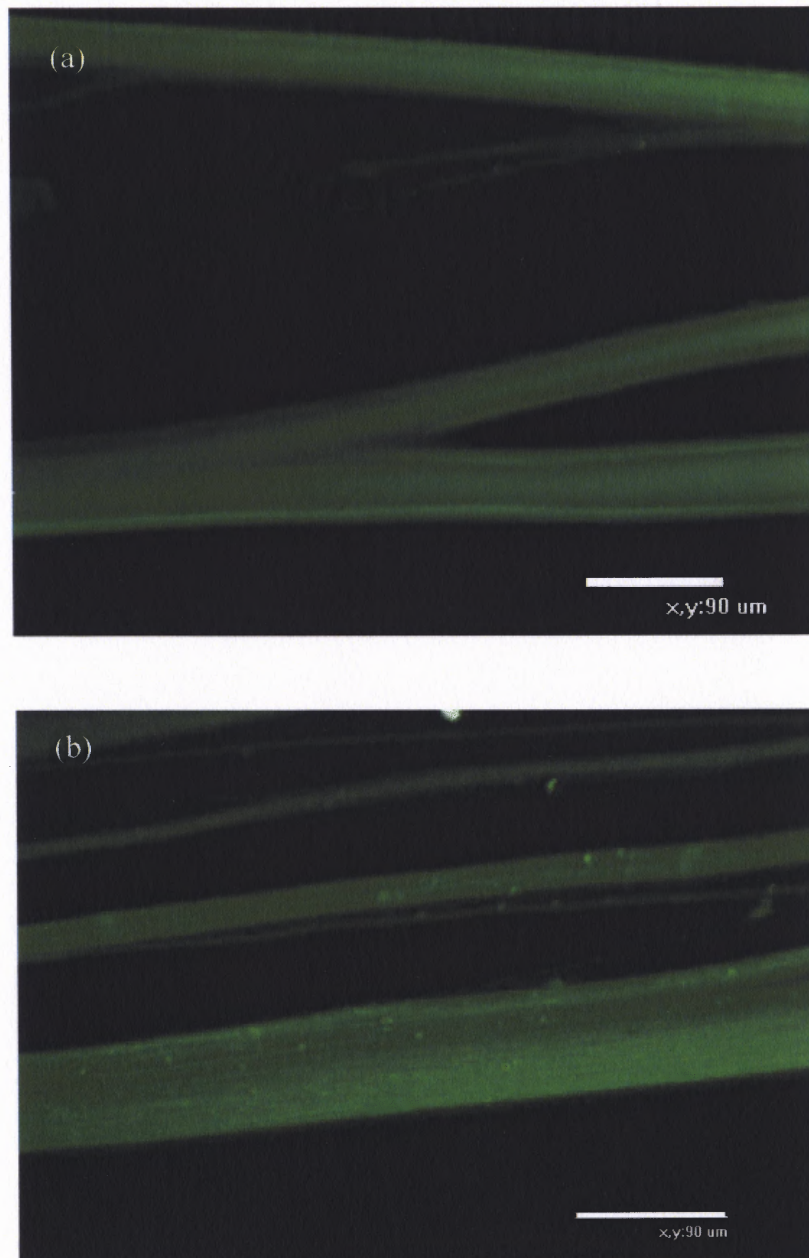
Figure 4.54 Confocal Images of typical axon bundles stretched using the 2D device. (a) bifurcating axon bundle, (b) Thick and thin axon bundles.

Figure 4.54 shows the confocal image of axon bundles stretched in 2D. Figure 4.54 (a) shows bifurcating axon bundle during stretch growth and Figure 4.54 (b) shows the typical thicknesses of an axon bundle observed during stretch growth using the current 2D device. It can be seen from these images that axons of different thicknesses are observed during stretch growth. The following section describes the quantification method used to calculate the cross sectional area of such axon bundles. It also discusses the axon profile observed by the quantification method.

4.3 Quantification of Axons Stretched in 2D

The samples prepared using the above procedure are viewed and imaged using the confocal microscope. The 3D scanning ability of the confocal microscope offers the benefit to calculate the thickness of each axon bundle and the 2D tissue formed. The cross-sectional area, along with the number of axons, can be used to estimate the axon density for a particular region of the tissue. The thickness of each axon bundle is determined using the confocal imaging software. The software allows the axon thickness to be divided into individual slices of equal thickness (z-dimension) giving a 2D image of each slice. A series of these 2D images of the slices in different planes are superimposed together to create a 3D image of the axon with a depth. The 3D image created is used to evaluate the cross sectional area of axons.

Figure 4.55 shows the schematic of the slices or layers through the thickness of the axon bundle in the z-dimension. When all the 2D images of each slice are

superimposed, a 3D image of the axon bundle is obtained as shown. The 2D image of each slice is the top view of individual layer showing the axons (green) and the empty spaces (black). The software of the confocal microscope helps to locate the top and the bottom planes of the axon bundle tissue and generates a thickness range between the respective planes. Depending on the range, the depth can then be "sliced" into several layers of equal thickness "z". The thickness chosen for each sample analyzed are described below.
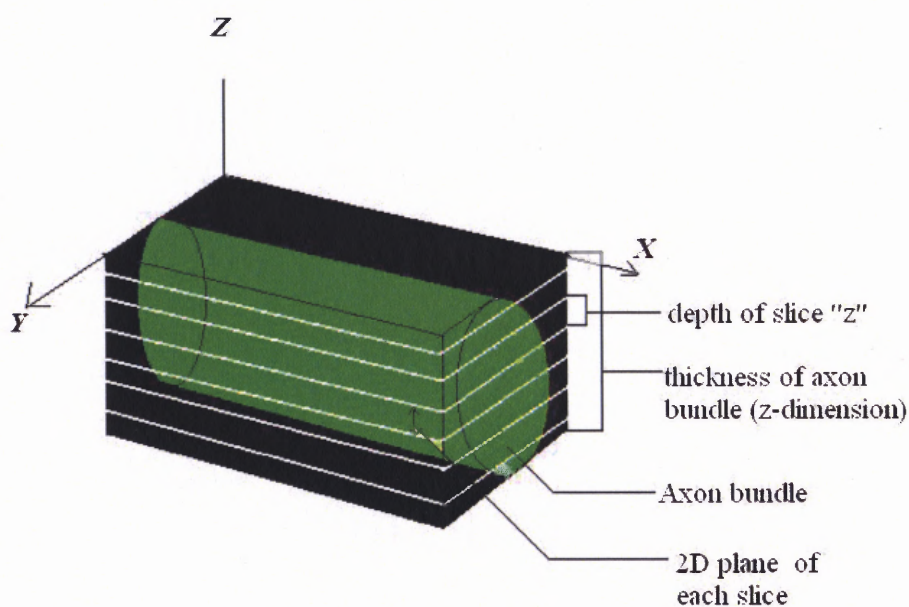
Figure 4.55 Schematic of the slices through the thickness of the axon bundle. Each slice produces a 2D image. When 2D images of all slices are combined, a superimposed image of the 3D axon bundle is produced.

Figure 4.56 (a) – (f) shows the image of the slices through two such axon bundles: (a) the top layer, when axons bundles just become visible, (c) the reference slice through the middle of the axon bundles, and (f) bottom layer of the axons. "Axon 1" is the thick axon bundle and "Axon 2" is the thinner one as shown in the figure.
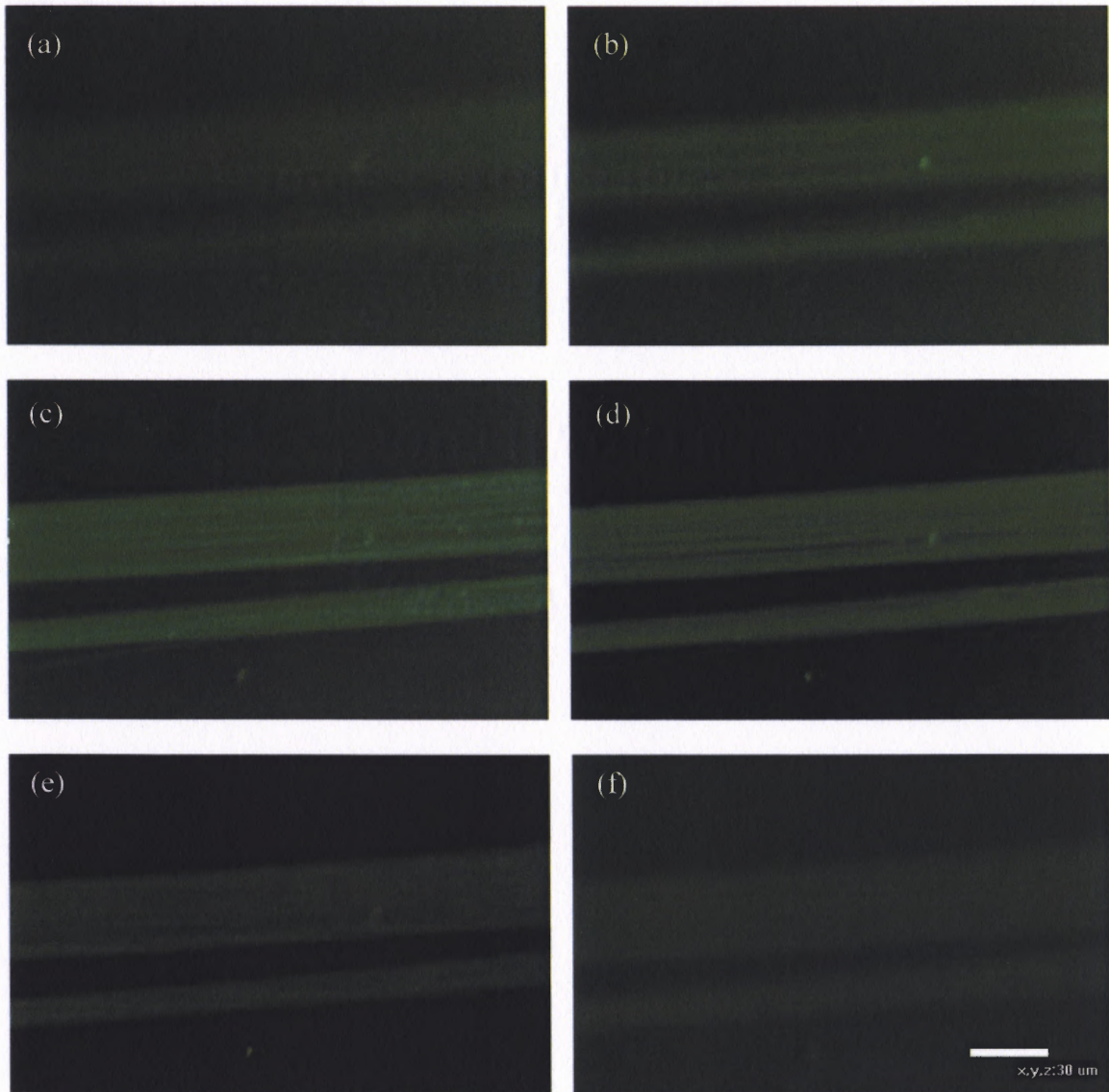
Figure 4.56 Image of slices through the axon bundle. (a) top slice, (c) reference slice, (f) bottom slice. Axon bundles at the reference or the middle slice are the most prominent. "Axon 1" is the thicker axon bundle and "Axon 2" is the thinner one. For each image, the axon width is calculated for both axons by drawing a region of interest using the Nikon EZ-C1 3.20 FreeViewer. The software then generates the value of the axon width. Average of the axon width, W, is calculated for a set of five different values for the same image.

Images of each slice are analyzed using the Nikon EZ-C1 3.20 FreeViewer. For individual images, the width "w" of labeled axon profiles is manually highlighted with a digital pen and the software generates the value of the axon width for each image. In order to minimize the error, the width is calculated at five separate points along the axon

bundle of the same image and the average value, W, is calculated. The standard deviation of the axon width values for each image is then used to calculate the error bar for the average axon width calculation. The top and bottom layer images tend to be of a lower resolution and hence the axon boundaries are not well defined. As a result for these images, the error bars of the average axon width are higher than the error bar of the axon width in the middle layers.

The cross-sectional area for axon bundles in each image, A_s, is obtained by the product of the average axon width "W" and the thickness "z" for each slice as given by:

$$A_S = W.z \qquad (4.1)$$

Here, A_s is the cross-sectional area for axon bundles in each image; W is the average axon width and z is the thickness of each slice.

The total cross-sectional area for the axon bundle, A, is given by the sum of the areas for each slice as:

$$A = \sum A_S \qquad (4.2)$$

Here, A is the total cross-sectional area for axon bundles.

The effect of the stretch growth rate of axons on the thickness of the axon bundles is discussed below. A stretch growth rate of (1) 6 mm/day, and (2) 1 cm/day for axons is used to measure the cross-sectional area. The regions showing most number of axons of varying thickness are used to calculate the axon width and the cross-sectional area. Calculations for the regions of interest are discussed in the following sections.

4.3.1 Axons Stretched Grown at a Rate of 6 mm/day

Figure 4.57 shows the confocal image of a region of stretched grown axons. This sample of axons has been stretched at a rate of 6 mm/day over a span of one week. The axons are fixed and mounted in glass cover slips by the method discussed earlier in this chapter. In this region, two zones of axons, as marked in the figure, are chosen for quantification.

Figure 4.58 is the magnified image of zone 1 showing "Axon 1" and "Axon 2". This image is the reference layer of the axons where maximum resolution is obtained and thus the boundaries of the axons are well defined. By means of the confocal imaging software, the thickness of this zone is measured to be 22 μm. This thickness is then divided into 10 slices each with a thickness, z, of 2.2 μm. Six of the ten slices are shown in Figure 4.56 (a) – (f).

88
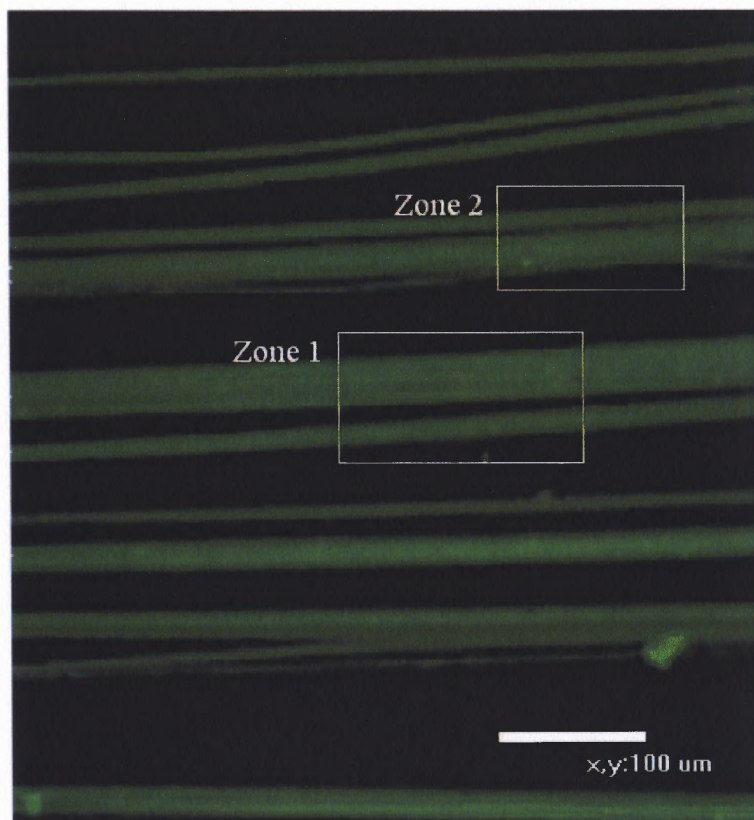
Figure 4.57 Confocal image of a region of stretched axon grown at a rate of 6 mm/day. The region shows the axon zones of interest: Zone 1 and Zone 2.
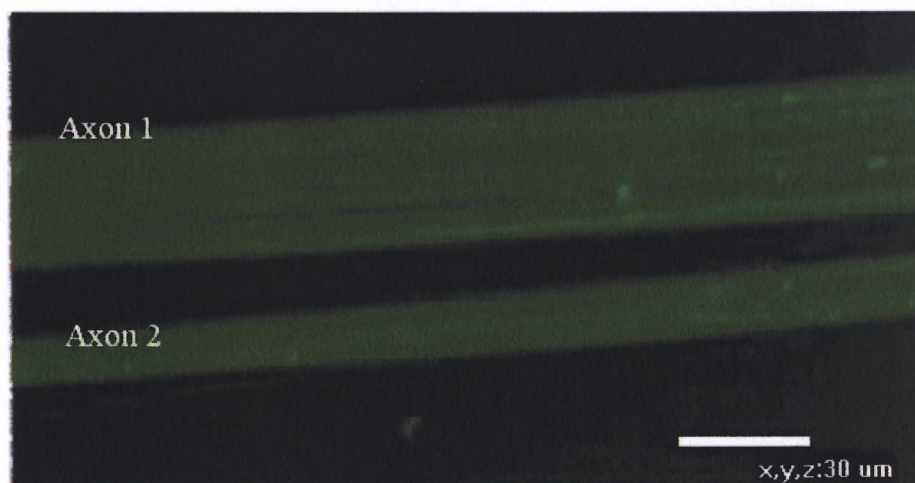
Figure 4.58 Magnified confocal image of the axons in Zone 1 of the region of axons shown in Figure 4.57. Zone 1 shows Axon 1 and Axon 2.

Figure 4.59 (a) shows the average axon width for "Axon 1" for each slice for a set of 10 slices. The x-axis represents the images numbers. Each image represents individual axon slices with a thickness of 2.2 μm. The y-axis represents the axon width in μm.

(a)   (b)
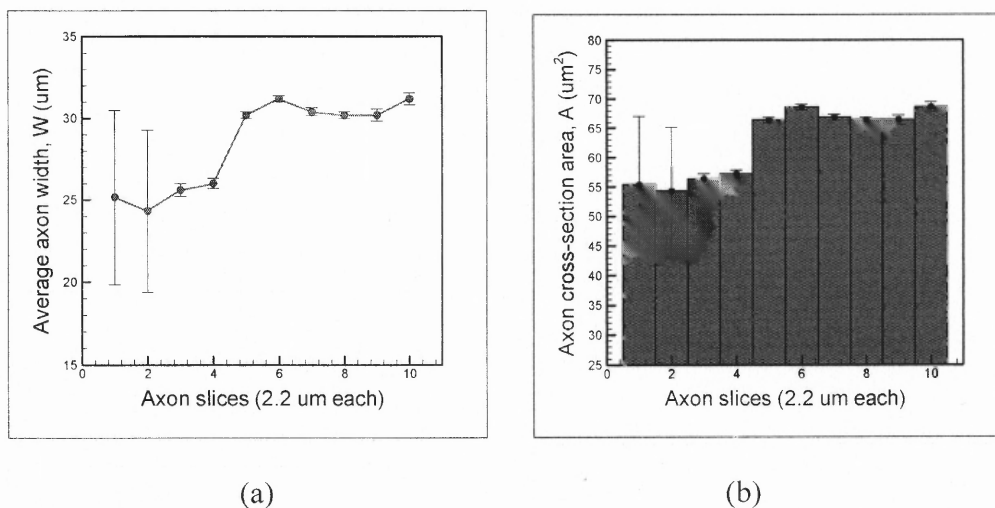
Figure 4.59 Axon 1 of Zone 1 (a) Axon bundle width for each image of individual slice of axon through the z-dimension with standard error. The x-axis represents the slice numbers having a thickness of 2.2 μm. The y-axis represents the axon width for each slice in μm. (b) Axon bundle cross-sectional area for each slice. The x-axis represents the number of slices and the y-axis represents the axon cross-section for each slice in μm^2 with error bar.

The graph shows an initial steep increase through the slices until the axon bundle width reaches a maximum and then the values gradually decreases. The standard error for the axon width for images 1 and 2 are seen to be 5.3 μm and 4.9 μm respectively. The top and the bottom slices, when imaged under the confocal microscope, are usually of lower resolution because less fluorescence light reaches the top and bottom layers. In these cases, the images being fluorescence images, adds a glow to the edges of the axons and make them appear thicker. That is why the axon width values tend to be higher for the initial and final image. The undefined axon edges also result in higher error bars for these

images. This phenomenon is observed for most cases of axons that have been quantified and are described below. Also, the axon widths in the initial images seem to be uneven, resulting in a greater error as compared to the axon widths in the images of the reference layers (middle of the slice) where the axon boundaries are clearly defined. At the reference layer, the axon bundle width reaches a maximum of 31 μm. The axon boundaries in the middle images are also clearly defined resulting is lower error: 0.2 μm for image 5, 0.24 μm for image 6 and 0.2 μm for image 7. The axon bundle width decreases in the later images showing that the width decreases through the z-dimension once the maximum is reached. The small increase in the axon bundle width at greater depths (images 8 and greater) is due to the blurry images of the fluorescence glow obtained at these sections.

Figure 4.59 (b) shows the bar graph of the axon cross-sectional area A_s, calculated for individual slices. Each slice thickness is 2 μm and the area for each bar of given by the product of the axon width and slice thickness as discussed earlier. The errors in the initial images are seen to be higher: 10.6 μm for image 1 and 9.9 μm for image 2, than the reference images: 0.4 μm for image 6. The pattern of the cross-sectional area is similar to that of the axon width, the axon cross-section being the maximum at the reference layer at 68.64 $μm^2$ and gradually decreasing to a value of 66.44 $μm^2$. The total cross-sectional area, A, as given by the sum of the areas in images 3 to 10 is calculated to be 517 $μm^2$. For the calculation of the cross-sectional area of the axon bundle, the values obtained by the initial images (image 1 and 2) are not taken into account because of the large error. Errors more than 5 μm are discarded for calculation purpose. The pattern from the axon bundle width reveals that the axon bundle is elliptical in shape.

Figure 4.60 (a) shows the average axon bundle widths for Axon 2 for each slice for a set of 10 slices. The standard error for the axon width for images 1, 2 and 3 are seen to be 0.58 μm, 0.7 μm and 0.74 μm respectively. The errors are higher than that of the middle images because of the undefined boundary regions in the initial images. It is seen that the axon bundle width gradually increases after image 3 reached a peak and then decreases. At the reference layer: image 6 (middle of the slice) axon bundle width reaches a maximum of 13.7 μm. The error here is 0.2 μm because the axon boundaries are clearly defined.

(a)   (b)
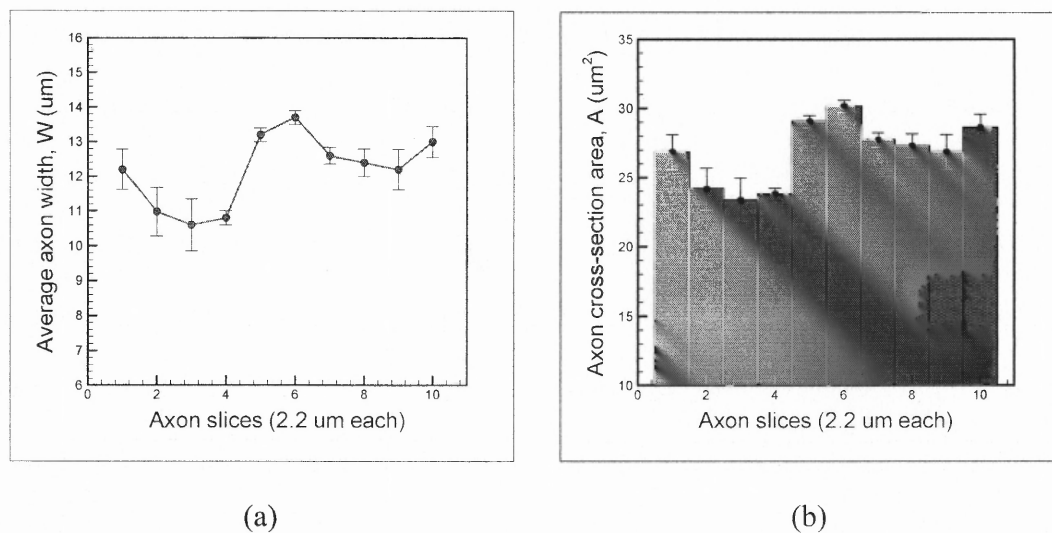
Figure 4.60 Axon 2 of Zone 1 (a) Axon bundle width for each image of individual slice or layer of axon through the z-dimension with standard error. The x-axis represents the slice numbers having a thickness of 2.2 μm. The y-axis represents the axon width for each slice in microns. (b) Axon bundle cross-sectional area for each slice. The y-axis represents the axon cross-section for each slice in μm^2 with standard error.

Figure 4.60 (b) shows the bar graph of the axon cross-sectional area for individual slices. The pattern of the cross-sectional area is similar to that of the axon width, the axon cross-section being the maximum at the reference layer at 30.14 μm^2 with an estimated error of 0.44 μm^2. Discarding the initial and the final images, because of the higher errors, the total cross-sectional area of the axon bundle is calculated to be 193.38 μm^2.

From the pattern of the values, it is observed that the axon bundle is approximately elliptical in shape through the thickness.

Figure 4.61 shows Zone 2 containing Axons 1 and 2. Zone 2 has previously been defined in the confocal image of Figure 4.57. Axon 2 is seen to split into a thinner axon bundle. For the calculations done below, this split section of the axon bundle is not taken into account because the bundle is not even throughout the images. This may lead to erroneous data. The thickness of this region as measured by the confocal microscope is 22 μm, divided into 10 slices, each 2.2 μm thick. The representation of the axon widths and the cross-sectional areas of the axon bundles shown in Figure 4.61 are discussed below.
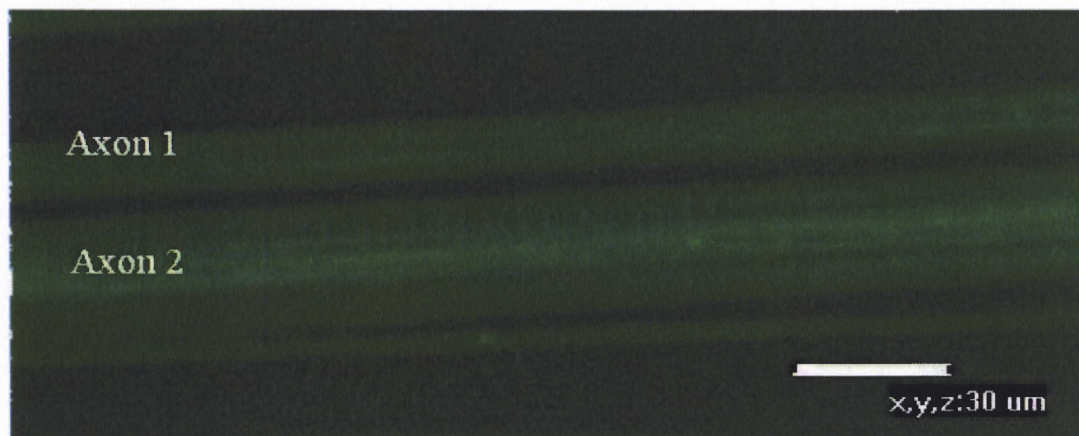
Figure 4.61 Magnified confocal image of the axons bundles in Zone 2 of the region of axons shown in Figure 4.57. Zone 2 shows Axon 1 and Axon 2. Axon 1 is the thinner axon bundle and Axon 2 is relatively thicker.

Figure 4.62 (a) shows the average axon bundle width for "Axon 1" in Zone 2 for each slice for a set of 10 slices. Unlike the axons described previously, the data represented in this graph has a minimum at image 5, 9.24 μm, and increasing axon bundle widths on either side. It can be inferred from this graph that, there may be two axons

present one on top of another, in the z-dimension in this particular layer. The points where the two axons bundles merge together, give the lowest axon width values. The errors, 0.2 μm – 0.26 μm, in these regions are also relatively less as compared to the top and bottom layers having an error of 1.35 μm and 0.68 μm, respectively. The peak value of the axon width on the either sides are 10.8 μm and 10 μms with an estimated error of 0.2 μm and 0.26 μm respectively. On either ends the axon bundle width tends to decrease.

Figure 4.62 (b) shows the graph of the axon cross-sectional areas for individual slices. The pattern of the cross-sectional area is similar to that of the axon bundle width, having a minimum of 16.93 μm^2 with an error of 1.08 μm^2 at image 6. The axon cross-section is the maximum on either side of the minimum: 21.6 μm^2 and 20 μm^2. The cross-sectional are gradually decreases through the z-dimension following a similar pattern of the axon width.

Figure 4.63 (a) shows the graphs of the width for "Axon 2" in Zone 2. The maximum axon bundle width calculated is to be 22.8 μm in image 5 (reference image) with an estimated error of 0.48 μm. On either side of the maximum the axon bundle width seems to decrease. This pattern represents that this axon bundle is circular in shape.

Figure 4.63 (b) shows the graph of the cross-sectional areas of each slice. The pattern of the cross-sectional area is similar to that of the axon width. The maximum cross-sectional area for the reference slice is calculated to be 50.16 μm^2 at image 5 with an error of 1.07 μm^2. The total cross sectional area for this axon bundle is calculated to be 388.96 μm^2.

(a)   (b)
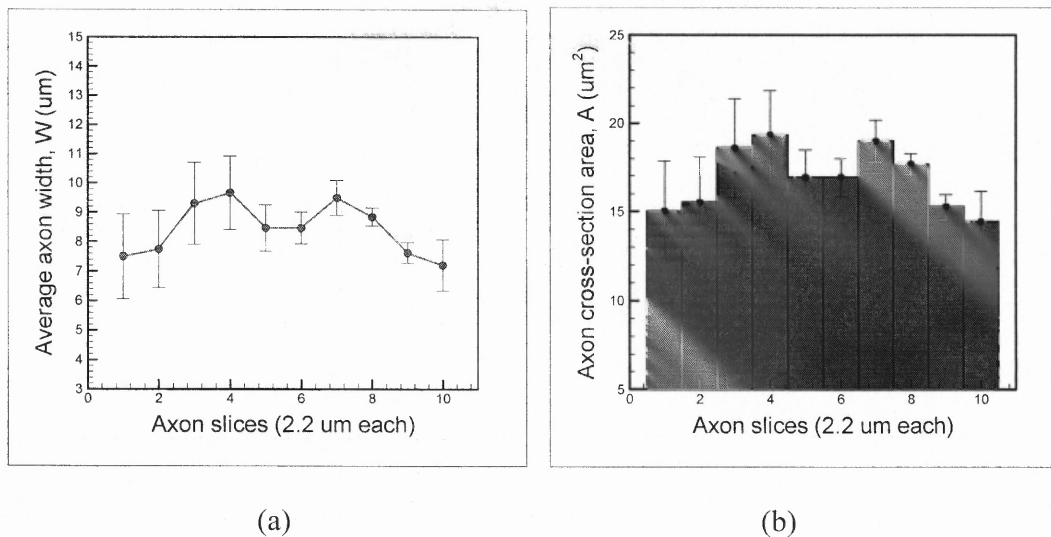
Figure 4.62 Axon 1 of Zone 2 (a) Axon bundle width for each image of individual slice or layer of axon through the z-dimension. The x-axis represents the slice numbers having a thickness of 2.2 μm. The y-axis represents the axon width for each slice in μm with error bar. (b) Axon bundle cross-sectional area for each slice. The y-axis represents the axon cross-section for each slice in μm^2 with error bars.

(a)   (b)
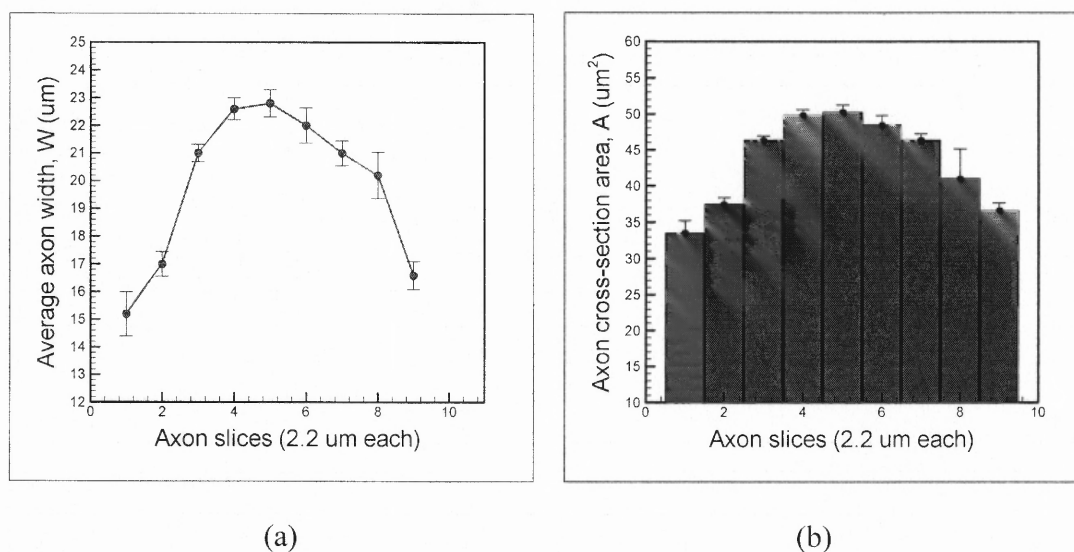
Figure 4.63 Axon 2 of Zone 2 (a) Axon bundle width for each image of individual slice or layer of axon through the z-dimension. The x-axis represents the slice numbers having a thickness of 2.2 μm. The y-axis represents the axon width for each slice in μm with error bars. (b) Axon bundle cross-sectional area for each slice. The y-axis represents the axon cross-section area for each slice in μm^2 with error bar.

4.3.2 Axons Stretched Grown at a Rate of 1 cm/day

Figure 4.64 is the confocal image of region of axon bundles stretched at a rate of 1 cm/day. The region consists of both thin and thick axon bundles. As shown in the image, Zone 1 and Zone 2 are defined in the figure. Quantification is carried for the axon bundles in the respective zones and the results are discussed below.

Figure 4.65 show the magnified confocal image of Zone 1 defined in Figure 4.64. Three axon bundles, Axon 1, Axon 2, and Axon 3 are seen here. This image is the reference layer of the axons where maximum resolution is obtained and thus the boundaries of the axons are well defined.
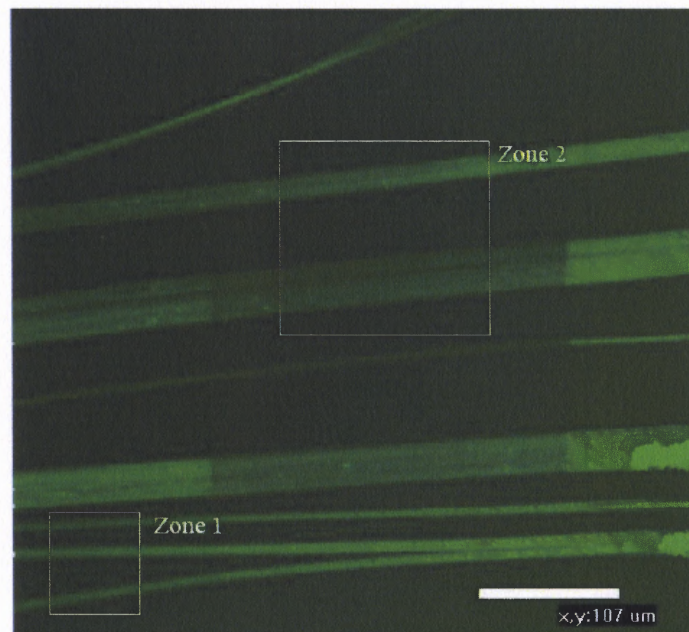
Figure 4.64 Confocal image of a region of axon stretched grown at a rate of 1 cm/day. The region shows the axon zones of interest: Zone 1 and Zone 2. Axon width and axon cross-sectional area for each zone is calculated using the EZ software.

By means of the confocal imaging software this zone of axons has been sliced into 23 layers in the z dimension to observe the axon bundle profile along the z-dimension resulting in a thickness of 1.0 μm for each slice.
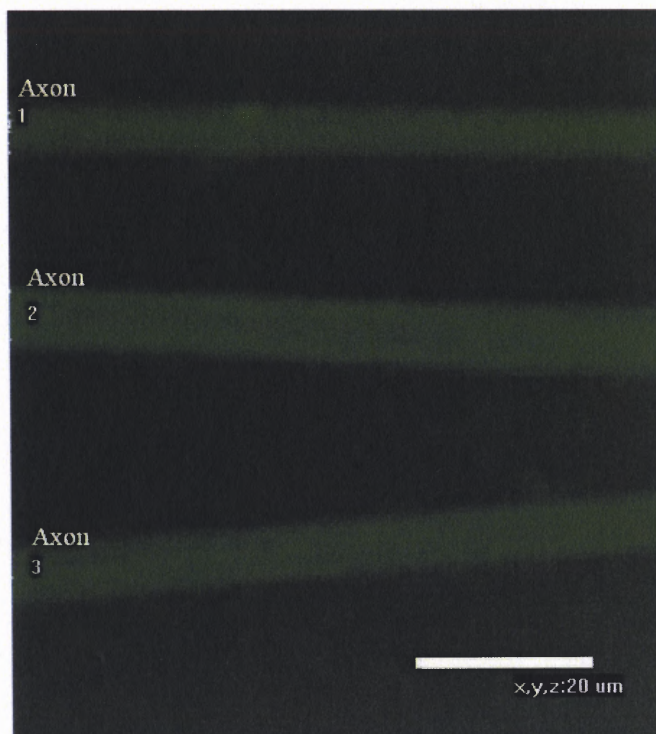
Figure 4.65 Zone 1: Magnified confocal image of the axons in zone 1 of the region of axons shown in Figure 4.64. Zone 1 shows Axon 1, Axon 2 and Axon 3.

Figure 4.66 (a) shows the graphs of the width for Axon 1 in Zone 1. Axon bundle width is calculated for a set of 23 images with slice thickness of 1 μm. The maximum axon bundle width calculated is 6.1 μm in image 8 with an estimated error of 0.06 μm. On either side of the maximum the axon width is seen to decrease to 4.62 μm in image 2 having an estimated error of 0.5 μm, and 3.82 μm for image 22 with an error of 0.21 μm. This pattern represents a circular shape of the axon bundle.

Figure 4.66 (b) shows the graph of the cross-sectional area of each slice. The pattern of the cross-sectional area is similar to that of the axon width. The maximum cross-sectional area is calculated to be 6.1 μm^2 for image 8 with an error of 0.06 μm^2. The sum of the cross-sectional areas for all the images gives the cross-sectional area for the axon bundle as 122.78 μm^2.
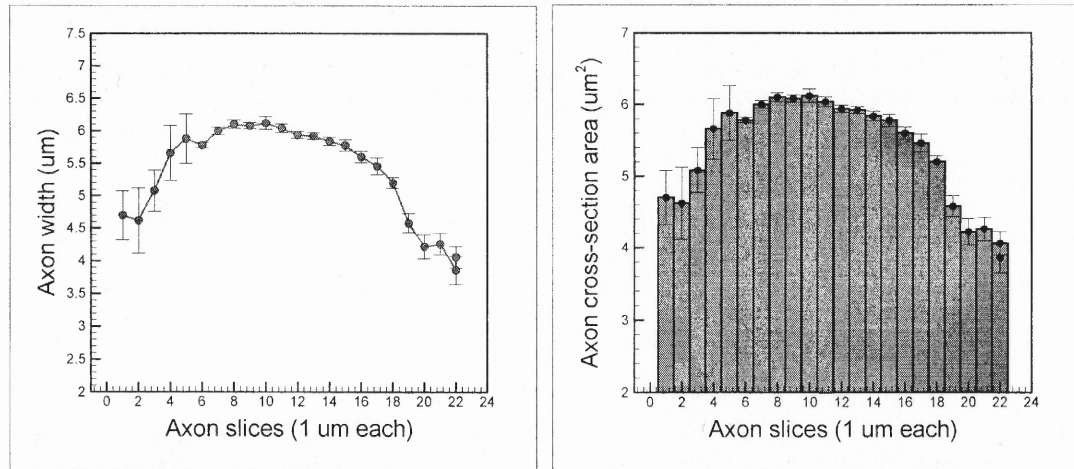
(a)   (b)

Figure 4.66 Axon 1 of Zone 1 (a) Axon bundle width for each image of individual slice of axon through the z-dimension with error bar. The x-axis represents the slice numbers having a thickness of 1 μm. The y-axis represents the axon width for each slice in μm. (b) Axon bundle cross-sectional area for each slice with standard error. The y-axis represents the axon cross-section for each slice in μm².

Figure 4.67 (a) shows the graphs of the width for Axon 2 in Zone 1. Axon bundle width is calculated for set of 23 images with slice thickness of 1 μm. The maximum axon bundle width calculated is to be 8.12 μm in image 16 with an estimated error of 0.02 μm. The errors for the initial (1 to 5) and final (18 to 24) images are higher than the middle images because of the undefined edges of the axon bundles. Figure 4.67 (b) shows the graph of the cross-sectional area of each slice which follows the pattern of the graph for the axon width. The maximum cross-sectional area is calculated to be 8.12 μm² for image 16 with an error of 0.02 μm². The cross-sectional area for the axon bundle given by the sum of cross-sectional areas for all the images is 164.47 μm². The shape of the axon is elliptical.

(a) (b)

Figure 4.67 Axon 2 of Zone 1 (a) Axon bundle width for each image of individual slice of axon through the z-dimension with error bar. The x-axis represents the slice numbers having a thickness of 1 μm. The y-axis represents the axon width for each slice in μm. (b) Axon bundle cross-sectional area for each slice with standard error. The y-axis represents the axon cross-section for each slice in μm^2.

Figure 4.68 (a) shows the graphs of the width for Axon 3 in Zone 1. Axon width is calculated for set of 23 images with slice thickness of 1 μm. The errors for the initial (1 to 5) and final (18 to 24) images are higher than the middle images because of the undefined edges of the axon bundles. The maximum axon width calculated is to be 5.94 μm. The pattern of the graph shows an elliptical axon width for the images through the z-dimension when compared to the previous graphs. Figure 4.68 (b) shows the graph of the cross-sectional area of each slice which follows the pattern of the graph for the axon width. The maximum cross-sectional area is calculated to be 5.94 μm^2. The axon bundle cross-sectional area, given by the sum of cross-sectional areas for all the images, is 136.26 μm^2.

(a)   (b)
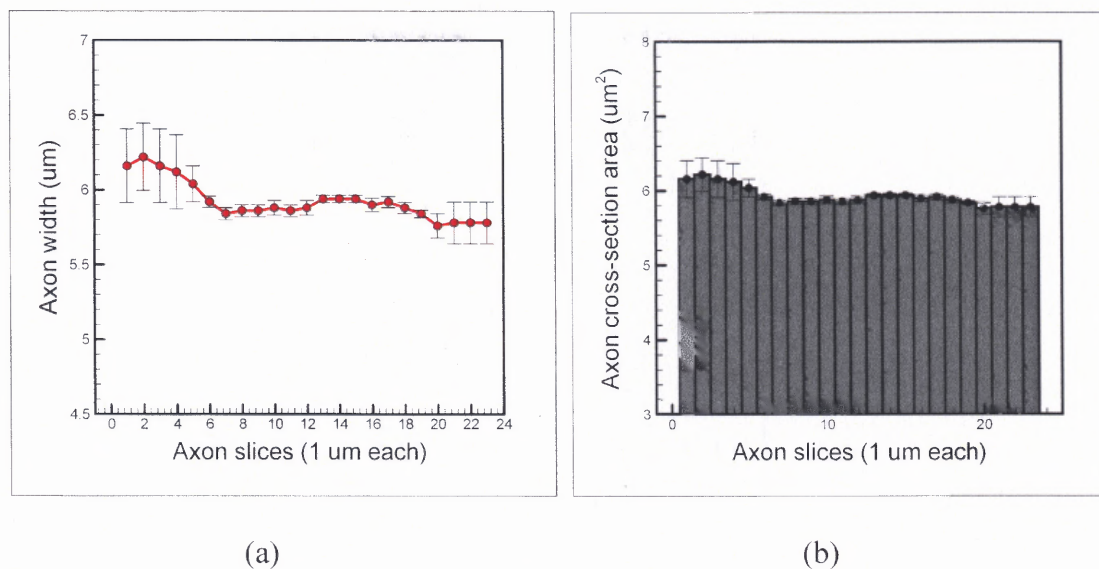
Figure 4.68 Axon 3 of Zone 1 (a) Axon bundle width for each image of individual slice of axon through the z-dimension with error bar. The x-axis represents the slice numbers having a thickness of 1 μm. The y-axis represents the axon width for each slice in μm. (b) Axon bundle cross-sectional area for each slice with standard error. The y-axis represents the axon cross-section for each slice in μm^2.
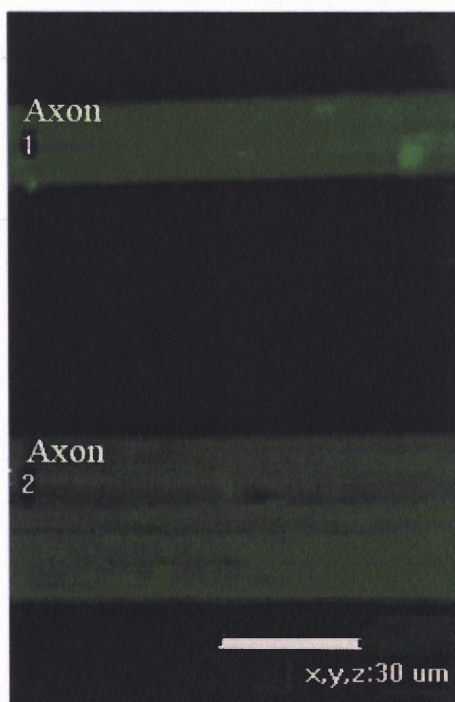
Figure 4.69 Zone 2: Magnified confocal image of the axons bundles in Zone 1 of the region of axons shown in Figure 4.64. Zone 2 shows Axon 1, and Axon 2.

Figure 4.69 show the magnified confocal image of zone 2 defined in Figure 4.64. Two axon bundles, Axon 1, and Axon 2 are seen here. This image is the reference layer of the axons where maximum resolution is obtained and thus the boundaries of the axons are well defined. By means of the confocal imaging software this zone of axons has been sliced into 10 layers in the z dimension to observe the axon bundle profile along the z-dimension resulting in a thickness of 3 μm.

Figure 4.70 (a) shows the graphs of the width for Axon 1 in Zone 2. Axon bundle width is calculated for set of 10 images with slice thickness of 3 μm. The maximum axon bundle width calculated is to be 16 μm in image 6 (reference image). On either side of the maximum the axon width is seen to decrease. However, the top and bottom images have a higher estimated error: (2.4 μm for image 1, 2.5 μm for image 2 and 0.6 μm for image 10) in comparison to the middle images (0.25 μm for image 5 and 0.0 μm for image 6) because of the undefined edges of the axon bundles in the images.

Figure 4.70 (b) shows the graph of the cross-sectional area of each slice which follows the pattern of the graph for the axon bundle width. The maximum cross-sectional area is calculated to be 48 μm^2 for image 6. The cross-sectional area for the axon bundle given by the sum of cross-sectional areas for images is 433.3 μm^2.

Figure 4.71 (a) shows the graphs of the width for Axon 2 in Zone 2. Axon bundle width is calculated for set of 10 images with slice thickness of 3 μm. The maximum axon bundle width calculated is to be 34.6 μm in image 6 (reference image) with an estimated error of 0.24 μm. On either side of the maximum the axon bundle width is seen to decrease. The axon width in seen to gradually increase, reach a maximum, and then gradually decrease to a value of 32 μm.

(a) (b)
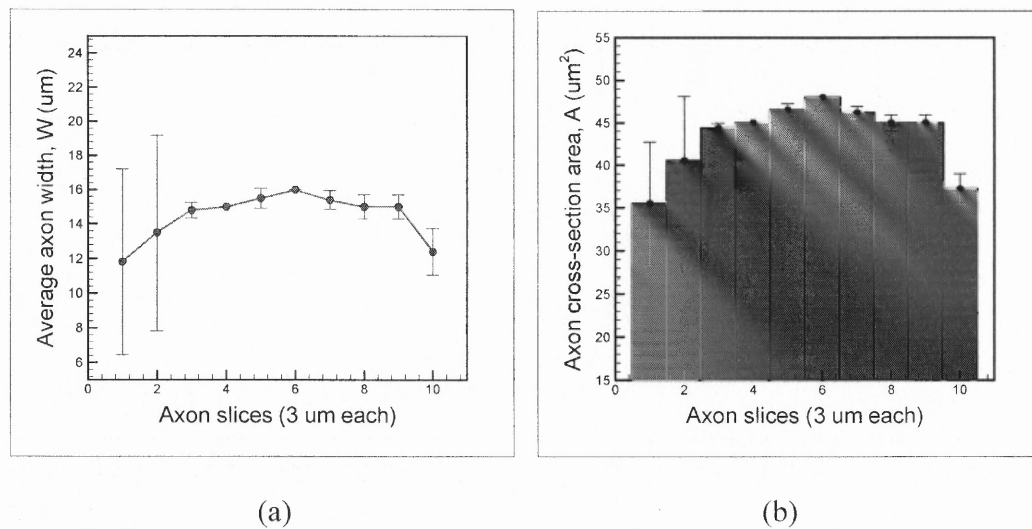
Figure 4.70 Axon 1 of Zone 2 (a) Axon bundle width for each image of individual slice of axon through the z-dimension with error bar. The x-axis represents the slice number having a thickness of 3 μm. The y-axis represents the axon width for each slice in μm. (b) Axon bundle cross-sectional area for each slice with standard error. The y-axis represents the axon cross-section for each slice in μm^2.

(a) (b)

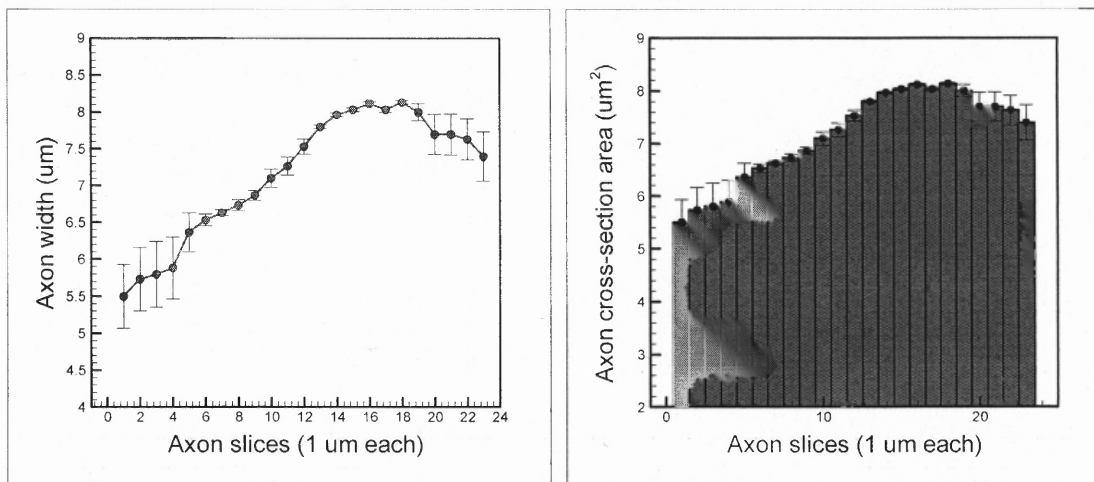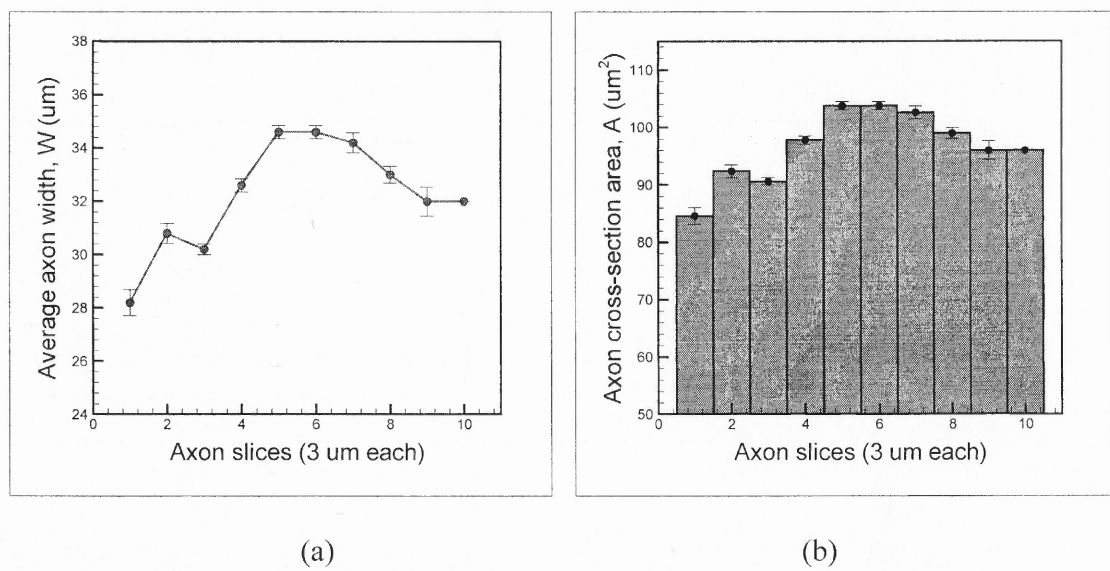**Figure 4.71** Axon 2 of Zone 2 (a) Axon bundle width for each image of individual slice of axon through the z-dimension with error bar. The x-axis represents the slice numbers having a thickness of 3 μm. The y-axis represents the axon width for each slice in μm. (b) Axon bundle cross-sectional area for each slice with standard error. The y-axis represents the axon cross-section for each slice in μm^2.

Figure 4.71 (b) shows the graph of the cross-sectional area of each slice which follows the pattern of the graph for the axon width. The maximum cross-sectional area is calculated to be 103.8 μm^2 for image 6. The cross-sectional area for the axon bundle given by the sum of cross-sectional areas for images 1 to 8 is 774.6 μm^2. The axon profile is seen to be circular.

Axon bundles stretched using the existing 2D stretch growth device has been imaged using the confocal microscopy. Quantification of the axon width using the Nikon EZ-C1 3.20 FreeViewer has been carried out for various axon bundles. The following table summarizes the axon profiles observed.

Table 4.2 Axon Bundle Cross-sectional Area and Axon Bundle Profile

Axon region	Total Cross-sectional area, A (μm^2)	Axon Profile
6 mm/day		
zone 1, axon 1	517.0	elliptical
zone 1, axon 2	193	elliptical
zone 2, axon 1	-	joined
zone 2, axon 2	388.96	circular
1 cm/day		
zone 1, axon 1	122	circular
zone 1, axon 2	164.47	elliptical
zone 1, axon 3	136.26	elliptical
zone 2, axon 1	433.3	elliptical
zone 2, axon 2	774.6	circular

From the patterns observed in the images through the thickness of the axon bundles, it can be inferred that most stretched axon bundles are somewhat elliptical in shape. Figure 4.72 summarizes the interpretation method. If the pattern seen is somewhat linear, the axon bundle is considered to be elliptical in shape through the cross-section. If

the pattern resulted in a curve with a maximum that was much higher than the initial and final values, the shape of the axon bundle is considered to be circular through the cross-section. A few bundles have two conjoined axons one on top of each other as seen in Figure 4.62. Other bundles seem to have a circular width throughout the thickness of the tissue as seen in Figure 4.68. Some axons are seen to split into a thin and a thick axon and this may lead to different values of the axon width depending upon which region of that particular axon is viewed. It is seen that the rate of axon stretch does not have an effect on the cross-sectional area of the axon bundles as seen in Table 4.2. The axon cross section varies from approximately 122 μm^2 to approximately 774.6 μm^2
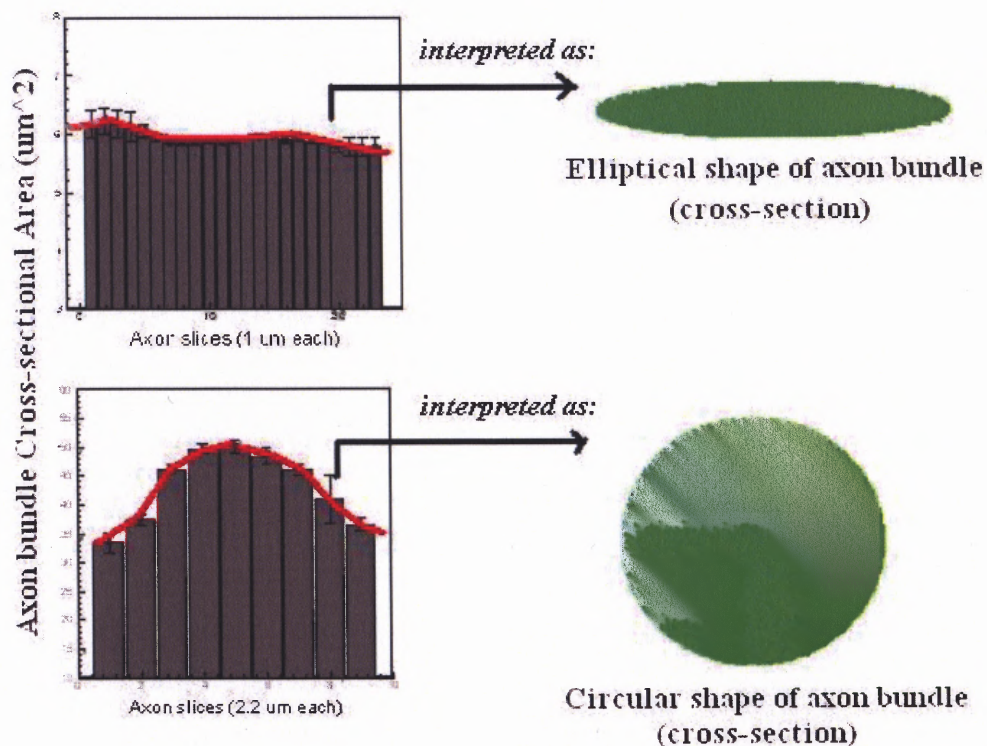
Figure 4.72 Interpretation of the shape of the axon bundles depending upon the pattern of the cross-sectional area.

Each axon bundle is made up of several axons. The quantification carried out above gives a preliminary idea of the cross-sectional area of axon bundles that result in 2D stretching. The more the area of the axon bundle, the more number of axons it has. A similar method of quantification can be used for measuring the axon bundle cross-sectional area for axons stretched using the 3D device. Measurement of the cross-sectional area of the 3D axon bundles would give us an insight into how the profile of axon bundles change during the process of stretching. If the axon bundle cross-sectional area (calculated using the above method) increases during the process of elongation, then we can interpret that the number of axons in the bundle is increasing for the 3D stretch growth and hence, the density of axons increase for the 3D setup.

It is believed that the EZ-C1 FreeViewer software gives room for erroneous data as it involves a manual process to define the region of interest. The average value and the standard error has been calculated but there still remains a certain degree of inaccuracy. In order to overcome the errors, a Matlab Image Analysis Program can be used. The program is under development by Yi Guo, Graduate student of the Biomedical Engineering Department at the New Jersey Institute of Technology. The Matlab program will allow for multiple image analysis simultaneously, generating an average width value of each axon bundle for individual 2D images.

4.3.3 Measurement of Axon Density Across a Region

The above sections describe the method of calculation for axon bundle cross-sectional area. The cross-sectional area of the axon bundles determine the density of axons, as discussed earlier. An alternative method to quantify the density of axon involves

calculating the coverage of a given area by axon bundles. This coverage can be quantified by calculating the ratio of the total cross-sectional area covered by axon bundles to the cross –sectional area of the region under consideration.

As done previously, the thickness range of a particular region of stretched axons is sliced in the z-dimension. Using the method of calculation described above, the cross-sectional area, A, of all the axon bundles visible in the region is calculated. The total cross-sectional area, covered by all the axon bundles in a given region, $T_{axon\text{-}bundles}$, is given by the sum of the individual cross-sectional areas, A, of each axon bundles as:

$$T_{axon-bundles} = \sum A \qquad (4.3)$$

Here, A is the cross-sectional area for each axon bundle and $T_{axon\ bundles}$ is total cross-sectional area of all the axon bundles.

The dimension of each region is found using the EZ-C1 FreeViewer software. The product of the dimension, y, of the region and the thickness of each slice, z, yields the cross—sectional area, Y, of the given region for each slice. The sum of the cross sectional areas for each slice, in turn, gives the total cross-sectional area of the region, T_{region}.

$$Y = y.z \qquad (4.4)$$

$$T_{region} = \sum Y \qquad (4.5)$$

Here, y is the dimension of the region, z is the thickness of each slice and Y is the cross-sectional area of the region for each slice. T_{region} is the total cross-sectional area of the region under consideration.

Thus, the percentage, P, of the area covered by all the axon bundles to that of the given region is calculated by:

$$P = (T_{axon-bundles} / T_{region}) * 100 \qquad (4.7)$$

Here, $T_{axon\ bundles}$, is the cross-sectional area covered by the axon bundles, T_{region} is the total cross-sectional area of the region under consideration, and P is the percentage of cross-sectional area covered by axon bundles to that of the given region.

Using the above method, two samples of axon regions have been analyzed as explained below. The percentage of axon coverage is calculated through the middle of each sample. By means of the confocal imaging software, the region of axons, Region 2 (as shown in Figure 4.73 (a)) has been sliced into 8 layers in the z dimension resulting in a thickness of 4.1 µm for each slice. For each image, the axon width, w, is calculated along the line specified in Figure 4.73 (a). This is done to ensure that a particular cross-sectional area across the region is analyzed, where the axons are uniform in shape through the z-dimension.

Figure 4.73 (b) shows the graph of the axon widths for all the axon bundles visible in the region in each slice. Figure 4.73 (c) gives the graph for the cross-sectional area, A, of individual axon bundles through the z-dimension. Using the method of calculation explained in Section 4.3.1, the sum of all the cross-sectional area is calculated to be 6776.89 µm². The cross-sectional area of the region under consideration is calculated to be 13677.6 µm². The percentage, P, of the area covered by the axon bundles to that of the region is found to be 49.54 %.

The region of axons, Region 2, (as shown in Figure 4.74 (a)) has been sliced into 8 layers in the z dimension resulting in a thickness of 3.05 µm. For each image, the axon

width, w, is calculated along the line specified in Figure 4.74 (a). This is done to ensure that a particular cross-sectional area across the region is analyzed, where the axons are uniform in shape through the z-dimension.

Figure 4.74 (b) shows the graph of the axon widths for all the axon bundles visible in the region in each slice. Figure 4.74 (c) gives the graph for the cross-sectional area, A, of individual axon bundles through the z-dimension. The sum of all the cross-sectional area is calculated to be 5807.81 μm^2. The cross-sectional area of the given region is calculated to be 16561.5 μm^2. The percentage, P, of the area covered by the axon bundles to that of the entire region then found to be 35.07 %.

The above method gives a good comparison for the area covered by the axon bundles in a defined region of interest. This technique may be applied across the entire width of the tissue spanned by stretched axons to exactly measure the area covered by axon bundles. The more the percentage of the region covered by stretched grown axons, the more is the axon density. Axons stretched in 3D cultures can also be quantified in a similar way. Since this method takes the z-dimension of the tissue into account, the axon bundles through multiple planes, as produced by the 3D cultures, can be measured properly.
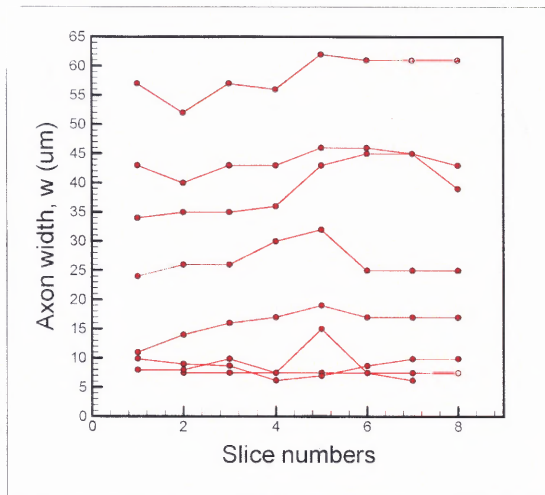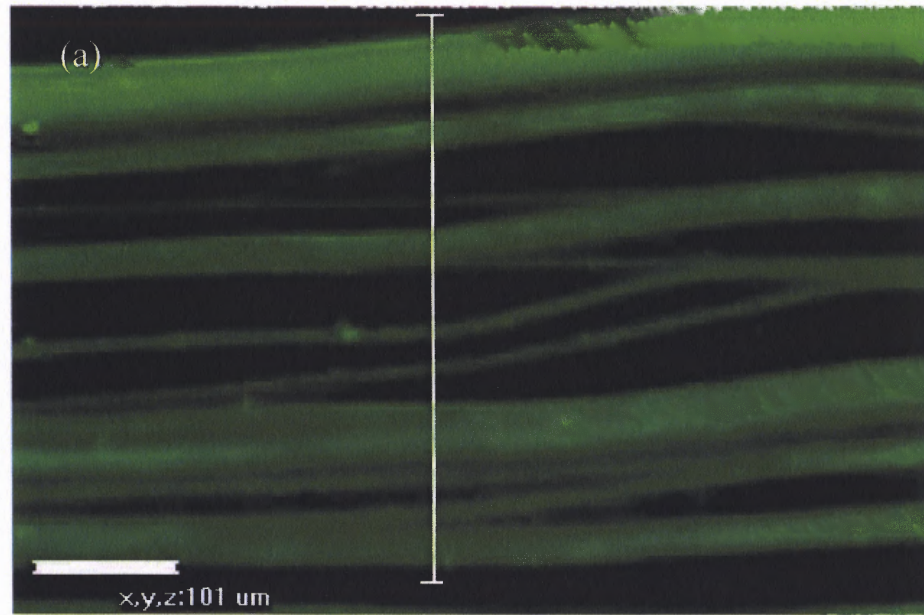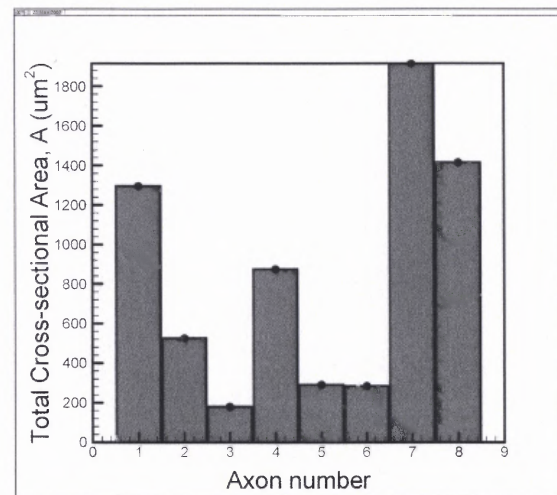
Figure 4.73 (a) Confocal image of Region 1 of axons stretched using the 2D device. (b) Axon bundle width for all the axon bundles visible in the region is plotted for each image. The x-axis represents the slice numbers and the y-axis represents the axon width in μm. (c) The total cross-sectional area for each axon bundle. The x-axis shows the axon number and the y-axis shows the cross-sectional area of each axon bundle through the z-dimension in μm^2.
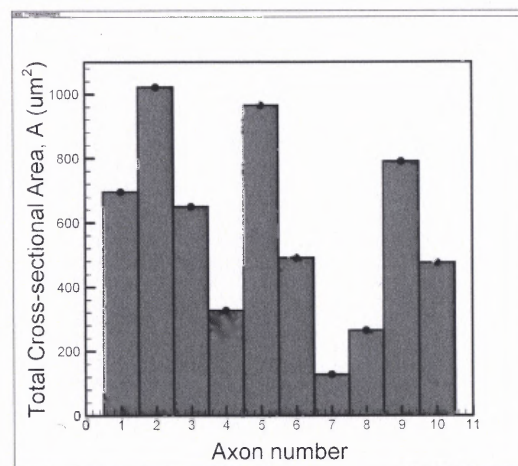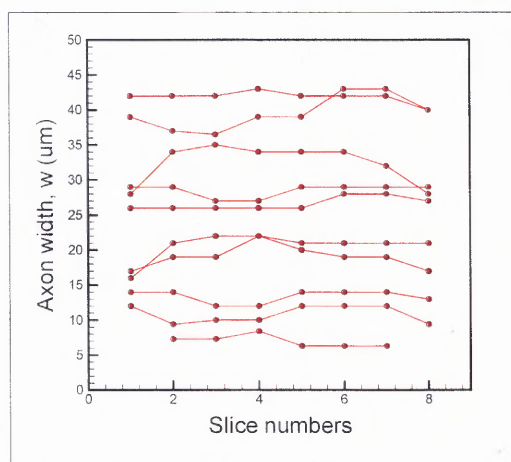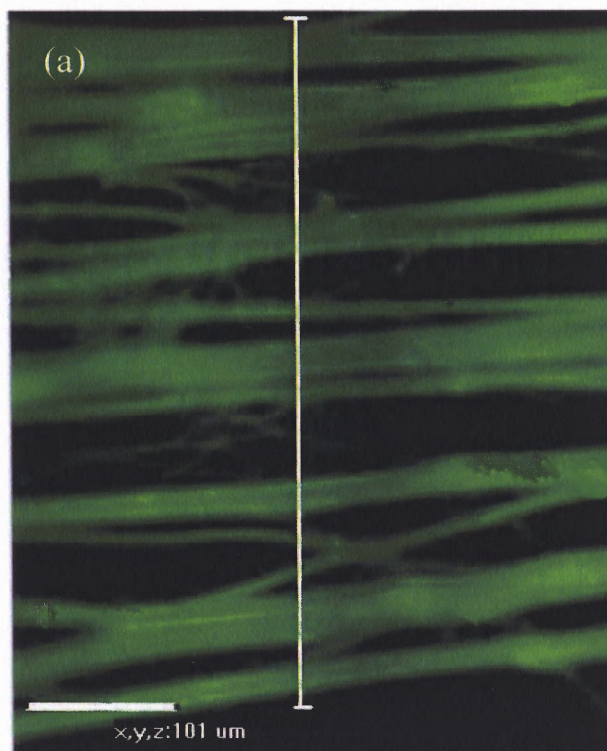
Figure 4.74 (a) Confocal image of Region 2 of axons stretched using the 2D device. (b) Axon bundle width for all the axon bundles visible in the region is plotted for each image. The x-axis represents the slice numbers and the y-axis represents the axon width in μm. (c) The total cross-sectional area for each axon bundle. The x-axis shows the axon number and the y-axis shows the cross-sectional area of each axon bundle through the z-dimension in μm^2.

4.4 Summary

Axons bundles stretched using the existing 2D stretch growth device has been imaged using the confocal microscopy. Using the Nikon EZ-C1 3.20 FreeViewer, the average axon width for each image of the slice through the axon bundle has been measured and the error for each calculation has been estimated for each value. The cross-sectional area of axon bundles have been calculated by the sum of the area for each image through the slice. The values have been graphed and the patterns observed confer that most axon bundles are circular or elliptical in shape when stretch grown. It can also be seen that the rate of axon stretch growth does not have an affect on cross-sectional area.

The observations about the axon bundle width and axon bundle cross sectional area give insight into the axon profile of stretch-grown axons, which can be a powerful tool in calculating the axon density of axons grown using the 2D verse the 3D system as discussed above.

CHAPTER 5

CONCLUSIONS AND FUTURE WORK

5.1 Conclusions

This section of the thesis highlights the main conclusions drawn on the basis of the work done so far on the modifications of the 2D axon stretch growth device to accommodate axons to be stretched in 3D cultures.

The 2D axon stretch growth device involves an *in vitro* tissue engineering method to rapidly elongate numerous axon bundles under the application of mechanical forces. The forces from stretching induce the longitudinal growth of axons at rates up to 1cm/day in comparison to the growth rate of axons by a growth cone which is approximately 1mm/day. Using the device axons can be stretched to a desired length of upto 10 cm in length at varying rates. The design of the existing 2D stretch growth device has been discussed in details in Chapter 1.

While the uni-axial axon growth achieved with the 2D system is fast and efficient there still remain a few limitations to this technique. Currently, axon stretch growth in 2D procedure is optimized and the stretch-growing axons from DRG cultures are at maximal density. Increasing the number and density of axons is required to optimize the final nerve construct formed by the stretched axons, as discussed previously. For this purpose, axons stretched in 3D cultures are required as the DRG explants will be distributed uniformly. The 3D cultures will add depth to the culture to allow axons to cross the interface in multiple planes.

In a transplantation study, stretch grown axons from the 2D system were supported in collagen hydrogel and rolled into a cylindrical structure to form a 3D construct. It was found that this procedure did not provide the mechanical stability for surgical purposes. Specifically, the extensive manipulation of axons in culture increased the potential of damaging the nervous tissue. The 3D cultures can solve this limitation as the final 3D culture can be matched to the geometrical confines of the rat spinal cord and eliminate the need to roll the 2D culture into a 3D construct. The mechanical properties of the 3D construct formed can be varied by forming a stiff hydrogel around the stretch grown axons just prior to transplantation.

The goal of this research is to increase the density and the total number of axons in the nerve construct. This will provide more nervous tissue for transplantation. This thesis explains the modifications made to the existing 2D axon stretch growth device to accommodate stretch growth of axon in 3D cultures. It is believed that 3D neuron cultures may help to improve the number and density of axons by allowing axons to grow in multiple planes at the same time thereby providing an improved transplantable nerve construct.

In order to design a functional 3D system, the modifications include two individual components: an attached component, which is kept stationary, and a towing component that separates two halves of the 3D neuronal culture. The complete design of the 3D axon stretch growth device has been described in details in Chapter 3. Collagen hydrogel forms the basis of the 3D cultures. The cultures in hydrogel are held in each component and the multiple layers of explants in the 3D cultures are physically separated by a biocompatible Nylon mesh. The mesh also preserves axon outgrowth from one

population of the neural culture into the other yet constrain the two half of the cultures inside each component. The essential parameters of the design are: (1) the dimensions of the 3D components (2) choice of the hydrogel for 3D culture (3) the porosity of the Nylon mesh used to separate the 3D cultures.

Experiments have been carried out to test the various parameters. The details of the experiments and the observations are discussed Chapter 3. The dimensions of the components are designed to fit against each lane and also help distribute the DRG explants uniformly throughout. The depth of each component is kept minimal so that DRG explants are dispersed more towards the front end, closer to the mesh to enable axons to grow efficiently across the mesh to the population of neurons on the other half of the 3D culture.

The functions and the purpose of the hydrogel are to support the DRG explants, provide nourishment and hold the 3D cultures in place inside each component. The mechanical properties of the hydrogel determines (1) the rate of axon outgrowth and (2) the mechanical stability. Both lower concentration gels (0.6mg/mL – 0.8mg/mL) and higher concentration gels (2mg/mL and 3.2mg/mL) have been tested in each component. Lower concentration gels are seen to leak out through the Nylon mesh unlike the higher concentration gels that are seen to maintain its structure. Leaking of the hydrogel is not preferred because it causes the 3D cultures to mix and no longer be separate. As such the higher concentration gels (2mg/mL and 3.2mg/mL) are used in the components it is able to suspend the DRG neurons.

Collagen hydrogel concentration of 2.0mg/mL and 3.2 mg/mL are tested with the "*medium*" and "*fine*" pore size Nylon mesh. Experimental observations show that

collagen hydrogel concentration does not affect the number of axons growing through the either pore size of the mesh but influences the rate of axon outgrowth and the time point.

The rate of axon growth through the mesh is slower in the stiffer hydrogel (3.2 mg/mL collagen concentration) when compared to the less stiff one (2.0 mg/mL). As seen from the phase contrast and the fluorescent images presented in Chapter Three, 2.0 mg/mL collagen hydrogel encourages a good rate of axon growth through the Nylon mesh of either pore size.

Time point is an important factor because it allows the time for axons to fully grow between the two 3D cultures and also determines when to start the elongation process. From the experimental observations described in Section 3.2.2, it can be concluded that the time it takes for all the axons to completely grow through the mesh is day 7. Axons from the DRG explants close to the mesh grow through within a period of 5 days. However, in order for the axons (originating from the DRG explants further away from the mesh) to cross the mesh, a period of one week is required. In all the images presented in Section 3.2.2, it can be seen that on day 7 the number and density of axons growing through the Nylon mesh is the optimal.

The Nylon mesh pore sizes of *fine* pore size (104 x 104 treads per inch or 50 μm x 50 μm) and *medium* pore size (30 x 30 treads per inch or 160 μm x 160 μm) are considered for the design. The pore sizes determine the number and density of axons growing between each pair of 3D components.

The Nylon mesh pore size has an evident effect on the number and density of axons growing through the mesh. Images presented in Section 3.2.2 exhibit that the *"fine"* pore size of the Nylon mesh obstructs the number of axons growing through the mesh

and so the density of axons on the opposite side of the mesh remains a lot less than that compared to the density around the DRG explants. The "*medium*" pore size, being bigger poses fewer barriers against axon outgrowth and allows almost all axons to grow through the mesh resulting in an equal density of axons on either side of the mesh. Hence, for the 3D design purpose, the "medium" pore size Nylon mesh optimizes the density of axons inbetween the two halves of the 3D cultures.

Using the optimal parameters, preliminary experiments have been run with the 3D axon stretch growth device. Cell culture protocol using the 3D axon stretch growth device has been established. Using the 3D system, axons have been stretched to 1cm and 0.6 cm in length at a rate of 1mm/day. This shows that the 3D components are able to stretch axons in the fashion discussed above.

In order to determine whether axons stretched in 3D increases the number and density of axons, as intended, the next step to this work involves the quantification of axons grown using the 3D system. However, before the quantification of the 3D stretch grown axons can be carried out, it is important to understand the axon profile of axon stretched using the 2D device and form a basis of comparison for the 3D stretched axons. Thus, axons in two separate samples, stretched using the existing 2D device (6 mm/day and 1 cm/day), have been quantified using confocal microscope. The method of imaging and calculation has been described in details in Chapter 4. The cross-sectional area of axon bundles have been calculated using the Nikon EZ-C1 3.20 FreeViewer. From the patterns of the axon width obtained it can be seen that axons are mostly elliptical and circular in shape. The axon cross section varies from approximately 122 μm^2 to

approximately 774.6 μm^2. No difference in the axon profile is seen for axons stretched at different rates.

The following section of this chapter discusses the future work that may be carried out to optimize the 3D design and to quantify the axons grown using the 3D system.

5.2 Future Work

The goal of the 3D modifications made to the existing 2D axon stretch growth device, is to improve the number and density of axons by allowing axons to grow in multiple planes at the same time thereby providing an improved transplantable nerve construct. The 3D components have been designed and the parameters have been optimized as discussed earlier. The 3D axon stretch growth device has shown to successfully stretch axons in 3D cultures.

The next step to this work involves the optimization of the 3D axon stretch growth device so as to fit the confines of the rat spinal cord and to determine whether the 3D system improves axon density.

Optimization of the design of the 3D components may help to make the process of 3D growth more efficient. From the experimental observations it is seen that for the axons originating from the DRG neurons that are further from the mesh take longer to grow through. In order to shorten the time frame and allow most axons to grow through the mesh, the depth, d, of each component can be further reduced to 1.5 mm instead of 3

mm. This will allow more DRG neurons to be pushed towards the mesh in a uniform fashion. This in turn will help increase the number of axons growing through the mesh.

Experimental observations show that the Nylon mesh of *"medium"* pore size allows most number of axons to grow through the 3D cultures and establishes a continuous flow of axons from one half of the culture to the other. However, during cell culture, the *"medium"* pore size of the Nylon mesh allows the culture media to flow out of the components because of the bigger pore size. As a result, media had to pipetted on top of the hydrogel inside each component every day. In order to prevent this, in the future 3D design, the height, h, of the 3D components can be decreased to 4 mm instead of 8 mm. This will make the components sit lower than the height of each lane of the base frame which is 5 mm. When the lane is filled, the media will form a trough and the components will be submerged in media. The DRG cells inside the hydrogel of each component will then be exposed to sufficient culture media.

Once the DRG cells are plated in the hydrogel in each component, the growth of the axons in the 3D cultures cannot be viewed under the microscope. This is because the base of the attached and the towing 3D components is made of PEEK plastic that is opaque and does not allow light to pass through. Hence, axon outgrowth from one half of the culture to the other through the Nylon mesh cannot be viewed once inside the components. In order to overcome this problem, the base of the future 3D components can be made out of glass. Glass being transparent will allow light to pass through and thus the axon outgrowth inbetween two halves of the culture can be properly viewed. This will also help to visualize the health of the culture and determine axon outgrowth inbetween each culture halves.

In order to quantify axons grown in 3D cultures, a similar method of quantification to the 2D, can be used. Axons grown using the 3D system can be fixed and labeled using the standards protocol of Immunocytochemistry as described in Section 4.2. Axons then can be cut away from the Nylon mesh and mounted between glass cover slips, in order to combine all the planes of axons onto a single 2D plane to create an axon sample similar to the ones prepared for the 2D system. The 3D axon samples can be viewed and imaged. The confocal microscope can help take images of the slices through the thickness of axon bundles. The cross-sectional area of axon bundles across the entire tissue can be calculated using thicker slice thickness. The ratio of the sum of all the axon bundle cross-sectional areas to that of the given region will yield an estimate of the regions in the tissue covered with axons.

Measurement of the cross-sectional area of the 3D axon bundles would give us an insight into how the profile of axon bundles change during the process of stretching. As mentioned earlier, each axon bundle is made up of numerous axons. If the axon bundle cross-sectional area increases during the process of elongation, then we can interpret that the number of axons in the bundle is increasing for the 3D stretch growth. The comparison of the values of the axon bundle cross-section area would show whether axons stretch grown in 3D yield similar area of cross sectional for axon bundles. If the area tend to be larger, then we can interpret that there are more axons in each axon bundle, hence, a higher axon density. It can be used to compare the axon bundle profiles for the 2D verses the 3D stretched axons.

As seen from the observations in Chapter 4, the measuring tool in EZ-C1 FreeViewer software could lead to erroneous data as it involves a manual process to

define the region of interest. The average value and the standard errors have been calculated but there still remains a certain degree of inaccuracy. In order to overcome the errors, Matlab Image Analysis Program can be used. The program is under development by Yi Guo, Graduate student of the Biomedical Engineering Department at the New Jersey Institute of Technology. The Matlab program will allow for multiple image analysis simultaneously, generating an average width value of each axon bundle for individual 2D images.

The findings of the research described above provides a basis to develop an optimized 3D axon stretch growth device that provides a foundation for developing a functional 3D nerve tissue construct. The experiments aimed at quantifying the number of axons in the 3D setup will give direction into optimizing the number and density of axons stretch grown using the 3D setup. If the 3D system is indeed successful in improving the density of axons, the research will provide insights into the 3D growth mechanisms of axons and an improved nerve construct for transplantation purposes can be developed.

REFERENCES

1   Retrieved from the world wide web: www.shepherd.org/resources/spinal.asp

2   Retrieved from the world wide web: www.spinalcord.org

3   Retrieved from the world wide web: www.cdc.gov/health/default.htm.

4   Ning Z., Yan H., Wen X., Tissue-engineering approaches for axonal guidance, *Brain. Res. Rev.* 49, (2005), 48-64

5   Bareyre F. M., Neuronal repair and replacement in spinal cord injury. *J Neurol Sci.* (2007), article in press.

6   Retrieved from the world wide web: www.laesieworks.com/spinal/ 1

7   Pfister B. *Cell and molecular tissue engineering*, Lecture notes, Spring 2007, New Jersey Institute of Technology.

8   Sherwood L., Human Physiology: from Cells to Systems, 5th Edition. Chapter 5.

9   Retrieved from the world wide web: www.bseinquiry.gov.uk/report/volume16

10   Retrieved from the world wide web: http://science.education.nih.gov

11   Schwab M.E., Bartholdi D., Degeneration and regeneration of axons in the lesioned spinal cord. *Physiol. Rev.* **76**, (1996), 319-70.

12   Jaina A., Young-Tae Kima, Robert J. McKeonb, Ravi V. Bellamkondaa, In situ gelling hydrogels for conformal repair of spinal cord defects, and localdelivery of BDNF after spinal cord injury. *Biomaterials* **27**, (2006), 497-504.

13   Pfister B. J., Iwata A., Taylor A. G., Wolf J. A., Meaney D. F., Smith D. H., Development of transplantable nervous tissue constructs comprised of stretch-grown axons., *J. Neurosci. Methods* **15**, (2006), 95-103.

14   Berry M., Post-injury myelin-breakdown products inhibit axonal growth: an hypothesis to explain the failure of axonal regeneration in the mammalian central nervous system. *Bibl. Anat.* **23**, (1982), 1-11.

15   Xie F., ZhengB., White matter inhibitors in CNS axon regeneration failure. *Exp. Neurol.* **11**, (2007), 4C:3.

16   Caroni P., Schwab M.E., Antibody against myelin-associated inhibitor of neurite growth neutralizes nonpermissive substrate properties of CNS white matter. *Neuron* **1**, (1988), 85-96.

17   Stichel C.C,. Muller H.W, Experimental strategies to promote axonal regeneration after traumatic central nervous system injury, *Prog. Neurobiol.* **56**, (1998), 119-148.

18   Dietz V., Curt A., Neurological aspects of spinal-cord repair: promises and challenges. *Lancet Neurol* **5**, (2006), 688-94.

19   Chau C.H., Shum D.K., Li H., Pei J., Lui Y.Y., Wirthlin L., Chan Y.S., Xu X.M., Chondroitinase ABC enhances axonal regrowth through Schwann cell-seeded guidance channels after spinal cord injury, *FASEB* **18**, (2004), 194-196.

20   Fornaro M., Tos P., Geuna S., Giacobini-Robecchi M.G., Battiston B., Confocal imaging of Schwann-cell migration along muscle–vein combined grafts used to bridge nerve defects in the rat. *Microsurgery* **21**, (2001), 153-155.

21   Guest J.D,. Rao A, Olson L., Bunge M.B., Bunge R.P., The ability of human Schwann cell grafts to promote regeneration in the transected nude rat spinal cord, *Exp. Neurol* **148**, (1997), 502-522.

22   Firouzi M., Moshayedi P., Saberi H., Mobasheri H., Abolhassani F., Jahanzad I., Raza M.,Transplantation of Schwann cells to subarachnoid space induces repair in contused rat spinal cord, *NeuroSci Lett* **402**, (2006), 66-70.

23   Ao Q., Wang A.J., Chen G.Q., Wang S.J., Zuo H.C., Zhang X.F., Combined transplantation of neural stem cells and olfactory ensheathing cells for the repair of spinal cord injuries. *Medical Hypothesis* **30**, (2007), 209-218.

24   Li Y, Field P.M, Raisman G. Repair of adult rat corticospinal tract by transplants of olfactory ensheathing cells, *Science* **277**, (1997), 2000-2002.

25   Ramon-Cueto A., Plant G.W., Avila J., Bunge M.B., Long-distance axonal regeneration in the transected adult rat spinal cord is promoted by olfactory ensheathing glia transplants, *J Neurol Sci* **18**. (1998), 3803-15.

26   X. Cao, Schoichet M.S., Delivering neuroactive molecules from biodegradable microspheres for application in central nervous system disorders, *Biomaterials* **20**, (1999), 329-339.

27   DeLucia T.A., Conners J.J., Brown T.J., Cronin C.M., Khan T., Jones K.J., Use of a cell line to investigate olfactory ensheathing cellenhanced axonal regeneration, *Anat. Rec* **271B**, (2003), 61-70.

28   Garcia-Alias G., Lopez-Vales R, Fores J., Navarro X., Verdu E., Acute transplantation of olfactory ensheathing cells or Schwann cells promotes recovery after spinal cord injury in the rat, *J Neurol Sci* **75**, (2004), 632-641.

29   Li Y., Field P.M., Raisman G., Repair of adult rat corticospinal tract by transplants of olfactory ensheathing cells, *Science* **277**, (1997), 2000-2002.

30   Ramer L.M., Au E., Richter M.W., Liu J., Tetzlaff W., Roskams A.J., Peripheral olfactory ensheathing cells reduce scar and cavity formation and promote regeneration after spinal cord injury. *J. Comp. Neurol* **473**, (2004), 1-15.

31   Ogawa Y., Sawamoto K., Miyata T., Miyao S., Watanabe M., Nakamura M., Bregman B.S., Koike M., Uchiyama Y., Toyama Y.,Okano H. Transplantation of in vitro-expanded fetal neural progenitor cells results in neurogenesis and functional recovery after spinal cord contusion injury in adult rats. *J Neurol Sci* **69**, (2002), 925-33.

32   Toda H., Takahashi J., Mizoguchi A.,. Koyano K, Hashimoto N., Neurons generated from adult rat hippocampal stem cells form functional glutamatergic and GABAergic synapses in vitro, *Exp. Neurol,* (2000): 66-76.

33   Veizovic T., Beech J.S., Stroemer R.P, Watson W.P., Hodges H., Resolution of stroke deficits following contralateral grafts of conditionally immortal neuroepithelial stem cells, *Stroke* **32**, (2001), 1012-1019.

34   McDonald J.W., Liu X.Z., Qu Y., Liu S., Mickey S.K., Turetsky D., Transplanted embryonic stem cells survive, differentiate and promote recovery in injured rat spinal cord. *Nat Med* **5**, (1999), 1410-2.

35   Keirstead H.S., Nistor G., Bernal G., Totoiu M., Cloutier F., Sharp K., Human embryonic stem cell-derived oligodendrocyte progenitor cell transplants remyelinate and restore locomotion after spinal cord injury. *J Neurol Sci* **19**, (2005), 4694-705.

36   Zeng X., RAO M. S.,Human embryonic stem cells: Long term stability, absence of senescence and a potential cell source for neural replacement. *J Neurol Sci* **145**, (2007), 1348-1358

37   Schultz S.S., Adult stem cell application in spinal cord injury. *Curr Drug Targets* (2005): 63-73.

38 Reier P.J., Cellular transplantation strategies for spinal cord injury and translational neurobiology. *NeuroRx* **1**, (2004), 424-51.

39 Griffith L.G., Emerging design principles in biomaterials and scaffolds for tissue engineering, *Ann. N. Y. Acad. Sci* **961**, (2002), 83-95.

40 Wang G., Yang Z., Xie H., Materials fabrication of tissue engineered peripheral nerve in vitro. (2000), 110-114.

41 Decherchi P., Lammari-Barreault N., Cochard P., Carin M., Rega P., Pio J., Pellissier J.F., Ladaique P., Novakovitch G., Gauthier P., CNS axonal regeneration with peripheral nerve grafts cryopreserved by vitrification: cytological and functional aspects. *Cryobiology* **34**, (1997), 214-239.

42 Gautier S.E., Oudega M., Fragoso M., Chapon P., Plant G.W, Bunge M.B., Parel J.M., Poly(alpha-hydroxyacids) for application in the spinal cord: resorbability and biocompatibility with adult rat Schwann cells and spinal cord, *J. Biomed. Mater* **42**, (1998): 642-654.

43 Yoshii S., Oka M., Shima M., Taniguchi A., Taki Y., Akagi M., Restoration of function after spinal cord transection using a collagen bridge, *J. Biomed. Mater* **70A**, (2004): 569-575.

44 Takezawa T., A strategy for the development of tissue engineering scaffolds that regulate cell behavior, *Biomaterials*. (2003), 2267-2275.

45 Peter P., Rainer M., Ahmed E., Klaus H., Werner K., Thomas W., Cornelius F., Maurice V., Ulrich B., Norbert W., The promotion of oriented axonal regrowth in the injured spinal cord by alginate-based anisotropic capillary hydrogels, *Biomaterials* **27**. (2006): 3560-3569.

46 Atala A., Tissue engineering of artificial organs, *J. Endourol* **14**, (2000): 49-57.

47 Lanza R.P., Langer R.S., Vacanti J., Principles of tissue engineering, *Academic Press*. (2000): 1-73.

48 Wen X, Studies in the Development of a Bridging Device for Guiding Regenerating Axons, (2003): 115.

49 Kidoaki S., Kwon I.K, Matsuda T., Mesoscopic spatial designs of nano- and microfiber meshes for tissue-engineering matrix and scaffold based on newly devised multilayering and mixing electrospinning techniques. *Biomaterials* **26**, (2005): 37-46.

50 Wen X., Webb K., Tresco P.A., Multi-filament entubulation bridging device for axonal guidance and regeneration, *Biomaterials*, (2001): 182.

51   Giles W. Plant a, Alan R. Harvey a,,, Traian V. Chirila, Axonal growth within poly (2-hydroxyethyl methacrylate) sponges infiltrated with Schwann cells and implanted into the lesioned rat optic tract. *Brain Res* 671, (1995): 119-130.

52   Liu, Y., Kim, D., Himes, B.T., Chow, S.Y., Schallert, T., Murray, M., Tessler, A., and Fischer, I. Transplants of fibroblasts genetically modified to express BDNF promote regeneration of adult rat rubrospinal axons and recovery of forelimb function. *J Neurol Sci* 19, (1999): 4370-4387.

53   Murray, M., Kim, D., Liu, Y., Tobias, C., Tessler, A., and Fischer, I. Transplantation of genetically modified cells contributes to repair and recovery from spinal injury. *Brain Res Rev* 40, (2002): 292-300.

54   Anderson, D.K., Howland, D., R., Reier, P. J., Fetal neural grafts and repair of the injuredspinal cord. *Brain Pathol* 5, (1995): 451-57.

55   Bray D., Axonal growth in Response to Experimentally applied Mechanical tension. *Dev Biology*, (1984): 379-389.

56   Dennerll T. J., Philip L., Robert E. B., Steven R. H., The Cytomechanics of Axonal Elongation and Retraction. *J.Cell Biology*. (1989): 3073-3083.

57   Heidemann S. R., Buxbaum R. E., Tension as a Regulator and Integrator of Axonal Growth. Cell Motility and the Cytoskeleton. 1990.

58   Jing Z., Phillip L., Vivian S., Timothy D., Robert E. B., Steven R. H., Tensile Regulation of Axonal Elongation and Initiation. *J Neurol Sci*. (1991): 1117-1 125.

59   Hitchcock P.F. Constant dendritic coverage by ganglion cells with growth of the goldfish's retina. (1987): 17-22.

60   Hitchcock P.F., Easter S.S. Retinal ganglion cells in goldfish: a qualitative classification into four morphological subtypes and a quantitative study of one of them. *J Neurol Sci*. (1986): 1037-1050.

61   Rebecca K., Skornia S. L., Effect of collagen gel stiffness on neurite extension, *J Biomaterials Sci* 15, (2004), 1521-1532.

62   Retrieved from the world wide web:http://probes.invitrogen.com